



NTNU – Trondheim
Norwegian University of
Science and Technology

Dynamic Analysis of Floating Bridges with Transverse pontoons

Ahnaf Rahman

Marine Technology

Submission date: June 2014

Supervisor: Bernt Johan Leira, IMT

Norwegian University of Science and Technology
Department of Marine Technology



I. ABSTRACT

The main objective of this thesis is to analyse the dynamic response of floating bridges with transverse pontoons, when subjected to harmonic regular wave loads. As a result, a simplified beam model of the Bergsøysundet floating bridge is established in the FEM software Abaqus. Additional “synthetic” floating bridge structures are subsequently built and analysed in a similar manner.

The pontoon model already developed in Genie by Abdillah Suyuthi is analysed in HydroD to obtain the pontoon’s structural model and hydrodynamic parameters. In addition to these parameters, by implementing his calculated data of mass and sectional properties of the bridge truss-work components, the simplified beam model of the bridge is developed in Abaqus. Taking the Bergsøysundet floating bridge model as the basis, “synthetic” bridge models are similarly assembled and studied. The effect of sideway mooring is also considered for some of the models.

Eigenfrequency analysis is then carried out in Abaqus in order to determine the frequency of the fundamental mode of a model. The eigenfrequency and added mass are updated by iteration until they are concurrent. Static and dynamic analysis are then carried out for the model. The regular wave load corresponding to the updated frequency of the mode is acquired from the hydrodynamic analysis in HydroD and applied in Abaqus.

Efficient techniques are presented to calculate the phase difference at each pontoon. This arises due to the combined effect of changing wave direction and shapes of the models.

A simplified method is employed to gauge the critical angle of wave heading. The effect of wave spreading is also assessed in a streamlined manner based on discussion with the supervisor.

Limitations with regard to the non application of full matrices of the pontoon’s structural model and hydrodynamic parameters are highlighted. Negatively damped sway motions are controlled by the application of external lateral dampers. Mixed results are obtained at the estimated critical angles. Better result is obtained by iteration of the responses for growing angles of wave heading. The wave spreading response result is satisfying.





II. PREFACE

This thesis has been written as the concluding assignment for my master's education at the Department of Marine Technology, NTNU. The assignment has been mainly to investigate the dynamic response of a number of floating bridge models subjected to harmonic regular waves.

This thesis is a culmination of the task I started as a Summer Intern at the department, which continued through my master's project. At that time, the focus was mainly on the dynamic response of the Bergsøysund floating bridge model. "Synthetic" bridge models have been developed and analysed as part of the thesis.

The scope of work was proposed by my supervisor at the department, Professor Bernt Johan Leira. I want to thank him from the bottom of my heart for his thought-provoking discussions and encouraging guidance throughout the entire task.

Finally, I would like to thank Abdillah Suyuthi, a former PhD student at the department, for his help and collaboration during the initial stages of this work. His created pontoon model was of immense support for my thesis.

Trondheim June 10th, 2014

Ahnaf Rahman





III. CONTENTS

I.	ABSTRACT.....	i
II.	PREFACE	iii
III.	CONTENTS.....	v
IV.	LIST OF FIGURES.....	ix
V.	LIST OF TABLES.....	xiii
1	INTRODUCTION.....	1
1.1	Project description.....	1
1.2	General.....	1
1.3	History of floating bridges.....	2
1.4	Types of floating bridges.....	3
1.5	Existing floating bridges	4
2	THEORY	11
2.1	Structural loads	11
2.2	Dynamic analysis.....	12
2.3	Time domain analysis.....	13
2.4	Non-linear static problems	13
2.4.1	Load incremental methods	14
2.4.2	Iterative methods.....	15
2.4.3	Combined methods.....	16
2.5	Eigenvalue analysis	17
3	ANALYSIS TOOLS	19
3.1	HydroD – Wadam analysis	19
3.2	Abaqus CAE	20
3.2.1	Eigenvalue extraction.....	20
3.2.2	Implicit dynamic analysis	20
4	BRIDGE MODELS IN ABAQUS	23
4.1	Curve bridge model - Bergsøysund Bridge.....	23
4.2	Straight bridge model	24
4.3	Elongated straight bridge model	25
4.4	Elongated curve bridge model.....	25
4.5	Elongated bridge models with sideway mooring lines	26



5	EIGENFREQUENCY ANALYSIS	27
5.1	Curve bridge model.....	27
5.2	Straight bridge model	28
5.3	Elongated straight bridge model	29
5.4	Elongated straight bridge model with mooring.....	30
5.5	Elongated curve bridge model	31
5.6	Elongated curve bridge model with mooring	32
6	STATIC RESPONSE	33
6.1	Curve bridge model.....	34
6.2	Straight bridge model	35
6.3	Elongated straight bridge model	36
6.4	Elongated curve bridge model.....	37
7	DYNAMIC RESPONSE.....	39
7.1	Calculation of critical angles	39
7.2	Calculation of phase angles	40
7.2.1	Phase angles of curve bridge model	40
7.2.2	Phase angles of straight bridge model.....	41
7.3	Sway response	42
7.3.1	Curve bridge model.....	43
7.3.2	Straight bridge model	45
7.3.3	Elongated straight bridge model.....	47
7.3.4	Elongated straight bridge model with mooring.....	49
7.3.5	Elongated curve bridge model	51
7.3.6	Elongated curve bridge model with mooring	53
7.4	Heave response.....	55
7.4.1	Curve bridge model.....	55
7.4.2	Straight bridge model	58
7.4.3	Elongated straight bridge model.....	60
7.4.4	Elongated straight bridge model with mooring.....	63
7.4.5	Elongated curve bridge model	65
7.4.6	Elongated curve bridge model with mooring	68
8	DISCUSSION.....	71
9	CONCLUSION.....	75



10 REFERENCES.....	77
APPENDIX A.....	I
APPENDIX B.....	III
APPENDIX C.....	IX
APPENDIX D.....	XIII



IV. LIST OF FIGURES

Figure 1: Floating Bridge: (a) continuous pontoon bridge; (b) separated pontoon bridge; (c) semi-submerged foundation; (d) bridges with gravity foundation; (e) long-spanned separated foundation [3]	4
Figure 2: Homer Hadley Bridge (left) and Lacey V. Murrow Memorial Bridge (right) [5].....	4
Figure 3: Hood Canal Bridge [6]	5
Figure 4: Governor Albert D. Rosellini Bridge [7].....	5
Figure 5: Admiral Clarey Bridge [8]	6
Figure 6: William R. Bennett Floating Bridge (right) and Kelowna Floating Bridge (left) [10]	6
Figure 7: Bergsøysund Bridge [11]	7
Figure 8: Nordhordland Bridge [12]	7
Figure 9: Galata Bridge [13]	8
Figure 10: West India Quay Floating Footbridge [14].....	8
Figure 11: Yumemai Bridge [15].....	9
Figure 12: Euler-Cauchy Incrementing [18]	14
Figure 13: Newton-Raphson Iteration [18]	15
Figure 14: No updating of $K_i(r)$ [18]	16
Figure 15: $K_i(r)$ updated after first iteration [18]	16
Figure 16: Combined incremental and iterative solution procedure [18]	17
Figure 17: Panel model of pontoon in HydroD	19
Figure 18: Sketch of the Bergsøysund Bridge	23
Figure 19: Model of Bergsøysund Bridge in Abaqus.....	24
Figure 20: Straight bridge model in Abaqus	24
Figure 21: Elongated straight bridge model in Abaqus.....	25
Figure 22: Elongated curve bridge model in Abaqus	25
Figure 23: Longitudinal section area of the pontoon	33
Figure 24: Static displacement along the curve bridge model	34
Figure 25: Static bending moment along the curve bridge model	34
Figure 26: Static displacement along the straight bridge model.....	35
Figure 27: Static bending moment along the straight bridge model.....	35
Figure 28: Static displacement along the elongated straight bridge model.....	36
Figure 29: Static bending moment along the elongated straight bridge model.....	36
Figure 30: Static displacement along the elongated curve bridge model	37
Figure 31: Static bending moment along the elongated curve bridge model	37
Figure 32: Concept diagram for calculation of critical angle of wave direction	39
Figure 33: Wave heading in straight bridge model [23]	40
Figure 34: Concept diagram for calculation of phase angles of curve bridge model	40
Figure 35: Concept diagram for calculation of phase angles of straight bridge models	41
Figure 36: Sway displacement at a point of a model with lateral dashpots.....	42
Figure 37: Sway displacement along the curve bridge model	43
Figure 38: Sway bending moment along the curve bridge model.....	43



Figure 39: Sway displacement along the curve bridge model	44
Figure 40: Sway bending moment along the curve bridge model	44
Figure 41: Sway displacement along the straight bridge model	45
Figure 42: Sway bending moment along the straight bridge model	45
Figure 43: Sway displacement along the straight bridge model	46
Figure 44: Sway bending moment along the straight bridge model	46
Figure 45: Sway displacement along the elongated straight bridge model	47
Figure 46: Sway bending moment along the elongated straight bridge model	47
Figure 47: Sway displacement along the elongated straight bridge model	48
Figure 48: Sway bending moment along the elongated straight bridge model	48
Figure 49: Sway displacement along the elongated straight bridge model with mooring	49
Figure 50: Sway bending moment along the elongated straight bridge model with mooring	49
Figure 51: Sway displacement along the elongated straight bridge model with mooring	50
Figure 52: Sway bending moment along the elongated straight bridge model with mooring	50
Figure 53: Sway displacement along the elongated curve bridge model	51
Figure 54: Sway bending moment along the elongated curve bridge model	51
Figure 55: Sway displacement along the elongated curve bridge model	52
Figure 56: Sway bending moment along the elongated curve bridge model	52
Figure 57: Sway displacement along the elongated curve bridge model with mooring	53
Figure 58: Sway bending moment along the elongated curve bridge model with mooring	53
Figure 59: Sway displacement along the elongated curve bridge model with mooring	54
Figure 60: Sway bending moment along the elongated curve bridge model with mooring	54
Figure 61: Heave displacement along the curve bridge model	56
Figure 62: Heave bending moment along the curve bridge model	56
Figure 63: Heave displacement along the curve bridge model	57
Figure 64: Heave bending moment along the curve bridge model	57
Figure 65: Heave displacement along the straight bridge model	58
Figure 66: Heave bending moment along the straight bridge model	59
Figure 67: Heave displacement along the straight bridge model	59
Figure 68: Heave bending moment along the straight bridge model	60
Figure 69: Heave displacement along the elongated straight bridge model	61
Figure 70: Heave bending moment along the elongated straight bridge model	61
Figure 71: Heave displacement along the elongated straight bridge model	62
Figure 72: Heave bending moment along the elongated straight bridge model	62
Figure 73: Heave displacement along the elongated straight bridge model with mooring	63
Figure 74: Heave bending moment along the elongated straight bridge model with mooring	64
Figure 75: Heave displacement along the elongated straight bridge model with mooring	64
Figure 76: Heave bending moment along the elongated straight bridge model with mooring	65
Figure 77: Heave displacement along the elongated curve bridge model	66
Figure 78: Heave bending moment along the elongated curve bridge model	66
Figure 79: Heave displacement along the elongated curve bridge model	67
Figure 80: Heave bending moment along the elongated curve bridge model	67
Figure 81: Heave displacement along the elongated curve bridge model with mooring	68



Figure 82: Heave bending moment along the elongated curve bridge model with mooring 69

Figure 83: Heave displacement along the elongated curve bridge model with mooring 69

Figure 84: Heave bending moment along the elongated curve bridge model with mooring 70

Figure 85: Maximum heave bending moment for the elongated straight bridge model..... 72

Figure 86: Wave spreading as a $\cos^2\theta$ function 73

Figure 87: Heave bending moment along the elongated straight bridge model for $\cos^2\theta$ wave spreading function 73

Figure 88: Concept diagram for calculation of phase angles of curve bridge model III

Figure 89: Concept diagram for calculation of phase angles of elongated curve bridge modelIV



V. LIST OF TABLES

Table 1: Classification of Floating Bridges and Tunnels [3].....	3
Table 2: Iteration of added mass for first sway eigenmode	27
Table 3: Eigenfrequencies of the curve bridge model	27
Table 4: Iteration of added mass for first sway eigenmode	28
Table 5: Eigenfrequencies of the straight bridge model.....	28
Table 6: Iteration of added mass for first sway eigenmode	29
Table 7: Eigenfrequencies of the elongated straight bridge.....	29
Table 8: Iteration of added mass for first sway eigenmode	30
Table 9: Eigenfrequencies of the elongated straight bridge with mooring.....	30
Table 10: Iteration of added mass for first sway eigenmode	31
Table 11: Eigenfrequencies of the elongated curve bridge	31
Table 12: Iteration of added mass for first sway eigenmode	32
Table 13: Eigenfrequencies of the elongated curve bridge with mooring	32
Table 14: Iteration of added mass for first heave eigenmode	55
Table 15: Iteration of added mass for first heave eigenmode	58
Table 16: Iteration of added mass for first heave eigenmode	60
Table 17: Iteration of added mass for first heave eigenmode	63
Table 18: Iteration of added mass for first heave eigenmode	65
Table 19: Iteration of added mass for first heave eigenmode	68
Table 20: Comparison between the eigenfrequencies of simplified and detailed Bergsøysund bridge models.....	71
Table 21: Important results of the dynamic analyses.....	72
Table 22: Bridge sections' properties	I
Table 23: Bridge mass data	I
Table 24: Material Data	I
Table 25: Phase angles of curve bridge model in sway	III
Table 26: Phase angles of curve bridge model in heave.....	IV
Table 27: Phase angles of elongated curve bridge model in sway	V
Table 28: Phase angles of elongated curve bridge model in heave.....	VI
Table 29: Phase angles of elongated curve bridge model with mooring in sway.....	VII
Table 30: Phase angles of elongated curve bridge model with mooring in heave	VIII
Table 31: Phase angles of straight bridge model in sway	IX
Table 32: Phase angles of straight bridge model in heave	IX
Table 33: Phase angles of elongated straight bridge model in sway.....	X
Table 34: Phase angles of elongated straight bridge model in heave	X
Table 35: Phase angles of elongated straight bridge model with mooring in sway	XI
Table 36: Phase angles of elongated straight bridge model with mooring in heave	XI





1 INTRODUCTION

1.1 Project description

Floating bridges are relevant for crossing of very deep and wide lakes or fjord systems. In order to compute the static and dynamic response of these bridges, the joint properties of the whole hydro-elastic system need to be accounted for. Only recently, the design of floating bridges has moulded into a more scientific form due to developments in the theory and computers programs for studying the hydrodynamic interactions between fluid and floating bodies.

The objective of this thesis was to outline methods for response analysis and illustrate the calculation procedure for some particular example bridge structures with transverse pontoons.

The following subjects were addressed as part of this work:

1. A review was made of existing floating bridges. Similarities and differences between the different bridges were highlighted.
2. The loads which act on such bridges were described and associated structural models were discussed. Corresponding methods for eigenfrequency, static and dynamic response analysis were elaborated and relevant numerical algorithms were described.
3. A simplified beam model of the Bergsøysundet floating bridge was established in the FEM software Abaqus. The theoretical background and numerical algorithms related to non-linear static and dynamic response analysis were reviewed. Calculations were subsequently performed for regular waves with different directions of propagation.
4. Additional "synthetic" bridge structures were subsequently constructed and analysed in a similar manner. As a first case, the true arch shape of Bergsøysundet bridge model was replaced with a straight-line geometry and analysed. Subsequently, additional bridge structures were established by increasing the span length for both the straight and curve bridges. The effect of sideways mooring lines on the elongated bridge models were also considered. The effect of wave spreading was also assessed in a simplified way.

1.2 General

A floating bridge is a bridge that floats on water, resting on top of barges or boat like pontoons, which support the bridge's deck and its dynamic loads. A floating bridge is basically a beam on an elastic foundation and supports. Vertical loads are



resisted by the buoyancy, whereas the transverse and longitudinal loads are resisted by a system of mooring lines or structural elements [1].

The selection of a floating bridge is based on a number of technical and economic reasons which can be summarized as follows [2]:

1. At deeper water depths the construction of a fixed foundation is very expensive and may be an inadequate design.
2. In regions with very soft mud lines where there is no possibility of fixed foundation construction or there is unacceptable loading capacity, a floating bridge would be a more rational design.
3. In ports with high tidal levels where large differences between the structure level and fixed quay elevation are exposed.
4. In earthquake regions, where by using a fixed foundation, an extreme dynamic response is expected.
5. In temporary projects when the structure is not needed after a period of time.
6. In projects when the ecological condition of the site is not expected to change.

According to M. Myint Lwin, for a site where the width of water is 2-5 km and the depth is 30-60 m, with the soft bottom extending another 30-60 m, a floating bridge is three to five times cheaper to construct than a long span fixed bridge, tube or tunnel [1].

1.3 History of floating bridges

Floating bridges have been in use from ancient times. 4000 years ago, the first floating bridges were boat bridges [3], which were used in many battles. Even today, military floating bridges, which are of temporary type, are being used to transport soldiers, vehicles and ammunition.

In 1874, a mobile wooden pontoon railroad bridge was built across the Mississippi River in Wisconsin, which was rebuilt regularly but finally abandoned. The Brookfield Floating Bridge, which is a 98 m long wooden bridge, is still in operation in Brookfield, Vermont [3].

In 1912, the old Galata Bridge, which consisted of 50 steel pontoons at a water depth of 41 m, was built across the Golden Horn, Istanbul [3]. It burned down in 1992.

1.4 Types of floating bridges

Floating bridges can be classified according to their spatial position, as shown in Table 1 and Figure 1 [3].

Table 1: Classification of Floating Bridges and Tunnels [3]

Types and Spatial Position	Description
1. Deeper than seabed	Underwater tunnel
2. Just beneath seabed	Immersed tunnel
3. Structure completely immersed in water	Submerged floating bridge or tunnel
4. Foundation completely submerged:	
I. Foundation(s) resting on seabed	Bridges with gravity foundation(s) (see Figure 1d)
II. Continuous foundation	Floating bridge with continuous submerged foundation
III. Separated foundation	Floating bridge with separated foundations
5. Semi-submerged foundations	Floating bridge with semi-submerged foundations (see Figure 1c)
6. Pontoon foundations	Floating bridge with pontoon foundations (see Figure 1b)
7. Pontoon girders	Continuous pontoon bridge (see Figure 1a)
8. Foundations secured at seabed	Conventional (land-based) bridges

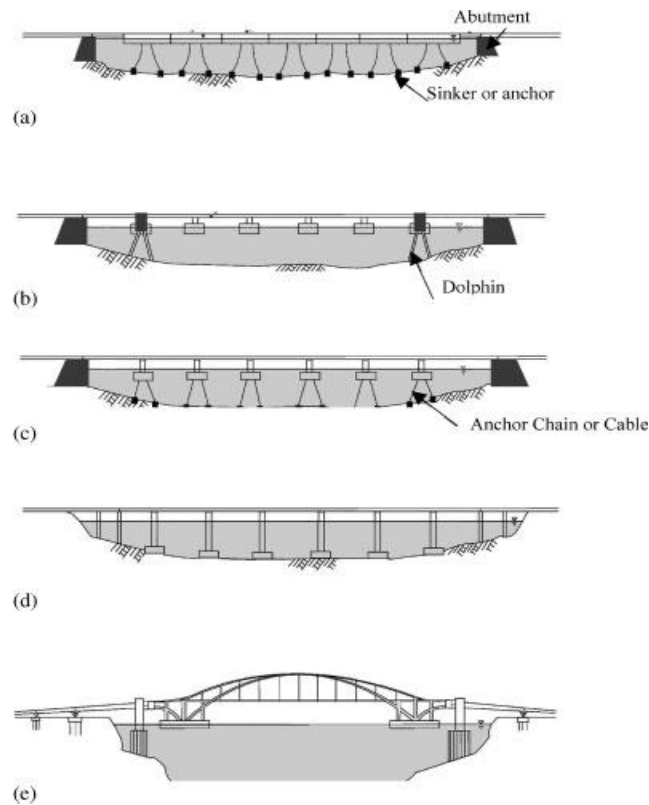


Figure 1: Floating Bridge: (a) continuous pontoon bridge; (b) separated pontoon bridge; (c) semi-submerged foundation; (d) bridges with gravity foundation; (e) long-spanned separated foundation [3]

1.5 Existing floating bridges

In 1940, the First Lake Washington Bridge also known as the Lacey V. Murrow Memorial Bridge was built in Seattle. See Figure 2. Its length is 2018 m and it consists of concrete pontoon girders [4].



Figure 2: Homer Hadley Bridge (left) and Lacey V. Murrow Memorial Bridge (right) [5]

The Hood Canal Bridge, shown in Figure 3, was constructed in 1961. At a length of 2398 m with the floating portion extending 1988 m, it is the world's longest floating bridge located in a saltwater tidal basin, and the third longest floating bridge overall [4].



Figure 3: Hood Canal Bridge [6]

The Second Lake Washington Bridge, also called the Governor Albert D. Rosellini Bridge (formerly known as the Evergreen Point Bridge) was constructed in 1963. At 2310 m, it is the longest floating bridge in the world [4]. See Figure 4.



Figure 4: Governor Albert D. Rosellini Bridge [7]

This was followed by the Third Lake Washington Bridge, also known as the Homer Hadley Bridge, in 1989. See Figure 2. At 1772 m, it is the fifth longest floating bridge in the world [4].

The Admiral Clarey Bridge, shown in Figure 5, was constructed at Pearl Harbor, Oahu Island, Hawaii in 1998. It is a floating concrete drawbridge of total length 1424 m and of width 13 m [4].



Figure 5: Admiral Clarey Bridge [8]

The Kelowna Floating Bridge, which was built on Lake Okanagan in British Columbia, Canada in 1958, was replaced by the William R. Bennett Floating Bridge in 2008. See Figure 6. The new design eliminates the lift span by providing a fixed, elevated approach structure with a navigation span on the west side of the bridge [9]. The middle portion of the bridge is comprised of the floating pontoon string, and the transition spans are provided from the east shore and the west approach structure to the pontoons [9].



Figure 6: William R. Bennett Floating Bridge (right) and Kelowna Floating Bridge (left) [10]

In 1992, the Bergsøysund Bridge was built at Bergsøyfjord near Kristiansund, Norway. It is a horizontally curved bridge with radius of curvature 1300 m and it is 845 m long. With a steel pipe truss superstructure, it rests on seven concrete pontoon foundations [3]. See Figure 7.



Figure 7: Bergsøysund Bridge [11]

The Nordhordland Bridge, as shown in Figure 8, is a combined cable stayed and pontoon bridge. It was built in 1994 in Hordaland, Norway. It is 1614 m long, with the floating part extending 1246 m [4]. Its basic design concepts are similar to the Bergsøysund Bridge but with a radius of curvature of 1700 m and a superstructure of steel box girders and flexible plates [3].



Figure 8: Nordhordland Bridge [12]

The Old Galata Bridge was replaced by a new one in December 1994. It is a bascule bridge, which spans the Golden Horn in Istanbul. It is 490 m long with a main span of 80 m [4]. See Figure 9.



Figure 9: Galata Bridge [13]

The 90 m long West India Quay floating footbridge was built in London's Docklands in 1996 [3]. See Figure 10. The bridge is 94 m long, with a U-shaped steel spine beam structure. The bridge is supported on eight foam filled pontoons [14].



Figure 10: West India Quay Floating Footbridge [14]

In 2000, the Yumemai Bridge was completed in Osaka, Japan. The bridge is shown in Figure 11. It is a 410 m long floating swing arch bridge with a main span of 280 m, and it is part of a 940 m long road crossing [3].



Figure 11: Yumemai Bridge [15]





2 THEORY

2.1 Structural loads

Floating pontoon bridges, namely continuous pontoon type and separate pontoon type, are generally expected to be in service life for 75-100 years with low cost maintenance cycle [1].

The important loadings on floating bridges can be classified as follows [3, 16]:

1. Self-Weight
2. Hydrostatic water pressure
3. Loads due to traffic
4. Ballasting and loads from equipment
5. Deformation loadings, e.g. creep, temperature, settlements, etc.
6. Wind loading
7. Wave loading: progressive and alternate
8. Effects of stratified flows (internal waves)
9. Water-level variations (tides, etc.)
10. Marine Growth and water absorption in concrete
11. Effect of tsunami
12. Snow load
13. Collision load
14. Ice load
15. Seiche (or secondary undulation)
16. Effect of earthquakes

A combination of the various loads above can lead to the most undesirable effect on the floating bridge. Using classical beam theory, it is easy to design for static loads, such as dead and live loads. For a concentrated load, P , acting from one end of a continuous floating structure, the maximum shear, moment, and deflection are given by [1]

$$V_{\max} = \frac{P}{2} \quad \text{Eq. 2.1}$$

$$M_{\max} = \frac{P}{2\lambda} \quad \text{Eq. 2.2}$$

$$V_{\max} = \frac{P\lambda}{2k} \quad \text{Eq. 2.3}$$

where k is the modulus of foundation

$$\lambda = 4 \sqrt{\frac{k}{4EI}} \quad \text{Eq. 2.4}$$

Winds and waves are the major environmental loads acting on a floating bridge. But these loads are difficult to predict. Wind blowing over water generates a sea state that induces horizontal, vertical and torsional loads on a floating bridge [3]. From a given wind history, the wave hindcast statistics can be accurately obtained after considering the wind direction, length of open water in wind direction (fetch) and refraction due to shallow water depth [16]. The design wind speed may be specified as the 10-min average at a height of 10m above the sea surface [3]. According to M. Myint Lwin, the normal and extreme storm conditions due to wind and wave are defined as the storm conditions that have a mean recurrence interval of 1 year and 100 years respectively [1].

Floating bridges should be designed so that they are comfortable to ride on during normal storm (1-yr storm) conditions and also so that they evade undesirable structural effects during extreme storm (100-yr storm) conditions [1]. In that case, the probability of non-exceedance P_n , which is the probability of the design load not occurring during the service life for the dominant natural action, may be expressed by means of the return period T and the expected service life Q [3] as

$$P_n = \left(1 - \frac{1}{T}\right)^Q \quad \text{Eq. 2.5}$$

From the point of view of risk management [3], a probability of about 50% looks reasonable since a probability of 100% corresponds to events occurring inevitably; while probability of zero corresponds to investing extra money or wasting money for events which never happen.

Irregular sea waves consist of many components of different frequency and therefore can be decomposed into many regular waves. Since the fundamental period of floating bridges is larger than that of conventional bridges, the long-period components of waves are important [3].

2.2 Dynamic analysis

The global responses of a floating bridge can be determined by dynamic analysis [1]. The basic approach to dynamic analysis is to solve the equation of motion, which is given by

$$Mx'' + Cx' + Kx = F(t) \quad \text{Eq. 2.6}$$

For prediction of dynamic response, the wave- structure interaction must be taken into account. As the bridge reacts to the incident waves, the motions of the bridge produce hydrodynamic effects generally characterized in terms of added mass and damping coefficients, which are frequency dependent. The equation of motion of a floating structure for a single degree of freedom system can be expressed as

$$(M + A)x'' + (C_1 + C_2)x' + (K + k)x = F(t) \quad \text{Eq. 2.7}$$



where,

x, x' and x''	= generalized displacement, velocity and acceleration at each degree of freedom
M	= structural mass-inertia
A	= frequency dependent added mass
C_1	= structural damping coefficient
C_2	= frequency dependent hydrodynamic damping coefficient
K	= structural stiffness coefficient (elastic properties, including the effects of mooring lines)
k	= hydrostatic stiffness coefficient
F(t)	= Wave excitation force acting on the structure

Numerical methods and computer programs have been established for computing the hydrodynamic coefficients of common cross sectional shapes. Structural configurations for which no or limited data exist, physical model testing is necessary to determine the basic sectional added mass, damping, and wave excitation loads [1]. Structural damping is an important source of damping in the structure and it significantly affects the responses. M. Myint Lwin assumes structural damping coefficient of 2 to 5% of critical damping for such analysis [1].

The equation of motion may be solved in the deterministic time-domain or in the probabilistic frequency-domain. The time-domain approach is time consuming and involves solving differential equations when the coefficients are constants. On the other hand, the frequency-domain approach is simple and involves fast calculations. It's very efficient in handling constant and frequency-dependent coefficients but it is applicable only for a linear system.

2.3 Time domain analysis

The commonly-used approaches for the time-domain analysis of floating structures are the direct time integration method and the method that uses the Fourier transform [17]. The equations of motion are discretized for both the structure and the fluid domain in the direct integration method. In the Fourier transform method, the frequency domain solutions for the fluid domain are first obtained. The results are then Fourier transformed for substitution into the differential equations for elastic motions. By using the finite element method or other suitable computational methods, these equations are then solved directly in the time domain.

2.4 Non-linear static problems

Various techniques for solving non-linear static problems exist. Three types of methods will be briefly explained, as described by T. Moan [18]. These are:

1. Incremental or Stepwise procedures
2. Iterative procedures
3. Combined methods

2.4.1 Load incremental methods

Incremental methods provide a solution of the non-linear problem by a stepwise application of the external loading. After each step, the displacement increment Δr is determined and all the increments are summed up to obtain the total displacement. Based on the known displacement and stress condition, the incremental stiffness matrix $K_I(r)$ is calculated and kept constant before a new load increment is applied. This method is also called Euler-Cauchy method. For load increment no. (m+1) it may be expressed as

$$\Delta R_{m+1} = \Delta R_{m+1} - R_m \quad \text{Eq. 2.8}$$

$$\Delta r_{m+1} = K_I(r_m)^{-1} \Delta R_{m+1} \quad \text{Eq. 2.9}$$

$$\Delta r_{m+1} = r_m + \Delta r_{m+1} \quad \text{Eq. 2.10}$$

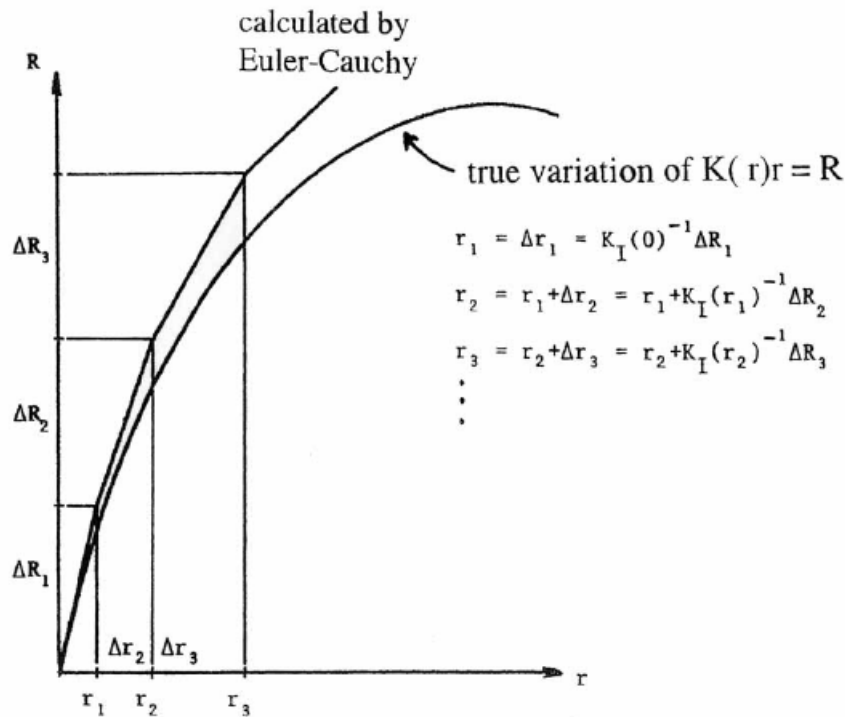


Figure 12: Euler-Cauchy Incrementing [18]

This method does not include fulfilment of the total equilibrium equation, $R=K_I(r)r$. Therefore, total equilibrium will not be fulfilled. This is illustrated by the deviation between the approximate and the true curve in Figure 12. The accuracy may be increased by reducing the load increment. Also, the load increment should be adjusted according to the degree of non-linearity. Computer programs are capable of choosing the load increment automatically.

2.4.2 Iterative methods

The most regularly used iterative method for solving non-linear structural problems is the Newton-Raphson method.

The Newton-Raphson algorithm to solve x for the problem: $f(x) = 0$ is

$$x_{n+1} = x_n - \frac{f(x_n)}{f'(x_n)} \quad \text{Eq. 2.11}$$

where $f'(x_n)$ is the derivative of $f(x)$ with respect to x , at $x = x_n$.

In this case, $K_i(\mathbf{r})$ represents the generalisation of the $\partial f / \partial x$ in Newton's method for a single degree of freedom system. Then by iteration, the following equation is solved

$$\mathbf{r}_{n+1} = \mathbf{r}_n - K_i^{-1}(\mathbf{r}_n) (\mathbf{R}_{int} - \mathbf{R}) \quad \text{Eq. 2.12}$$

The basic principle for this iteration is illustrated in Figure 13 for a single degree of freedom system. This method requires $K_i(\mathbf{r})$ to be established for each iterative step, which is time consuming. By updating $K_i(\mathbf{r})$ less frequently, fewer efforts are required. Modified Newton-Raphson iteration is beneficial since there is limited loss of rate of convergence. There are two alternatives for the modified Newton-Raphson methods, one which requires no updating of $K_i(\mathbf{r})$ and the other one where $K_i(\mathbf{r})$ is updated after the first iteration.

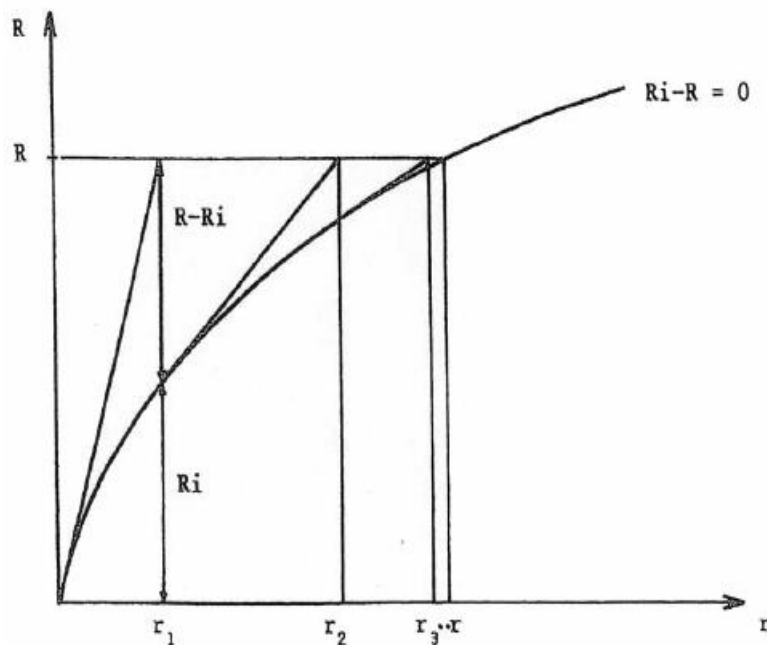


Figure 13: Newton-Raphson Iteration [18]

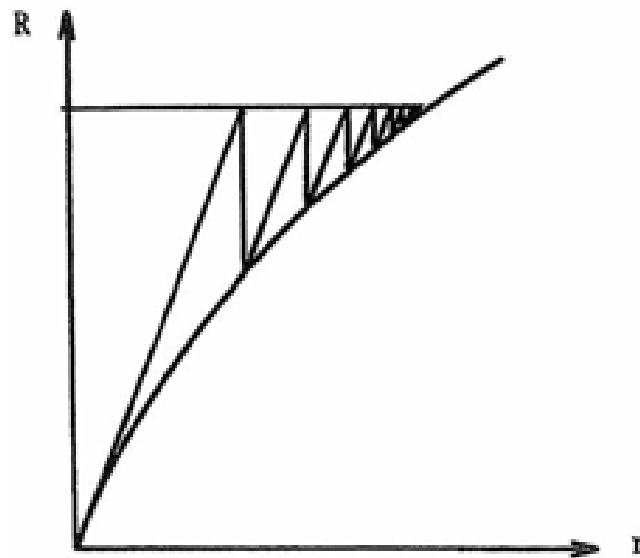


Figure 14: No updating of $K_i(r)$ [18]

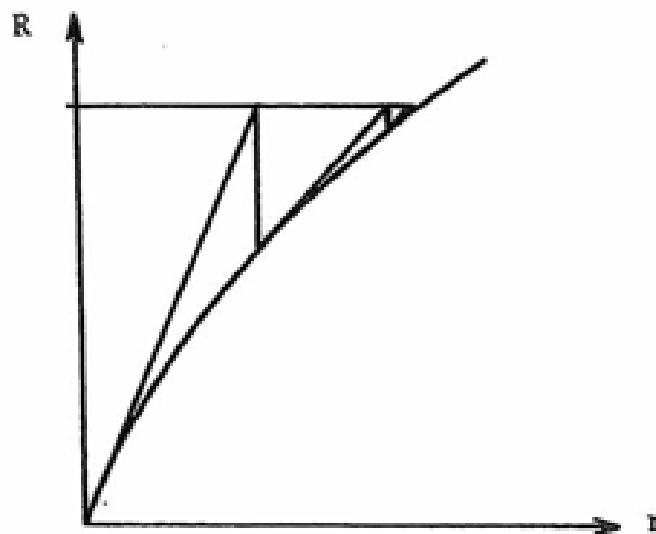


Figure 15: $K_i(r)$ updated after first iteration [18]

2.4.3 Combined methods

Incremental and iterative methods are frequently combined. The external load is applied in increments and in each increment equilibrium is achieved by iteration. Figure 16 illustrates a combination of Euler-Cauchy incrementation and a modified Newton-Raphson iteration.

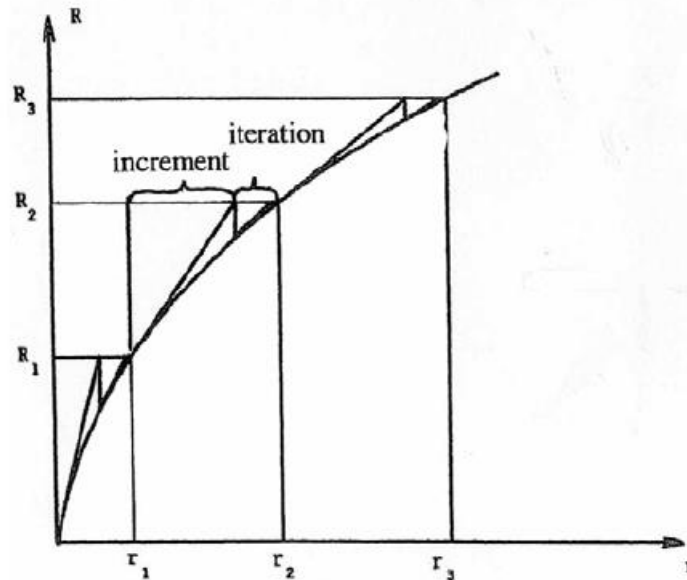


Figure 16: Combined incremental and iterative solution procedure [18]

The procedure is carried out by applying loading according to Eq. 2.9 followed by iteration at each load level by Eq. 2.12. The modified Newton-Raphson method is often used keeping the gradient $K_i(r)$ constant during several iteration cycles. The iteration is stopped when acceptable accuracy is achieved.

2.5 Eigenvalue analysis

The eigenfrequencies and the corresponding eigenmodes are usually solved by application of the classical eigenvalue problem [19]:

$$(\mu^2[M] + \mu[C] + [K]) \{\phi\} = 0 \quad \text{Eq. 2.13}$$

where $[M]$ is the mass matrix, which is symmetric and positive definite; $[C]$ is the damping matrix; $[K]$ is the stiffness matrix, which may include large displacement effects, such as “stress stiffening”, and, therefore, may not be positive definite or symmetric; μ is the eigenvalue; and $\{\phi\}$ is the eigenvector, which represents the mode of vibration [19].

The eigensystem represented by Eq. 2.13 in general will have complex eigenvalues and eigenvectors. This system can be symmetrized by assuming that $[K]$ is symmetric and by neglecting $[C]$ during eigenvalue extraction. The symmetrized system only has real squared eigenvalues, μ^2 and real eigenvectors.

For symmetric eigenvalue problems, it is also assumed that $[K]$ is positive semidefinite. In this case μ becomes an imaginary eigenvalue, $\mu=i\omega$, where ω is the circular frequency and the eigenvalue problem can be written as

$$(-\omega^2[M] + [K]) \{\phi\} = 0. \quad \text{Eq. 2.14}$$



3 ANALYSIS TOOLS

3.1 HydroD – Wadam analysis

The panel model of the waterborne pontoon, modelled in Genie by Abdillah Suyuthi, was analysed in HydroD for calculating the added mass and hydrodynamic damping coefficient. See Figure 17. These hydrodynamic frequency dependent effects can be explained as the effects caused by the interaction of the oscillating impenetrable pontoons with the surrounding liquid medium.

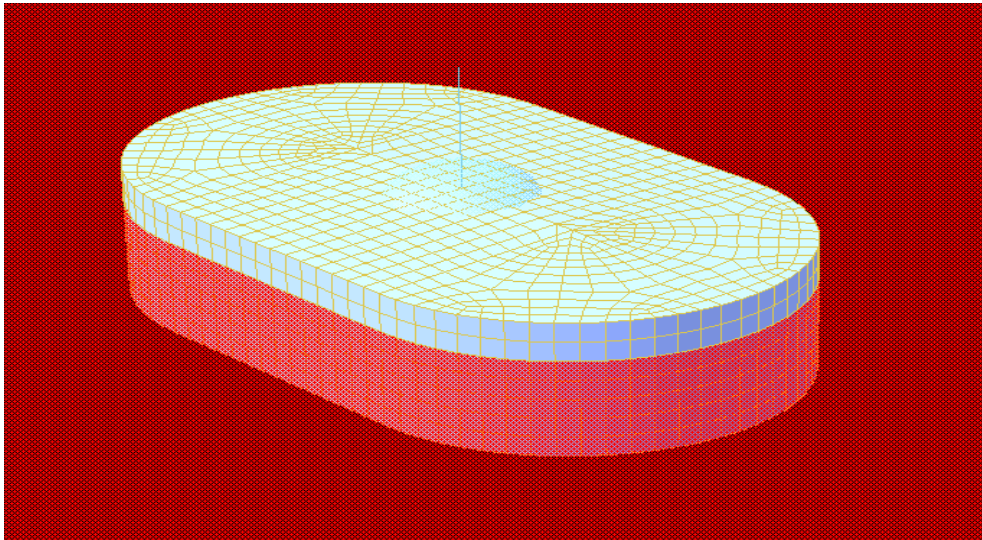


Figure 17: Panel model of pontoon in HydroD

As the pontoons oscillate, waves are generated which are forced around the geometry and results in dynamic pressure. This pressure depends on the acceleration of the geometry and therefore creates a frequency dependent problem [20].

The frequency independent effects like the pontoon's mass and hydrostatic stiffness coefficient were also acquired from HydroD. The amplitude of wave excitation force, which is a function of both wave frequency and wave direction, was also obtained from the Wadam analysis.

The Wadam analysis results were implemented for the construction as well as the analysis of the bridge models in Abaqus. Although the Bergsøysundet floating bridge has two sets of pontoons, test results of this pontoon have been used to represent the other pontoons of that bridge model.

3.2 Abaqus CAE

The most employed software in this thesis was Abaqus CAE, which is finite element modelling software. Eigenfrequency, static and time domain dynamic analyses were carried out using this software.

3.2.1 Eigenvalue extraction

The eigenvalue problem is solved by Lanczos Eigen Solver in Abaqus. The solver is an extended version of the Inverse Power Method, where blocks of frequencies are evaluated incrementally [19].

$$[M]([K] - \sigma[M]^{-1})[M]\{\phi\} = \theta[M]\{\phi\} \quad \text{Eq. 3.1}$$

where σ is a converging shift and θ is the eigenvalue. A new shift is formed after each convergence. Results from the analysis are transformed to frequencies as shown below

$$\omega^2 = \frac{1}{\theta} + \sigma \quad \text{Eq. 3.2}$$

3.2.2 Implicit dynamic analysis

For the time domain analysis, dynamic implicit method was used with a time step of 0.25 seconds. The theory presented here is from the Abaqus manual [19].

The equation of virtual work with the d'Alembert's part included is given by

$$\int_V \mathbf{f} \delta \mathbf{v} dV = \int_V \mathbf{F} \cdot \delta \mathbf{v} dV - \int_V \rho \ddot{\mathbf{u}} \cdot \delta \mathbf{v} dV \quad \text{Eq. 3.3}$$

where ρ is the material density, \mathbf{u} is the displacement, \mathbf{F} is the external body force and \mathbf{f} is the body force at a point.

The d'Alembert's term is more effectively described in terms of reference volume and reference density as

$$\int_{V_0} \rho_0 \ddot{\mathbf{u}} \cdot \delta \mathbf{v} dV_0 \quad \text{Eq. 3.4}$$

The finite element approximation of the integrals to equilibrium, as utilised by Abaqus, is given by

$$M^{NM} \ddot{\mathbf{u}}^M + I^N - P^N = 0 \quad \text{Eq. 3.5}$$

where M^{NM} is the consistent mass matrix, I^N is the internal force vector and P^N is the external force vector.

The balance of d'Alembert's forces weighted average of static forces is given by

$$M^{NM}\ddot{u}^M|_{t+\Delta t} + (1 + \alpha)(I^N|_{t+\Delta t} - P^N|_{t+\Delta t}) - \alpha(I^N|_t - P^N|_t) + L^N|_{t+\Delta t} = 0 \quad \text{Eq. 3.6}$$

where $L^N|_{t+\Delta t}$ is the sum of the Lagrange multiplier forces associated with degrees of freedom N . The Newmark formula is used for displacement and velocity integration

$$u|_{t+\Delta t} = u|_t + \Delta t \dot{u}|_t + \Delta t^2((1/2 - \beta)\ddot{u}|_t + \beta\ddot{u}|_{t+\Delta t}) \quad \text{Eq. 3.7}$$

$$\dot{u}|_{t+\Delta t} = \dot{u}|_t + \Delta t((1 - \gamma)\ddot{u}|_t + \gamma\ddot{u}|_{t+\Delta t}) \quad \text{Eq. 3.8}$$

where

$$\beta = \frac{1}{4}(1 - \alpha)^2, \quad \gamma = \frac{1}{2} - \alpha \quad \text{and} \quad -\frac{1}{3} \leq \alpha \leq 0. \quad \text{Eq. 3.9}$$

In the automatic time increment method, some noise might occur if no damping ($\alpha = 0$) is used. Numerical damping values around -0.05 ($\alpha = -0.05$) will effectively remove this noise as well as keep the low frequency responses, which are of interest, unaffected.

The half-step residual method finds the residual error in Eq. 3.5 at time step $t+\Delta t/2$. Linearly varying accelerations are assumed, which gives

$$\ddot{u}|_\tau = (1 - \tau)\ddot{u}|_t + \tau\ddot{u}|_{t+\Delta t}, \quad 0 \leq \tau \leq 1 \quad \text{Eq. 3.10}$$

Since $t+\Delta t$ is already solved for, the current step must fulfil the following

$$-\Delta u|_t = \tau^3 \Delta u|_{t+\Delta t} + \tau(1 - \tau^2)\Delta t \dot{u}|_t + \tau^2(1 - \tau)\frac{\Delta t^2}{2}\ddot{u}|_t \quad \text{Eq. 3.11}$$

$$\dot{u}|_\tau = \frac{\gamma}{\beta\tau\Delta t}\Delta u|_\tau + (1 - \gamma/\beta)\dot{u}|_t(1 - \frac{\gamma}{2\beta})\tau\Delta t\ddot{u}|_t$$

and

$$\ddot{u}|_\tau = \frac{1}{\beta\tau^2\Delta t^2}\Delta u|_\tau - \frac{1}{\beta\tau\Delta t}\dot{u}|_t + (1 - \frac{1}{2\beta})\ddot{u}|_t$$

The equilibrium residual magnitude can be obtained at any instance within a time step. The residual at the half time step is obtained by combining Eq. 3.5 and Eq. 3.11

$$R^N|_{t+\Delta t/2} \stackrel{def}{=} M^{NM}\ddot{u}^M|_{t+\Delta t/2} + (1 + \alpha)(I^N|_{t+\Delta t/2} - P^N|_{t+\Delta t/2}) - \alpha(I^N|_t - P^N|_t) + L^N|_{t+\Delta t/2} \quad \text{Eq. 3.12}$$

$$-P^N|_{t+\Delta t/2} - \frac{1}{2}\alpha(I^N|_t - P^N|_t + I^N|_{t-} - P^N|_{t-}) + L^N|_{t+\Delta t/2}$$

where $R^N|_{t+\Delta t/2}$ is set to a suitable part of the forces that are acting in the dynamic system.



4 BRIDGE MODELS IN ABAQUS

In this thesis, four simplified bridge models were constructed and analysed. These are:

1. Actual curve bridge model - Bergsøysund Bridge
2. Straight bridge model
3. Elongated straight bridge model
4. Elongated curve bridge model

Along with the calculated parameters from the hydrodynamic analysis, Abdillah Suyuthi's calculated figures of the bridge components' mass and section properties were implemented as part of the construction of the bridge models in Abaqus. These can be found in Appendix A.

4.1 Curve bridge model - Bergsøysund Bridge

The Bergsøysund Bridge has a radius of curvature of 1300 m and a length of 845 m, with a steel pipe truss superstructure. Located at a water depth of 320 m, it rests on seven concrete pontoon foundations. A simplified beam model of this bridge was built in Abaqus.

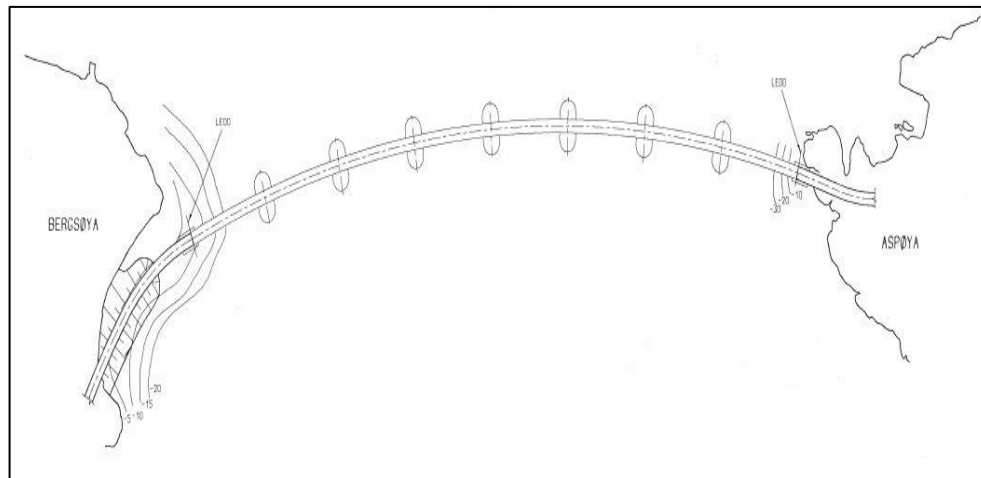


Figure 18: Sketch of the Bergsøysund Bridge

The arc of the bridge consisting of the truss-work was modelled using two node linear beam elements – B31. Details of this element can be found in the Abaqus documentation [19] and therefore has not been discussed in this study.

The position of the pontoons was denoted by point masses, which were connected to the truss-work by vertical cylindrical sections, modelled with rigid beam elements. Equivalent cross-section properties of the truss-work and the vertical connections were applied. The hydrodynamic damping and hydrostatic stiffness were incorporated in the model in terms of dashpots and springs respectively, at the pontoons.

The boundary condition applied at the bridge ends was such that the bridge is a simply supported beam in the vertical plane, but a fixed beam in the horizontal plane.

Similarly, the rest of the models were constructed in Abaqus.

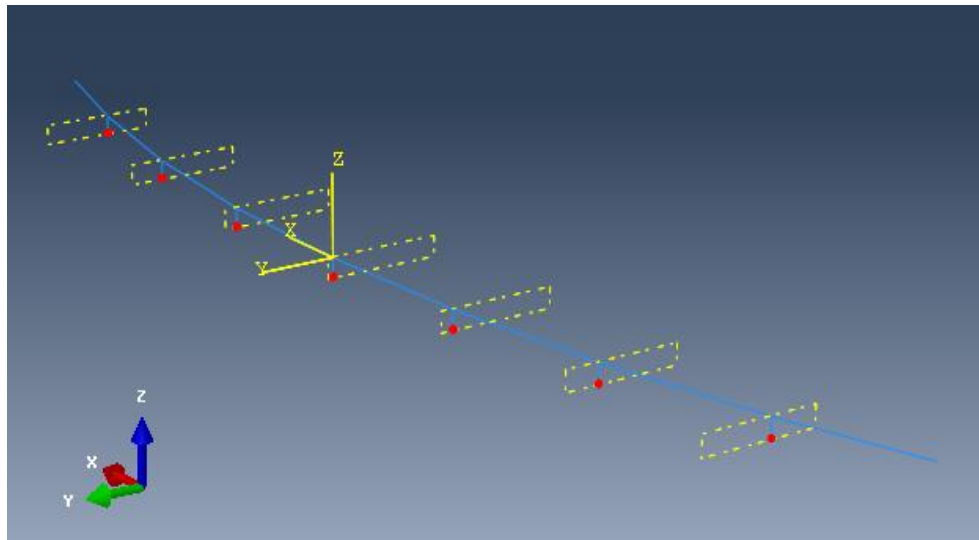


Figure 19: Model of Bergsøysund Bridge in Abaqus

4.2 Straight bridge model

In the simplified version of the Bergsøysund Bridge, the arc of the bridge was replaced by a straight truss-work model, as illustrated in Figure 20. The length of the straight bridge is 795.42 m, equal to the chord length of the curve bridge. The pontoons were positioned at an average distance of 105.33 m.

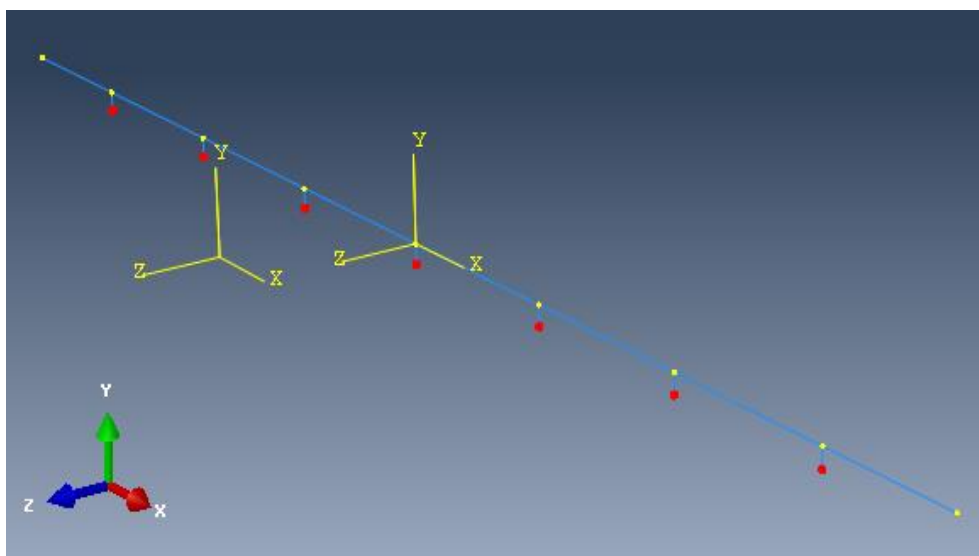


Figure 20: Straight bridge model in Abaqus

4.3 Elongated straight bridge model

The straight bridge model was elongated to twice its length, to 1600 m, with 15 pontoons. See Figure 21. The spacing between the pontoons was kept equal to the original spacing of 105.33 m.

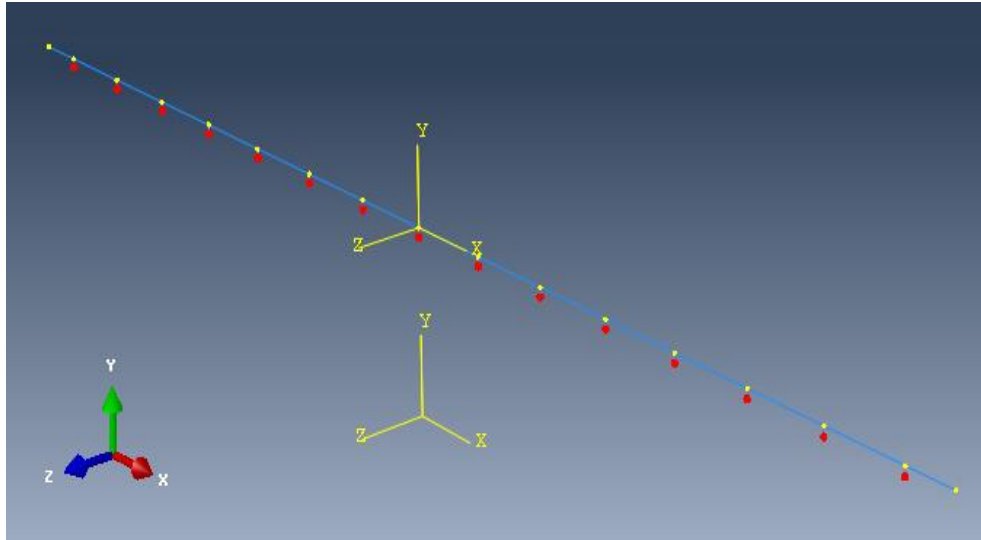


Figure 21: Elongated straight bridge model in Abaqus

4.4 Elongated curve bridge model

By keeping the radius of curvature equal to 1300 m, the elongated curve bridge model was constructed for a chord length of 1600 m with 15 pontoons, as shown in Figure 22. The pontoons were parallel positioned at 105.33 m interval.

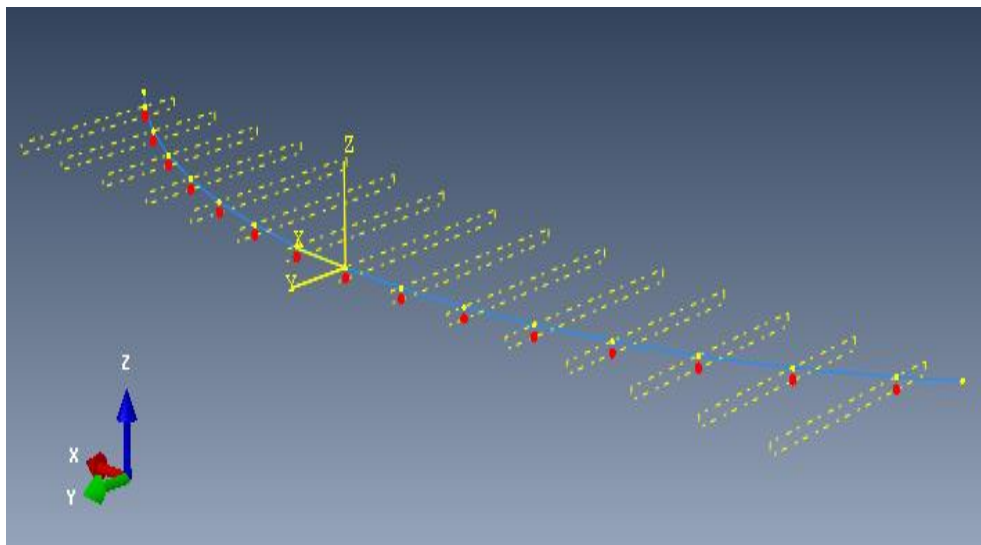


Figure 22: Elongated curve bridge model in Abaqus



4.5 Elongated bridge models with sideway mooring lines

Long floating bridges are influenced by lateral forces like waves, currents and winds. As a result, sideway mooring line of stiffness 3 MN/m [21] was applied at each pontoon position for the elongated models. The mooring lines were modelled in the form of lateral springs. The sideway mooring lines would provide the nonlinear horizontal support for the bridges under transverse wave loading [21].

All the analyses of the elongated bridge models were performed with and without sideway mooring lines.

5 EIGENFREQUENCY ANALYSIS

For each of the bridge models, the first ten eigenfrequencies were obtained using Abaqus. The added mass applied was updated by iteration in order to find the actual added mass corresponding to the first eigenfrequency. The final value of the added mass was then utilized in order to obtain the rest of the frequencies.

5.1 Curve bridge model

Table 2: Iteration of added mass for first sway eigenmode

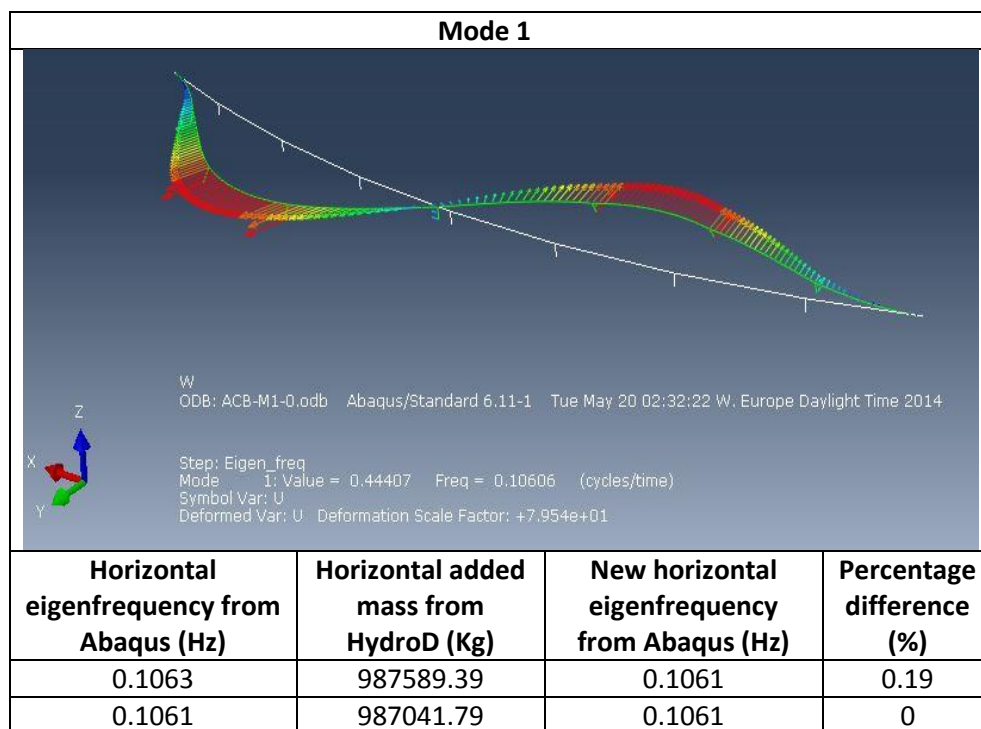


Table 3: Eigenfrequencies of the curve bridge model

Eigenmode No.	Eigenfrequency (Hz)
1	0.1061
2	0.1332
3	0.1762
4	0.1904
5	0.1924
6	0.2555
7	0.2778
8	0.2929
9	0.3296
10	0.3613

5.2 Straight bridge model

Table 4: Iteration of added mass for first sway eigenmode

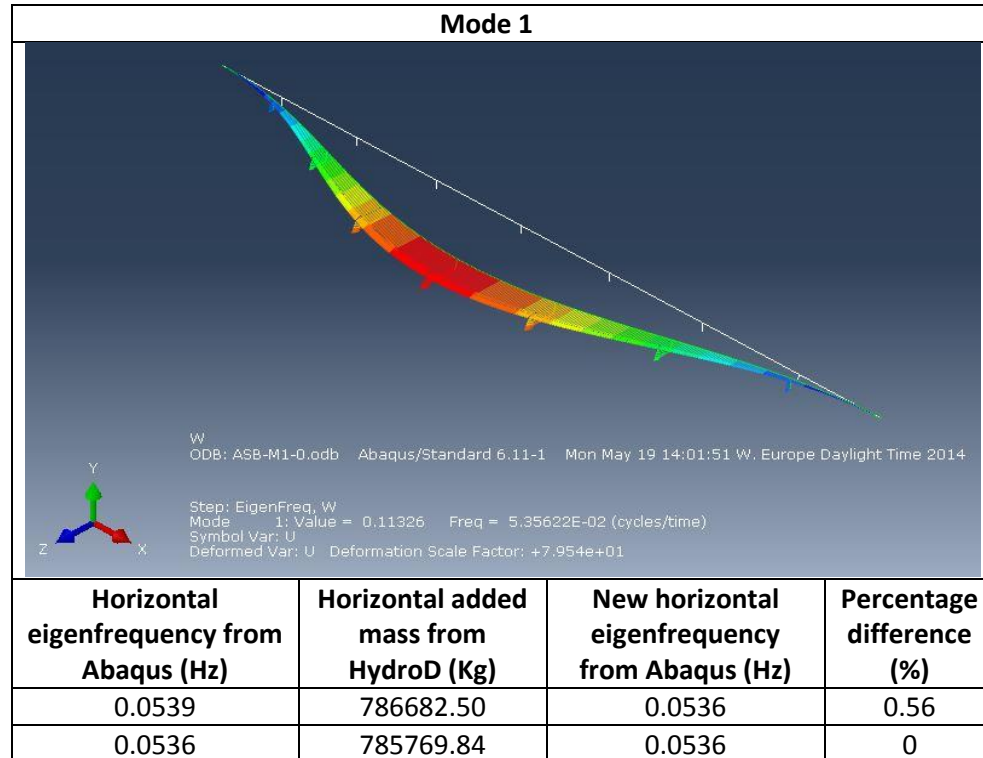


Table 5: Eigenfrequencies of the straight bridge model

Eigenmode No.	Eigenfrequency (Hz)
1	0.0536
2	0.1354
3	0.1797
4	0.1923
5	0.1932
6	0.2427
7	0.2433
8	0.2962
9	0.3395
10	0.3555

5.3 Elongated straight bridge model

Table 6: Iteration of added mass for first sway eigenmode

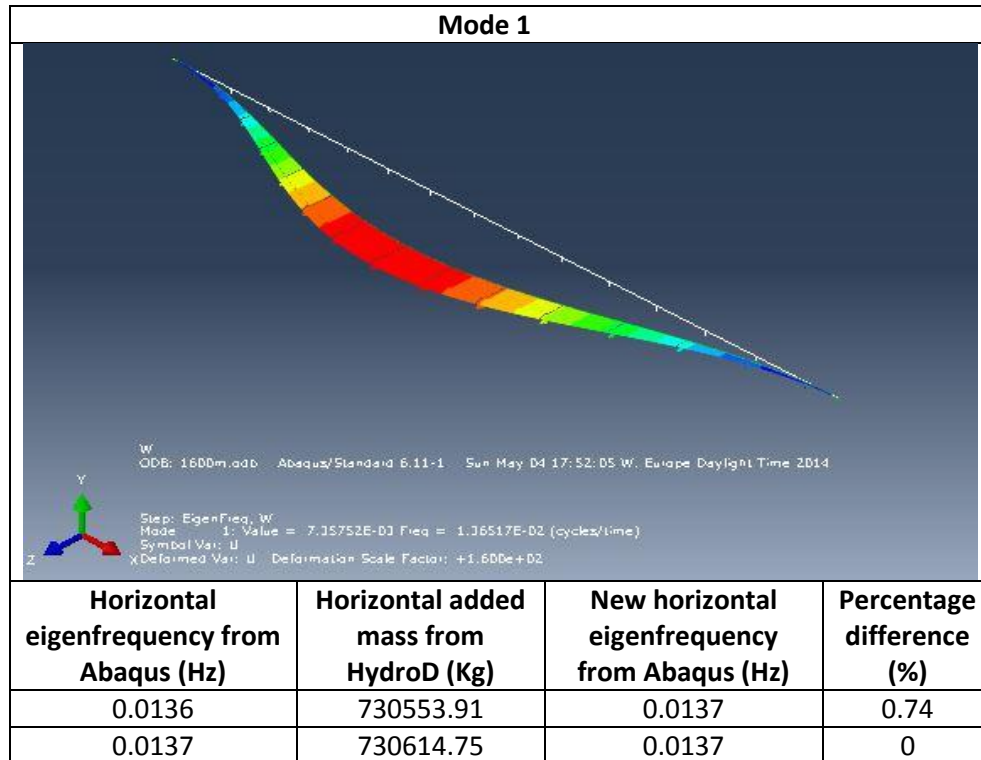


Table 7: Eigenfrequencies of the elongated straight bridge

Eigenmode No.	Eigenfrequency (Hz)
1	0.0137
2	0.0364
3	0.0695
4	0.1113
5	0.1533
6	0.1620
7	0.1799
8	0.1807
9	0.1845
10	0.1926

5.4 Elongated straight bridge model with mooring

Table 8: Iteration of added mass for first sway eigenmode

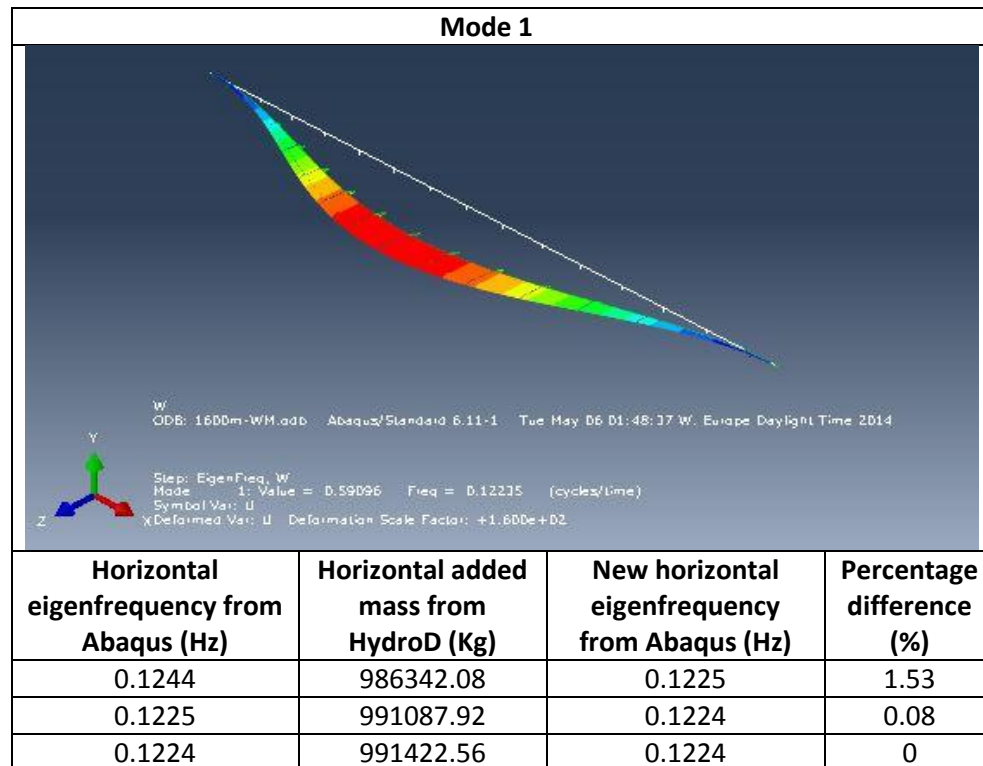


Table 9: Eigenfrequencies of the elongated straight bridge with mooring

Eigenmode No.	Eigenfrequency (Hz)
1	0.1224
2	0.1287
3	0.1419
4	0.1585
5	0.1655
6	0.1751
7	0.1759
8	0.1795
9	0.1890
10	0.1958

5.5 Elongated curve bridge model

Table 10: Iteration of added mass for first sway eigenmode

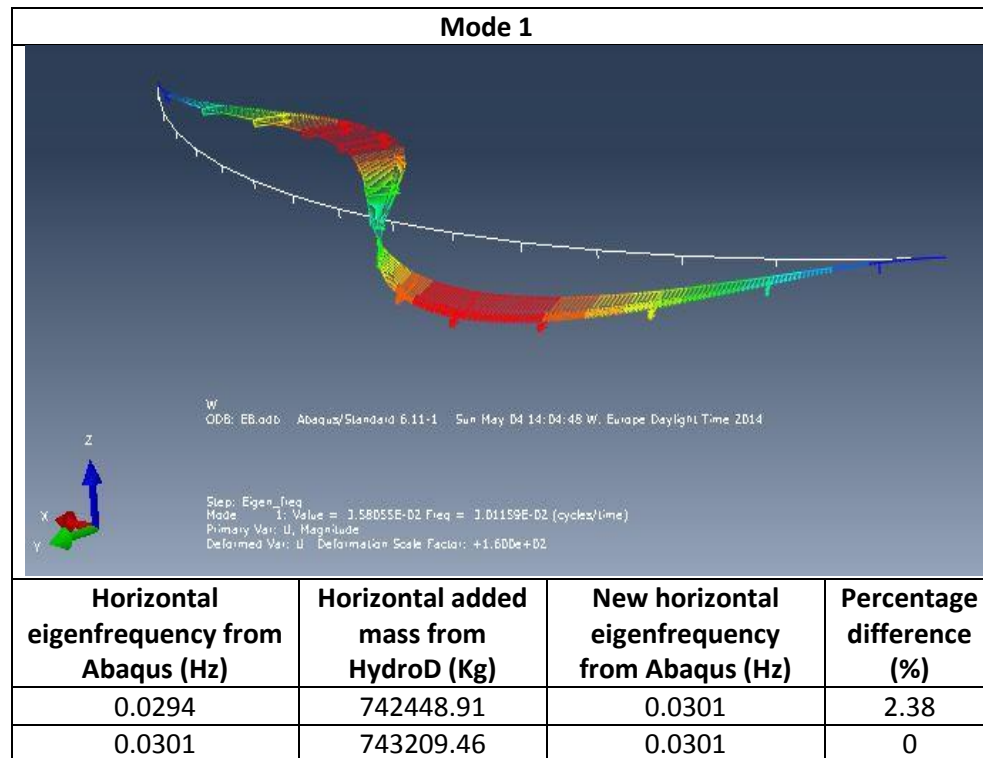


Table 11: Eigenfrequencies of the elongated curve bridge

Eigenmode No.	Eigenfrequency (Hz)
1	0.0301
2	0.0545
3	0.0980
4	0.1229
5	0.1459
6	0.1793
7	0.1794
8	0.1820
9	0.1892
10	0.1916

5.6 Elongated curve bridge model with mooring

Table 12: Iteration of added mass for first sway eigenmode

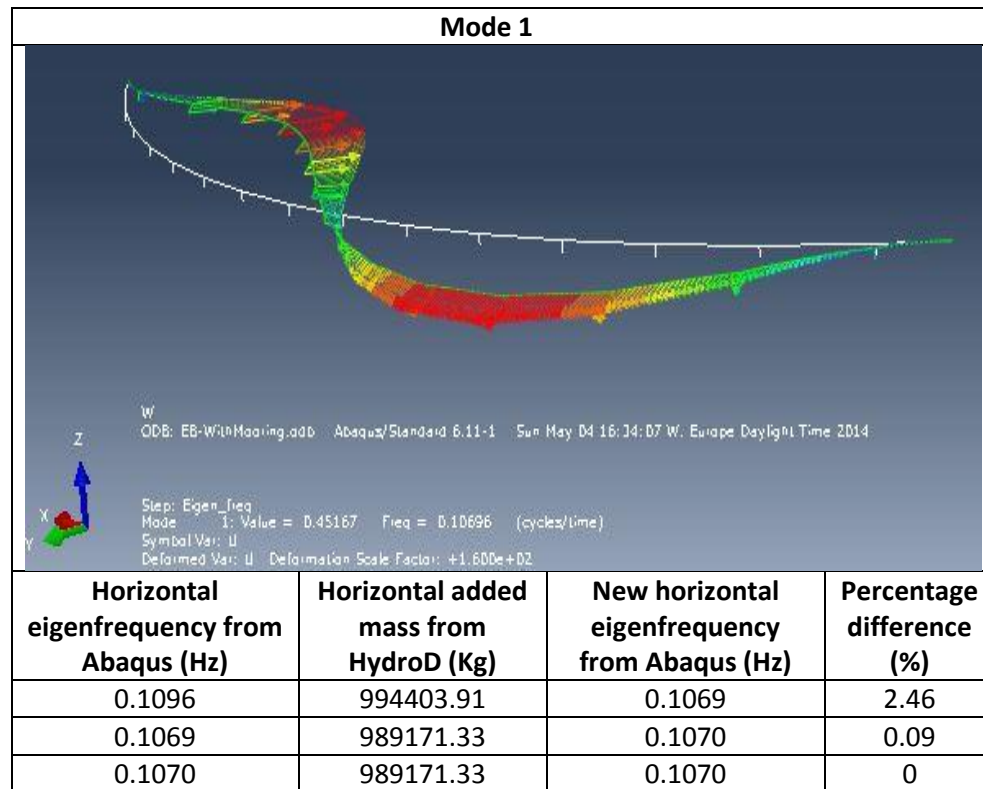


Table 13: Eigenfrequencies of the elongated curve bridge with mooring

Eigenmode No.	Eigenfrequency (Hz)
1	0.1070
2	0.1282
3	0.1497
4	0.1610
5	0.1748
6	0.1750
7	0.1775
8	0.1798
9	0.1847
10	0.1997

6 STATIC RESPONSE

Static analysis was carried out for the lateral drag force, computed by Morison's equation, corresponding to currents of 1 m/s. The longitudinal section of the pontoon is shown in Figure 23.

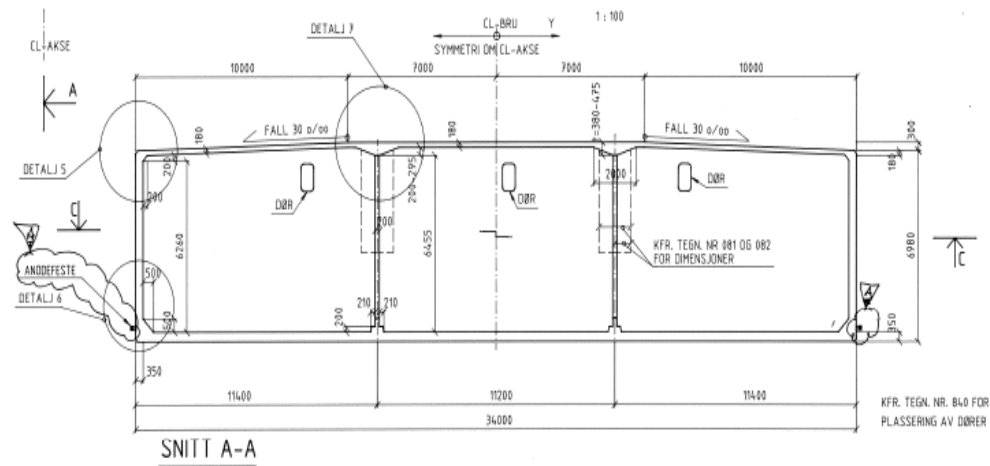


Figure 23: Longitudinal section area of the pontoon

$$F_d = 0.5 \times \rho \times C_d \times A \times v^2 \quad \text{Eq. 6.1}$$

where F_d is the horizontal drag force; ρ is the density of sea water; C_d is the drag coefficient; A is the cross-sectional area of the body perpendicular to the flow direction; and v is the velocity of the current.

For a draft of 5 m, A is rectangular. Therefore, C_d is taken as 2.1 [22].

$$F_d = 0.5 \times 1025 \times 2.1 \times (34 \times 5) \times 1^2$$

$$\therefore F_d = 182962.5\text{N}$$

For this sway (lateral) load, the static displacement and bending moment distribution along the models were determined in Abaqus.



6.1 Curve bridge model

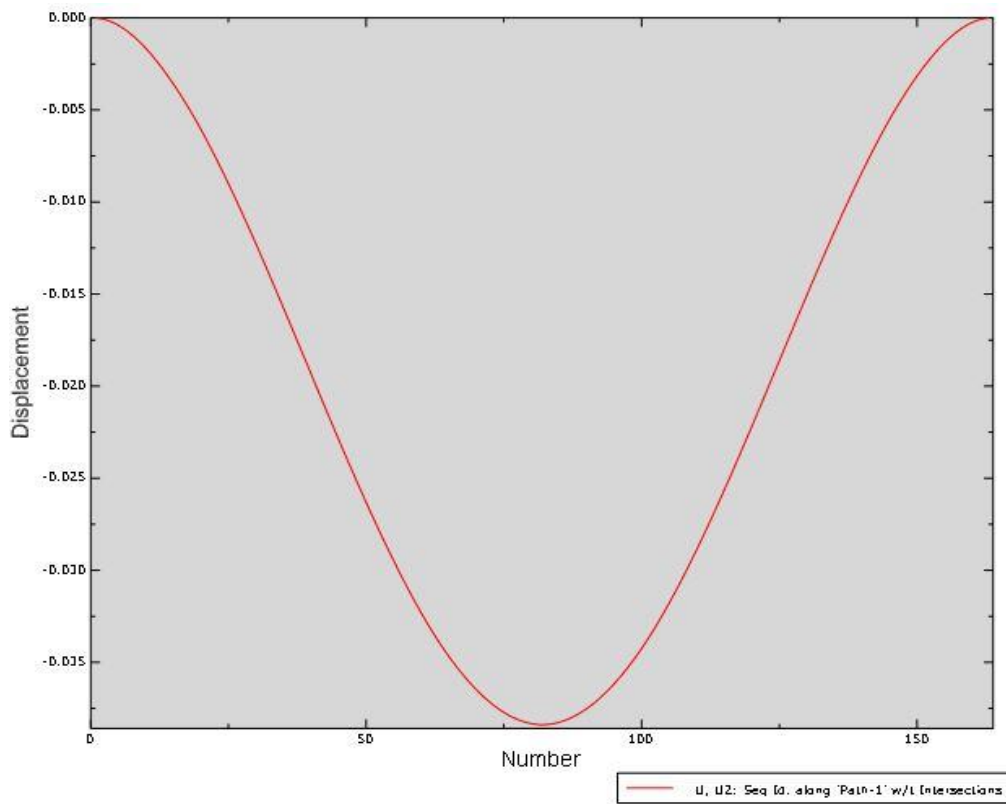


Figure 24: Static displacement along the curve bridge model

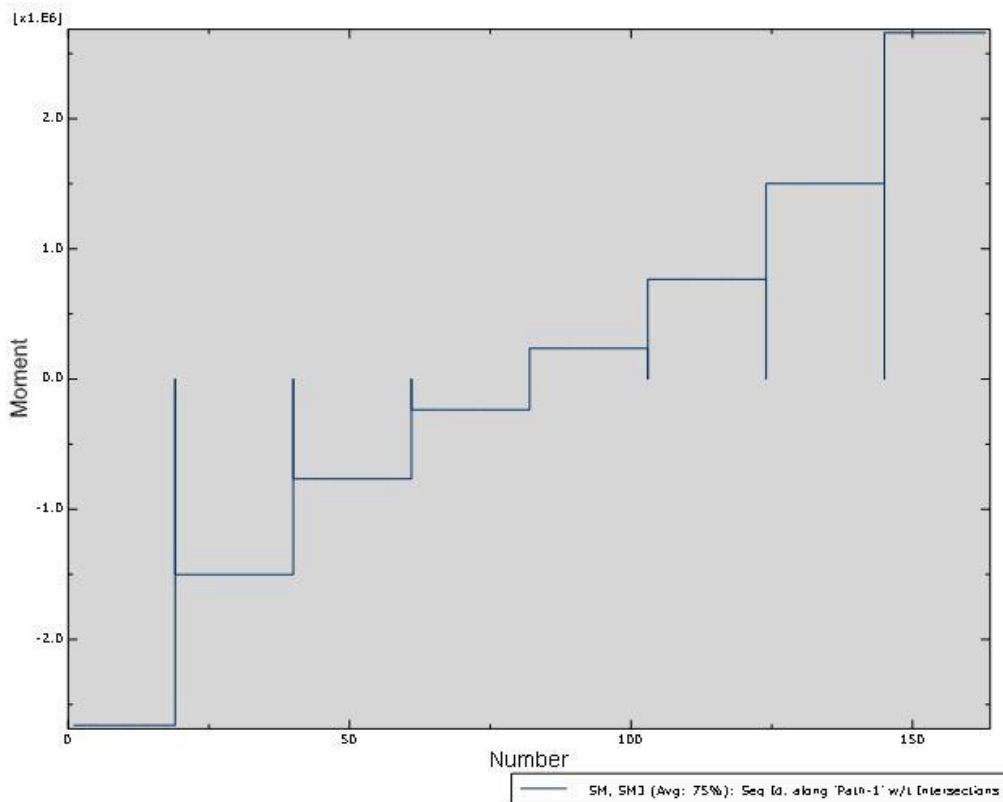


Figure 25: Static bending moment along the curve bridge model



6.2 Straight bridge model

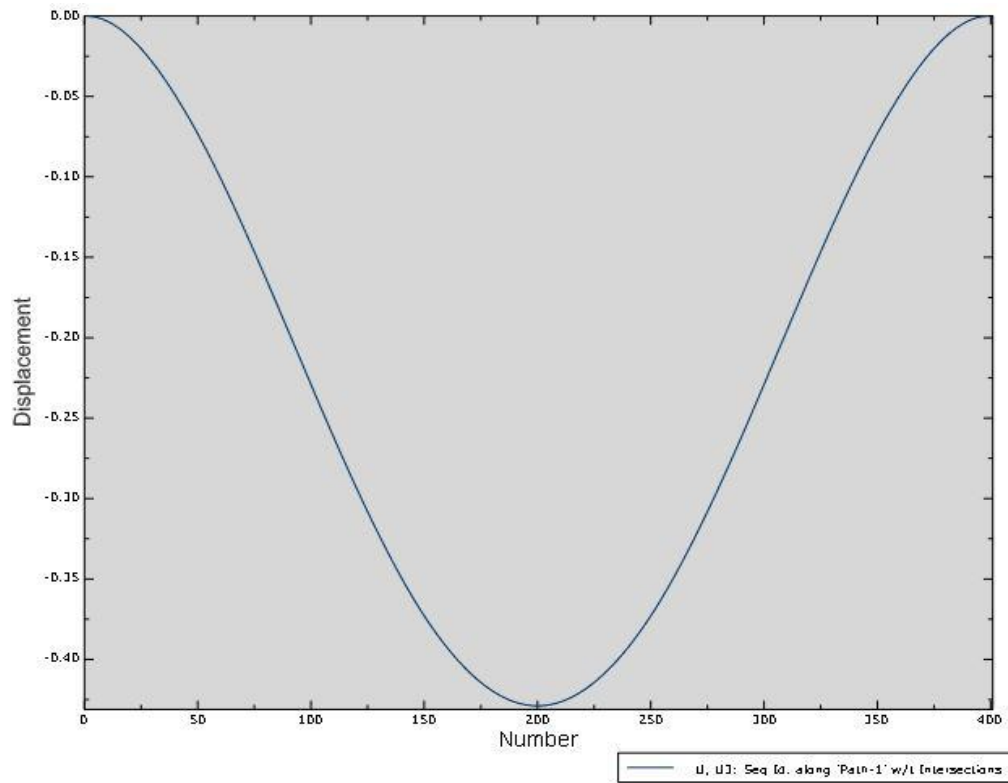


Figure 26: Static displacement along the straight bridge model

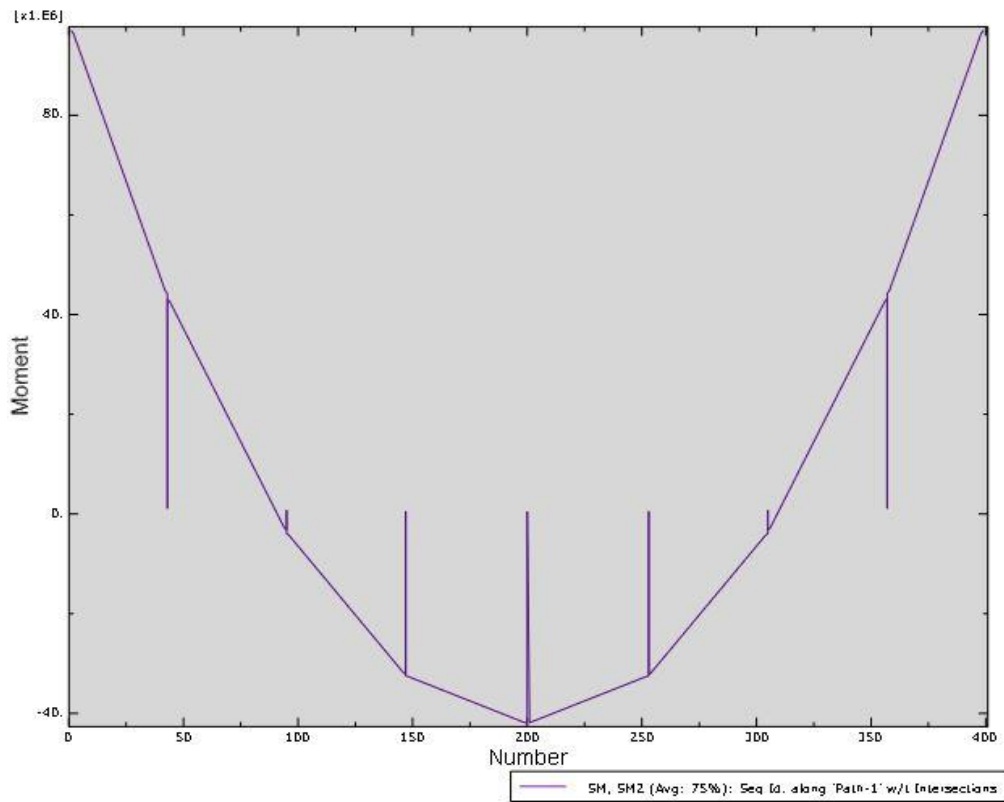


Figure 27: Static bending moment along the straight bridge model

6.3 Elongated straight bridge model

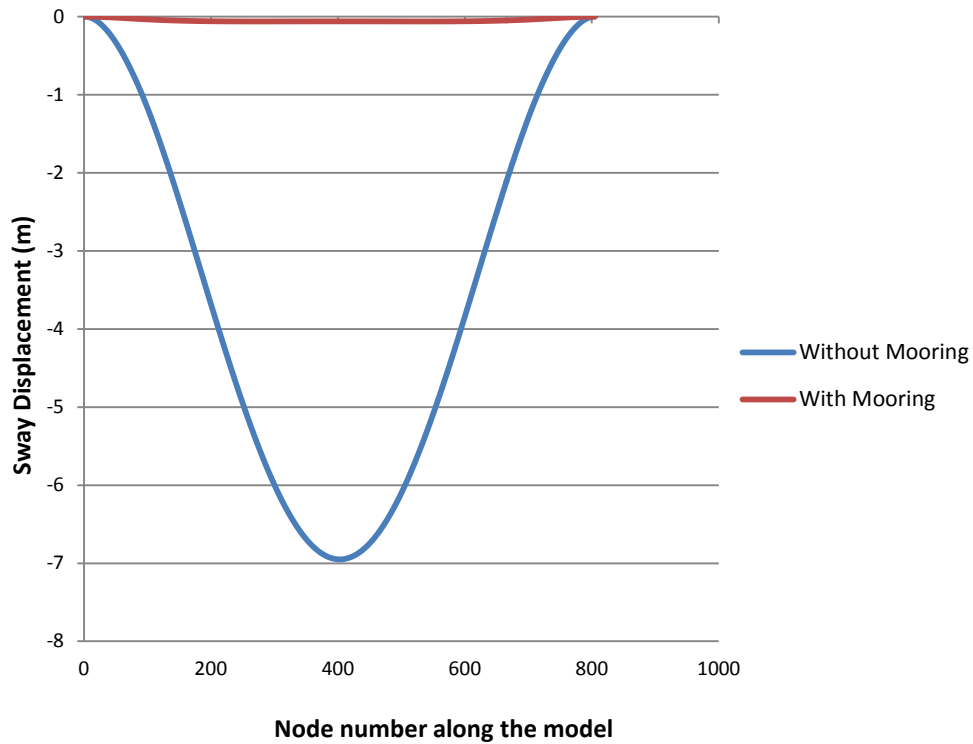


Figure 28: Static displacement along the elongated straight bridge model

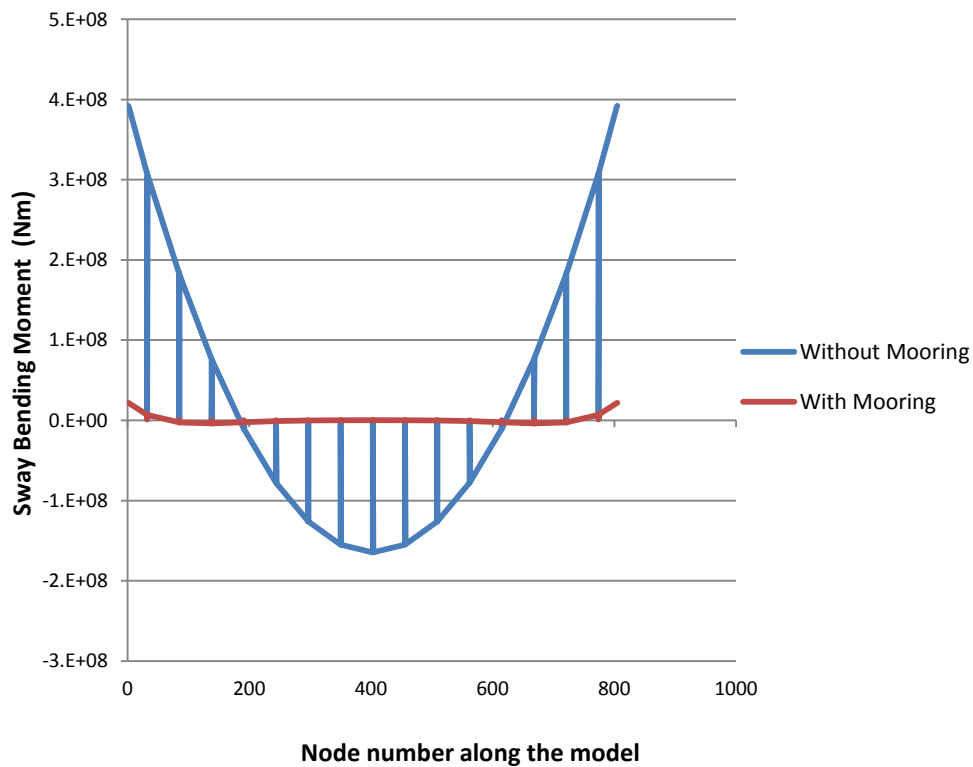


Figure 29: Static bending moment along the elongated straight bridge model

6.4 Elongated curve bridge model

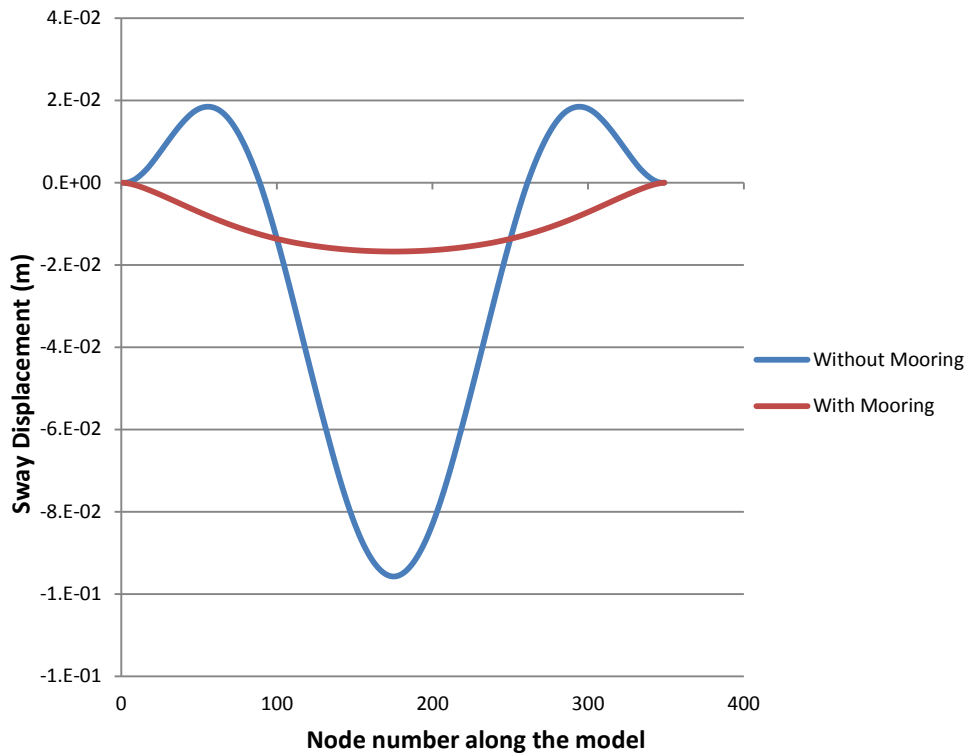


Figure 30: Static displacement along the elongated curve bridge model

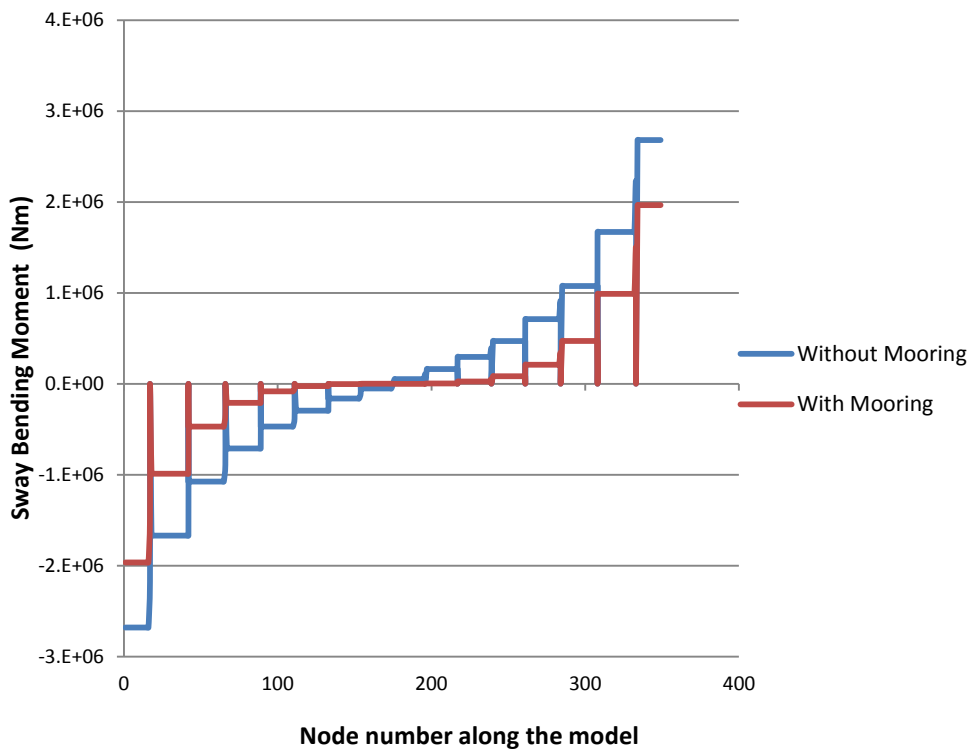


Figure 31: Static bending moment along the elongated curve bridge model



7 DYNAMIC RESPONSE

Dynamic analysis of all the models was carried out in Abaqus. The models were subjected to harmonic wave loads corresponding to their first horizontal and vertical eigenfrequencies. The sway and heave responses of the models were mainly studied. In each case, the phase difference of loading at each pontoon was considered. All analyses were performed for a wave heading of 0 deg. as well as for the estimated critical angle of each mode.

7.1 Calculation of critical angles

As suggested by Professor Bernt J. Leira, the critical angle of wave direction was calculated by employing a technique of superposition of the respective mode shape with half wavelength.

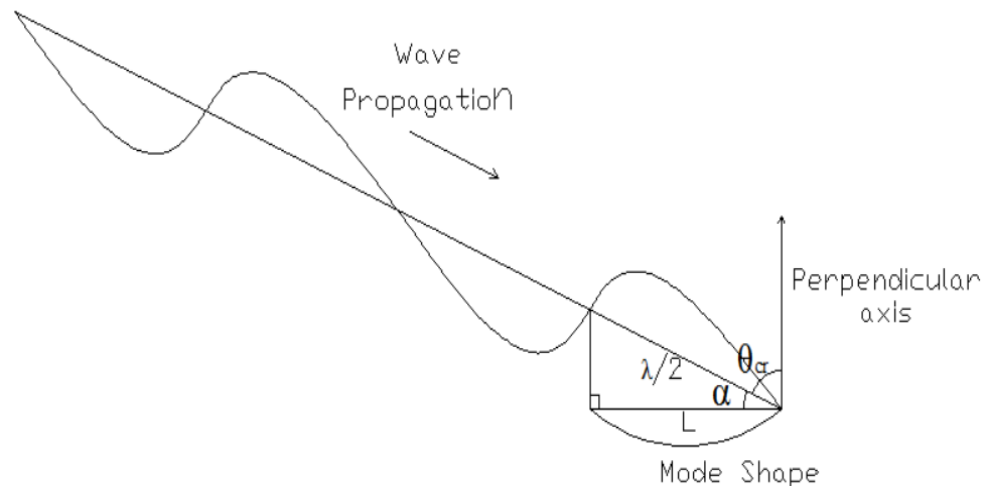


Figure 32: Concept diagram for calculation of critical angle of wave direction

$$\alpha = \cos^{-1} \left(\frac{L/p}{\lambda/2} \right) \quad \text{Eq. 7.1}$$

where L is a model's length; p is the number of peaks and troughs of a given mode shape along L; λ is the wavelength; and θ_{cr} is the critical angle of wave heading. In this thesis, the wavelength was approximated by the formula

$$\lambda = 1.56 \times T^2 \quad \text{Eq. 7.2}$$

where T is the period of the wave. The critical angle is obtained by

$$\theta_{cr} = 90 - \alpha \quad \text{Eq. 7.3}$$

For certain mode frequencies,

$$\cos \alpha = \left(\frac{L/p}{\lambda/2} \right) > 1$$

For such cases, the following formula was applied

$$\cos \alpha = \left(\frac{L/p}{n \times \lambda/2} \right) \quad \text{Eq. 7.4}$$

where n is the smallest possible odd-valued integer which gives a solution.

7.2 Calculation of phase angles

Phase difference arises at each pontoon due to the combined effect of changing wave direction and shapes of the models. Phase difference exists for the curve bridge models, even for a head on wave. For any other direction of the wave, phase difference also arises in the straight bridge models.

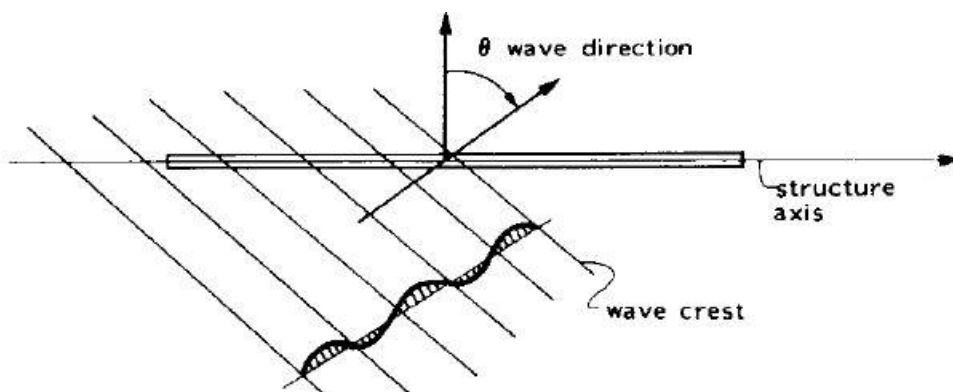


Figure 33: Wave heading in straight bridge model [23]

7.2.1 Phase angles of curve bridge model

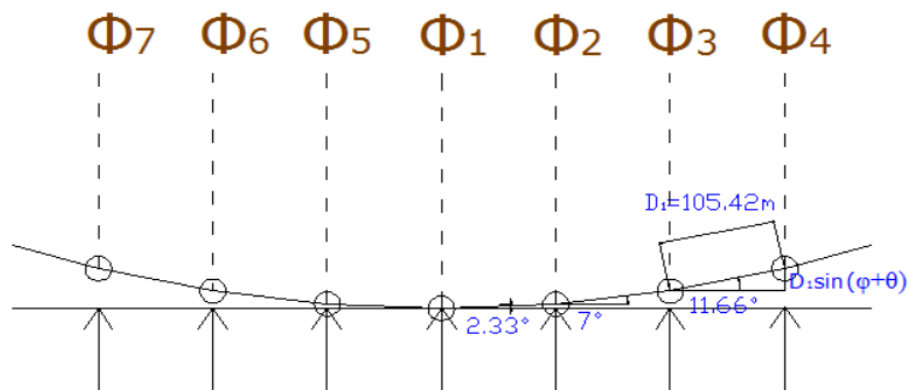


Figure 34: Concept diagram for calculation of phase angles of curve bridge model

For a wave direction of θ deg. and eigenperiod T,

$$\Phi_1 = 0 \quad \text{Eq. 7.5}$$

$$\Phi_2 = \Phi_1 + \left\{ \frac{2\pi}{\lambda} \times D_1 \times \sin(\varphi_1 + \theta) \times \frac{180}{\pi} \right\} \quad \text{Eq. 7.6}$$

$$\Phi_3 = \Phi_2 + \left\{ \frac{2\pi}{\lambda} \times D_1 \times \sin(\varphi_2 + \theta) \times \frac{180}{\pi} \right\} \quad \text{Eq. 7.7}$$

$$\Phi_4 = \Phi_3 + \left\{ \frac{2\pi}{\lambda} \times D_1 \times \sin(\varphi_3 + \theta) \times \frac{180}{\pi} \right\} \quad \text{Eq. 7.8}$$

$$\Phi_5 = \Phi_1 + \left\{ \frac{2\pi}{\lambda} \times D_1 \times \sin(\varphi_1 - \theta) \times \frac{180}{\pi} \right\} \quad \text{Eq. 7.9}$$

$$\Phi_6 = \Phi_5 + \left\{ \frac{2\pi}{\lambda} \times D_1 \times \sin(\varphi_2 - \theta) \times \frac{180}{\pi} \right\} \quad \text{Eq. 7.10}$$

$$\Phi_7 = \Phi_6 + \left\{ \frac{2\pi}{\lambda} \times D_1 \times \sin(\varphi_3 - \theta) \times \frac{180}{\pi} \right\} \quad \text{Eq. 7.11}$$

where D_1 is the shortest distance between the pontoons; Φ_i is the phase difference at pontoon no. i; and φ_i is the angle of curvature at pontoons no. i.

Likewise, for the elongated curve bridge model, the phase difference at each pontoon was found for a given wave direction and mode eigenperiod. The phase angles used for the curve bridge models can be seen in Appendix B.

7.2.2 Phase angles of straight bridge model

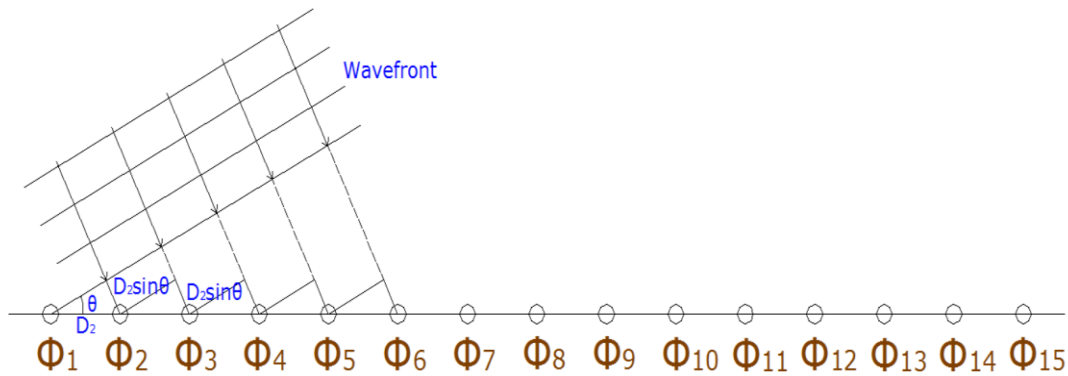


Figure 35: Concept diagram for calculation of phase angles of straight bridge models

For a wave direction of θ deg. and eigenperiod T,

$$\Phi_1 = 0 \quad \text{Eq. 7.12}$$

$$\Phi_2 = \Phi_1 + \left(\frac{2\pi}{\lambda} \times D_2 \times \sin \theta \times \frac{180}{\pi} \right) \quad \text{Eq. 7.13}$$

$$\Phi_3 = \Phi_2 + \left(\frac{2\pi}{\lambda} \times D_2 \times \sin \theta \times \frac{180}{\pi} \right) \quad \text{Eq. 7.14}$$

$$\Phi_4 = \Phi_3 + \left(\frac{2\pi}{\lambda} \times D_2 \times \sin \theta \times \frac{180}{\pi} \right) \quad \text{Eq. 7.15}$$

$$\Phi_5 = \Phi_4 + \left(\frac{2\pi}{\lambda} \times D_2 \times \sin \theta \times \frac{180}{\pi} \right) \quad \text{Eq. 7.16}$$

$$\Phi_6 = \Phi_5 + \left(\frac{2\pi}{\lambda} \times D_2 \times \sin \theta \times \frac{180}{\pi} \right) \quad \text{Eq. 7.17}$$

$$\Phi_7 = \Phi_6 + \left(\frac{2\pi}{\lambda} \times D_2 \times \sin \theta \times \frac{180}{\pi} \right) \quad \text{Eq. 7.18}$$

where D_2 is the distance between the pontoons. Similarly, for the elongated straight bridge model, the phase difference at each pontoon was calculated for a given wave direction and mode eigenperiod. The phase angles used for the straight bridge models can be seen in Appendix C.

7.3 Sway response

For a given model, the pontoons were exposed to a head on harmonic wave load of the same frequency as the sway mode. The corresponding sway force coefficient was calculated from the hydrodynamic analysis of the pontoon model in HydroD. The cosine component of the sway force coefficient was employed for different wave directions. The sway displacement and sway bending moment distribution along the models were evaluated at the time instant when maximum response took place.

Negatively damped sway responses were observed for all the models even after application of significant numerical damping ($\alpha = -1/3$), in addition to the lateral hydrodynamic damping force. As a consequence, artificial damper in the form of lateral dashpot was used at each pontoon. Iteration was carried out until stability was achieved at 1.3MN/m.

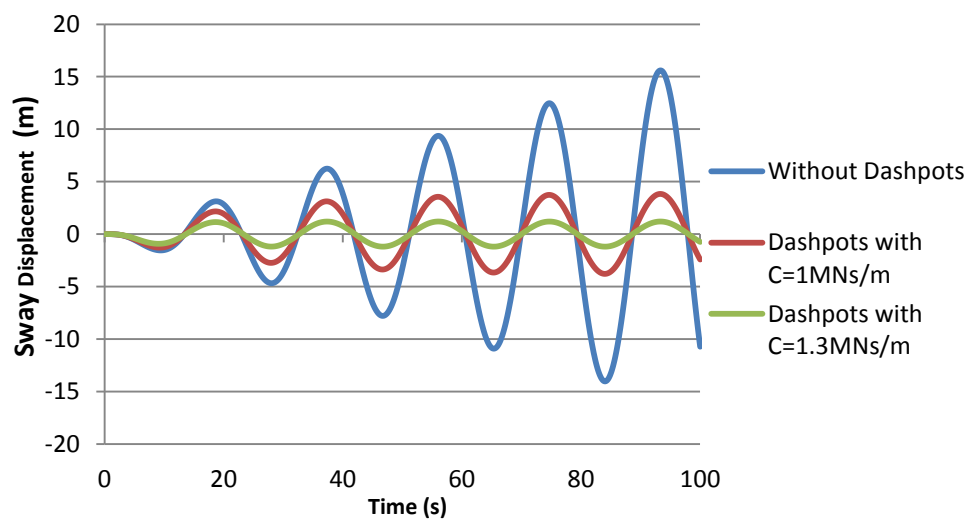


Figure 36: Sway displacement at a point of a model with lateral dashpots



7.3.1 Curve bridge model

$$F(t) = (-1325320 \cdot \cos\theta) \cdot \sin(0.6666t + \Phi_i) \quad \text{Eq. 7.19}$$

For $\theta = 0$ deg.

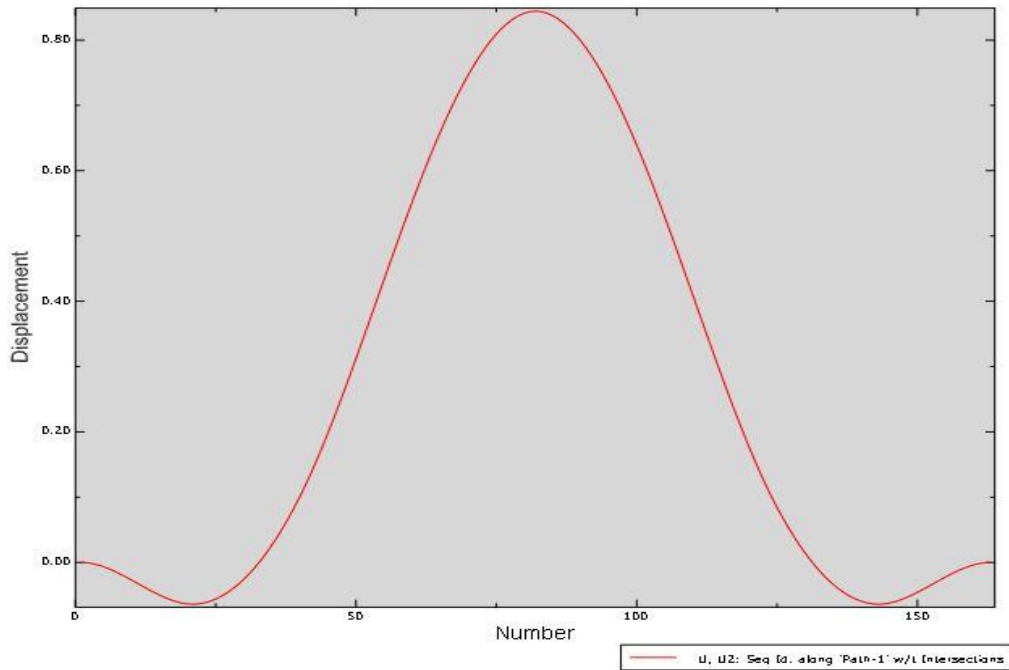


Figure 37: Sway displacement along the curve bridge model

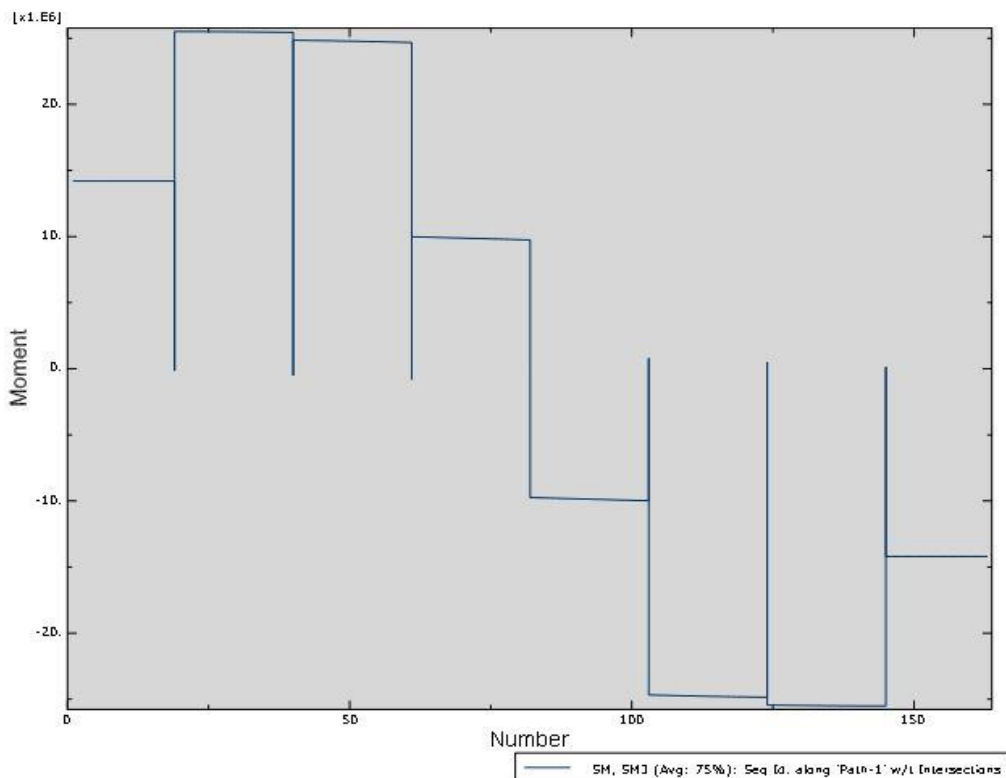


Figure 38: Sway bending moment along the curve bridge model



For $\theta_{cr} = 55.1$ deg.

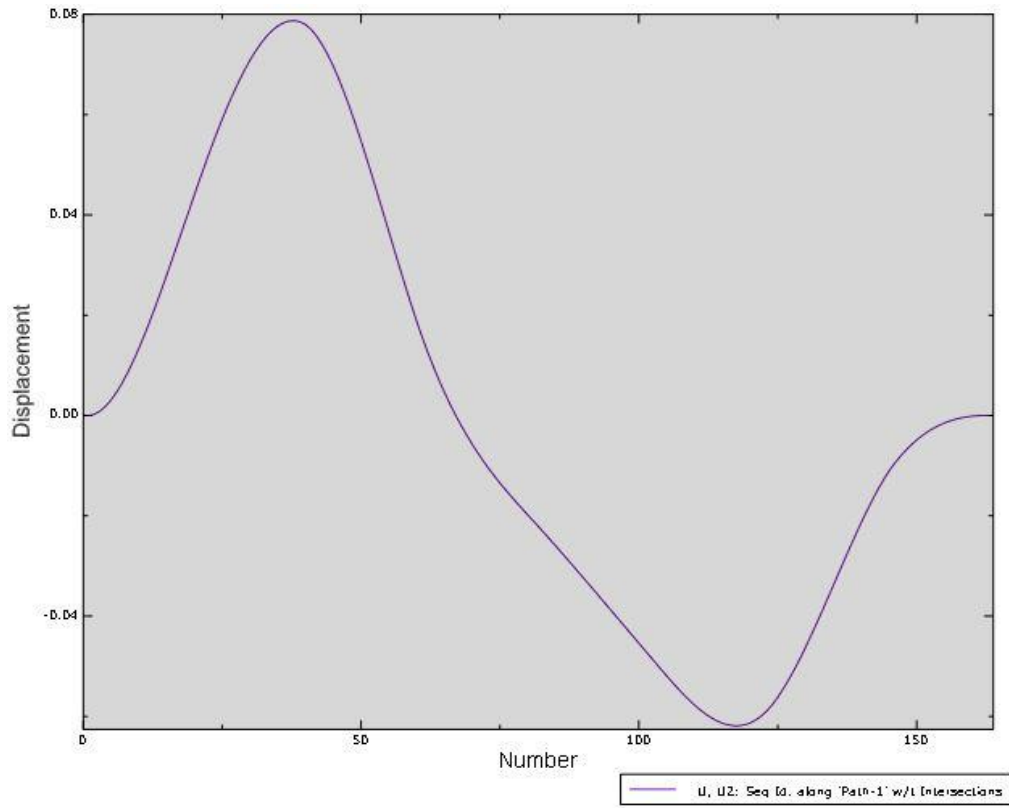


Figure 39: Sway displacement along the curve bridge model

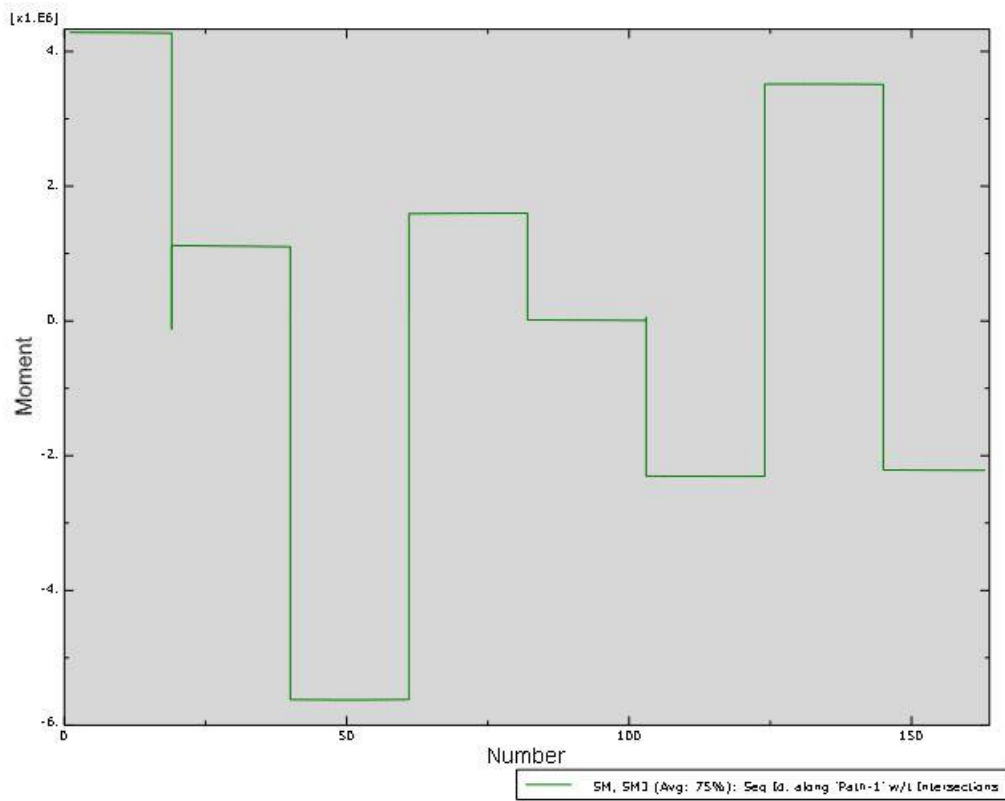


Figure 40: Sway bending moment along the curve bridge model



7.3.2 Straight bridge model

$$F(t) = (-413809 \cdot \cos\theta) \cdot \sin(0.3368t + \Phi_i) \quad \text{Eq. 7.20}$$

For $\theta = 0$ deg.

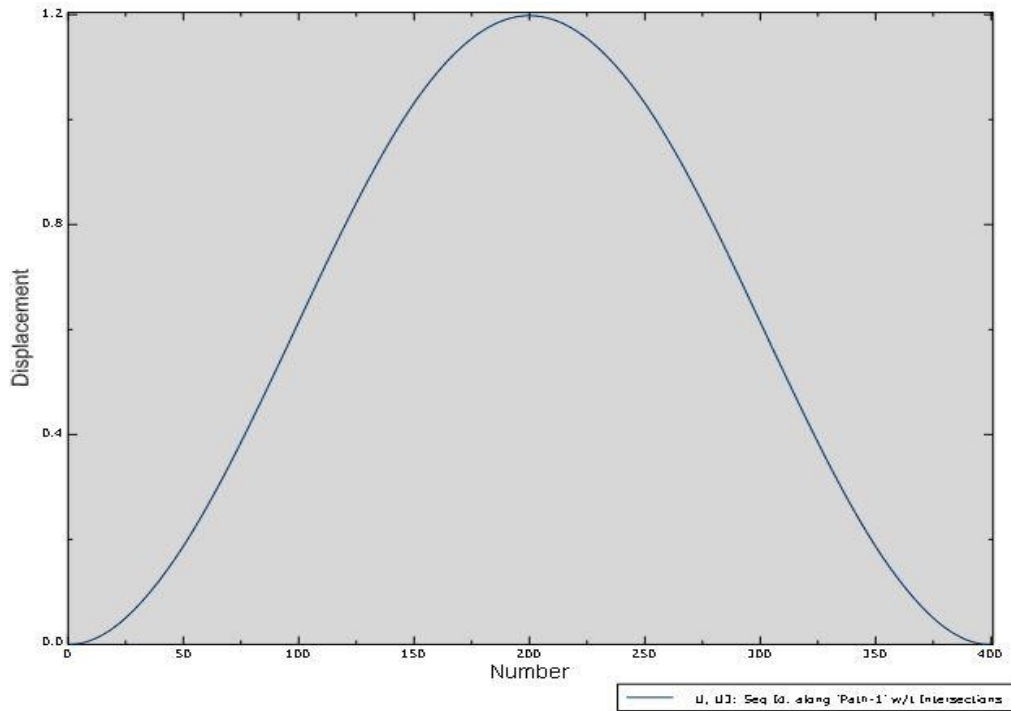


Figure 41: Sway displacement along the straight bridge model

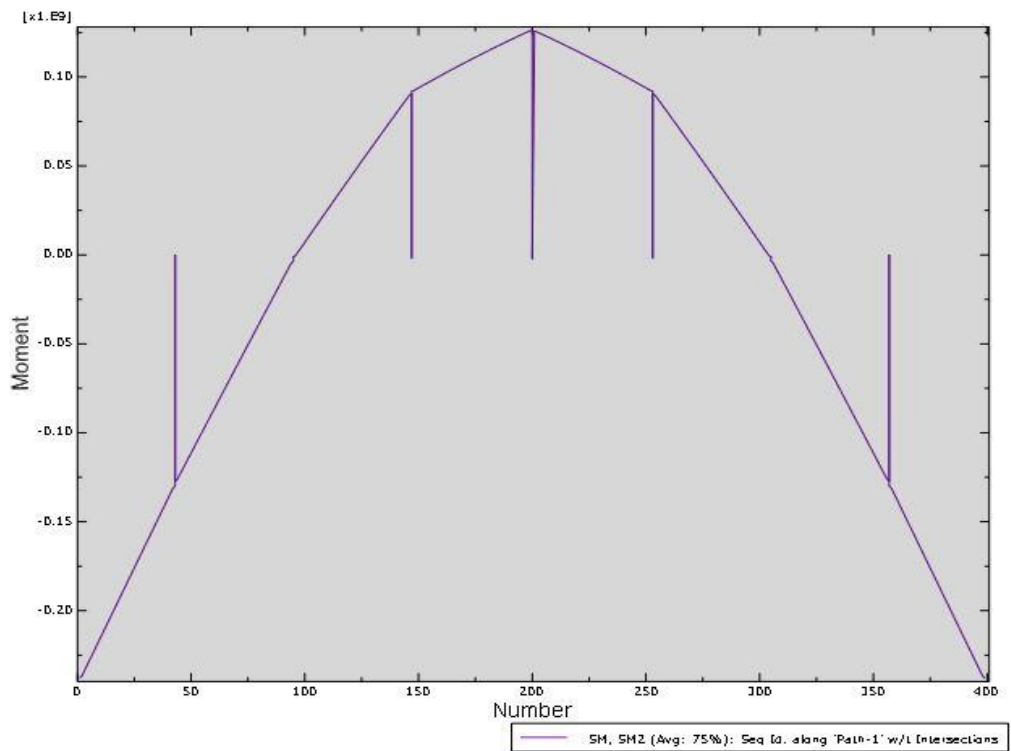


Figure 42: Sway bending moment along the straight bridge model



For $\theta_{cr} = 77.5$ deg.

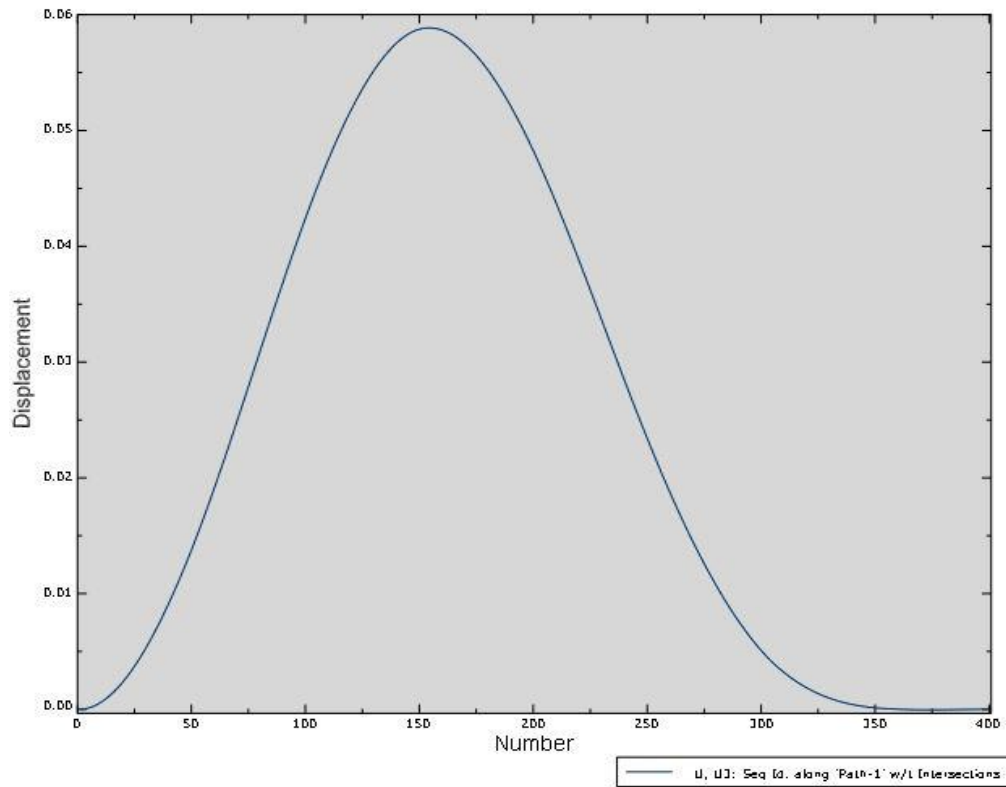


Figure 43: Sway displacement along the straight bridge model

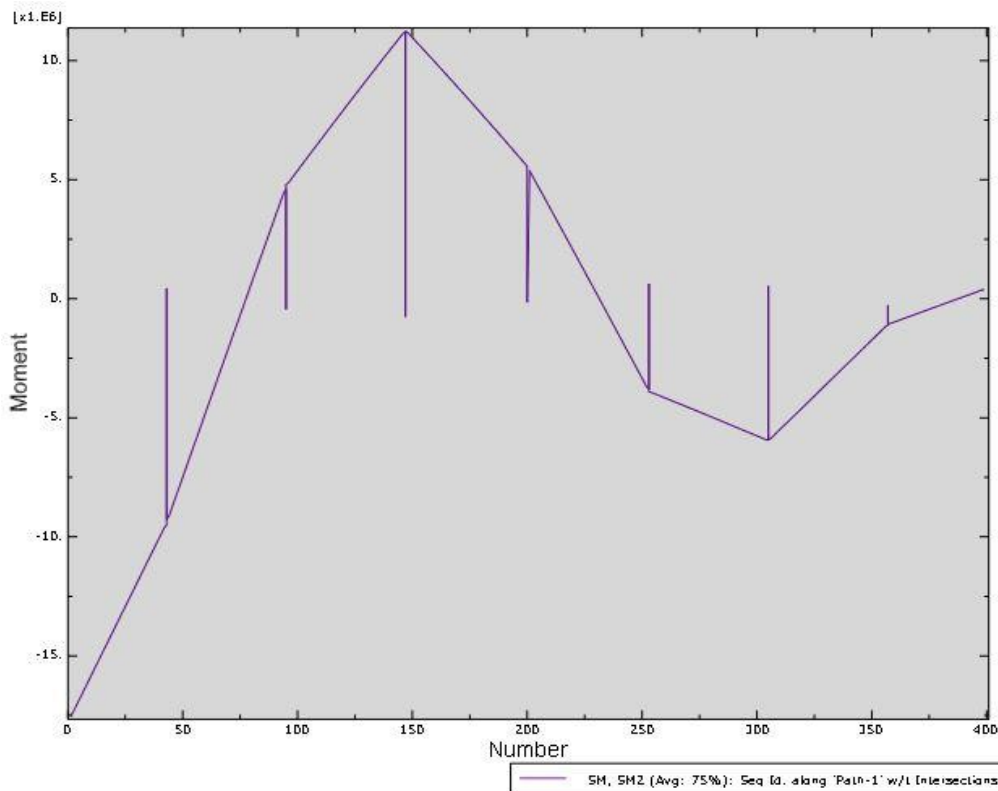


Figure 44: Sway bending moment along the straight bridge model

7.3.3 Elongated straight bridge model

$$F(t) = (-60863 \cdot \cos\theta) \cdot \sin(0.0861t + \Phi_i) \quad \text{Eq. 7.21}$$

For $\theta = 0$ deg.

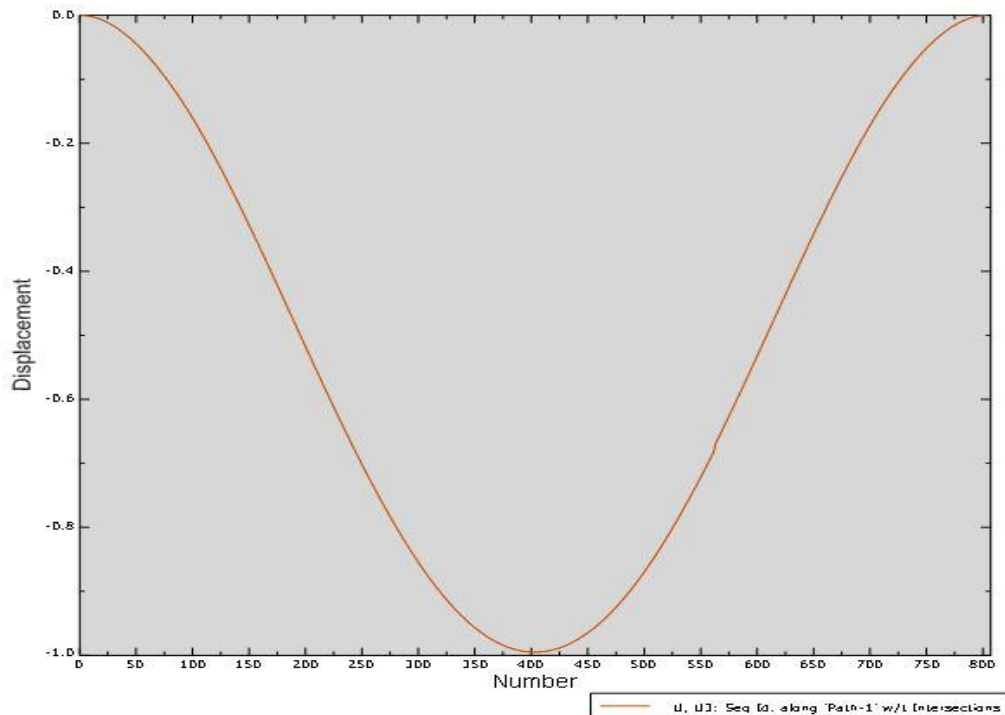


Figure 45: Sway displacement along the elongated straight bridge model

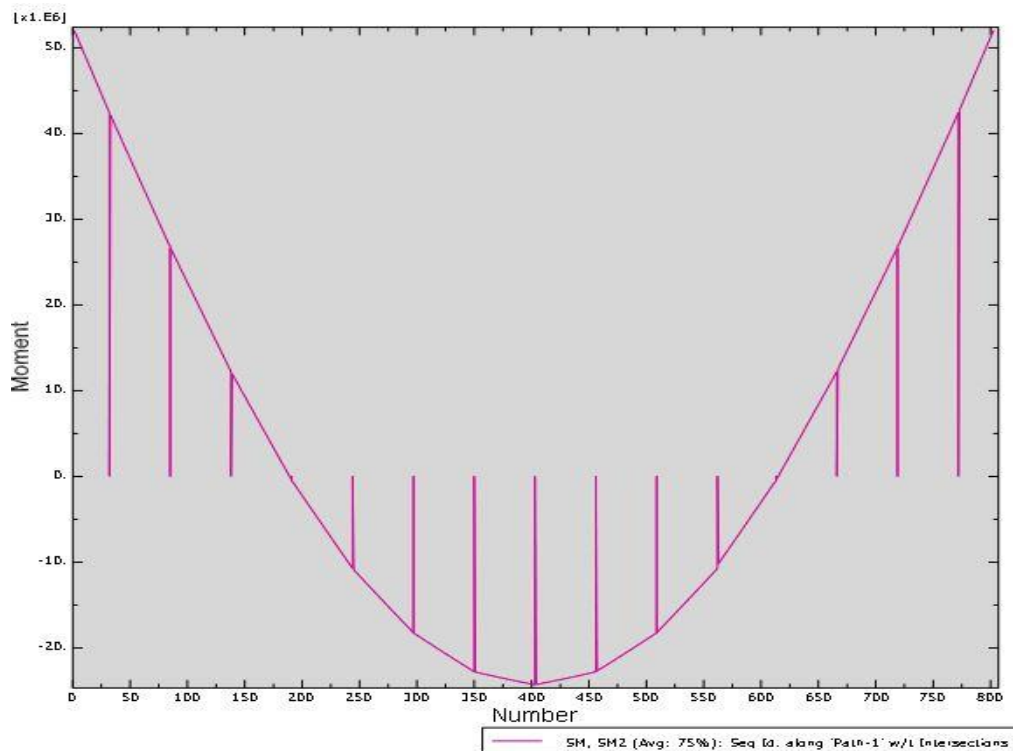


Figure 46: Sway bending moment along the elongated straight bridge model



For $\theta_{cr} = 22.6$ deg.

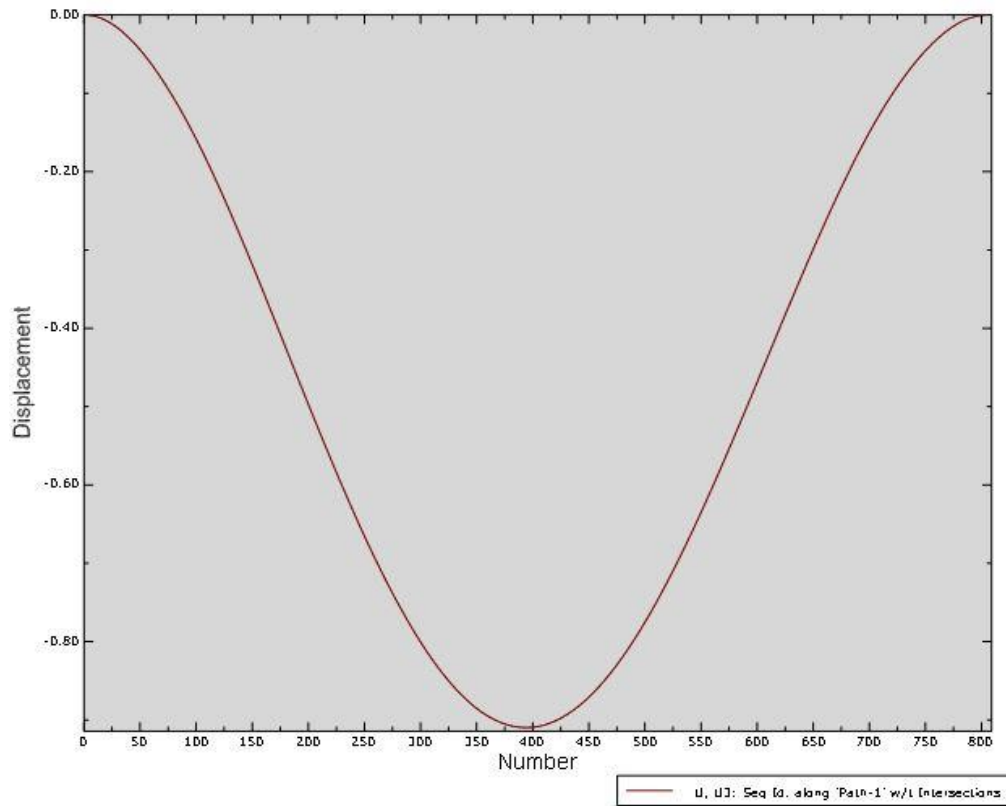


Figure 47: Sway displacement along the elongated straight bridge model

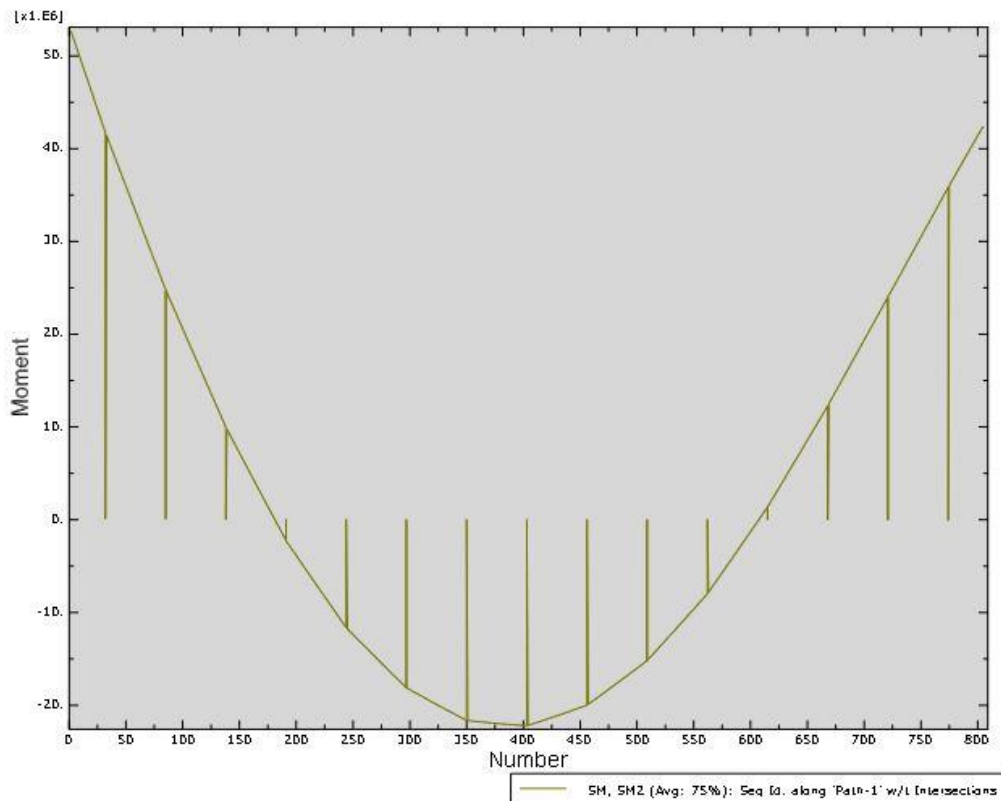


Figure 48: Sway bending moment along the elongated straight bridge model

7.3.4 Elongated straight bridge model with mooring

$$F(t) = (-1512750 \cdot \cos\theta) \cdot \sin(0.7691t + \Phi_i) \quad \text{Eq. 7.22}$$

For $\theta = 0$ deg.

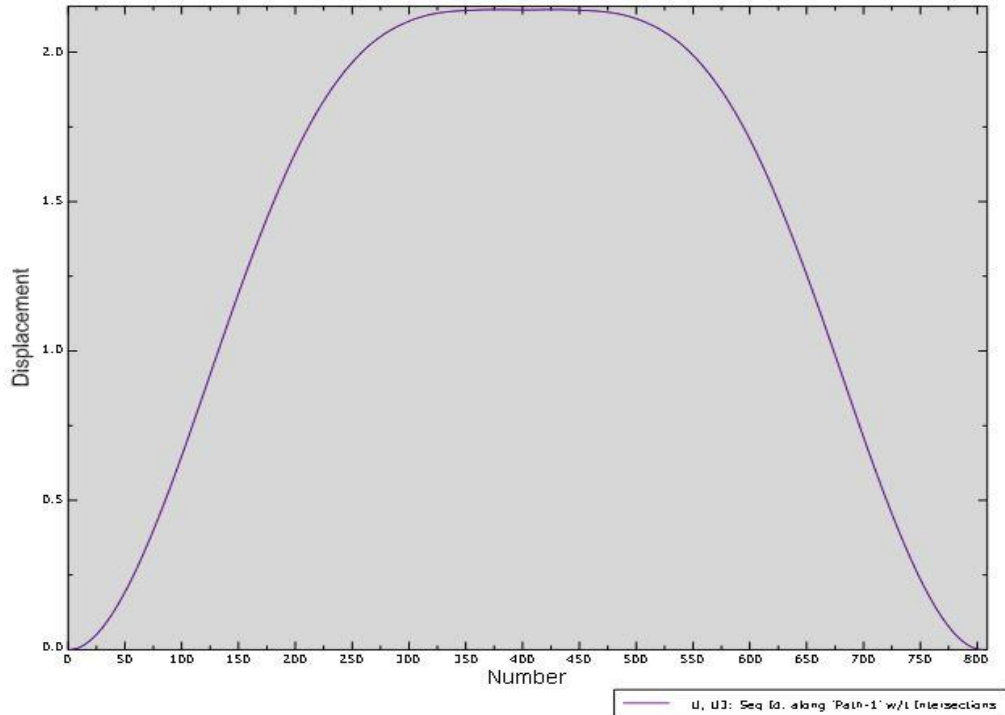


Figure 49: Sway displacement along the elongated straight bridge model with mooring

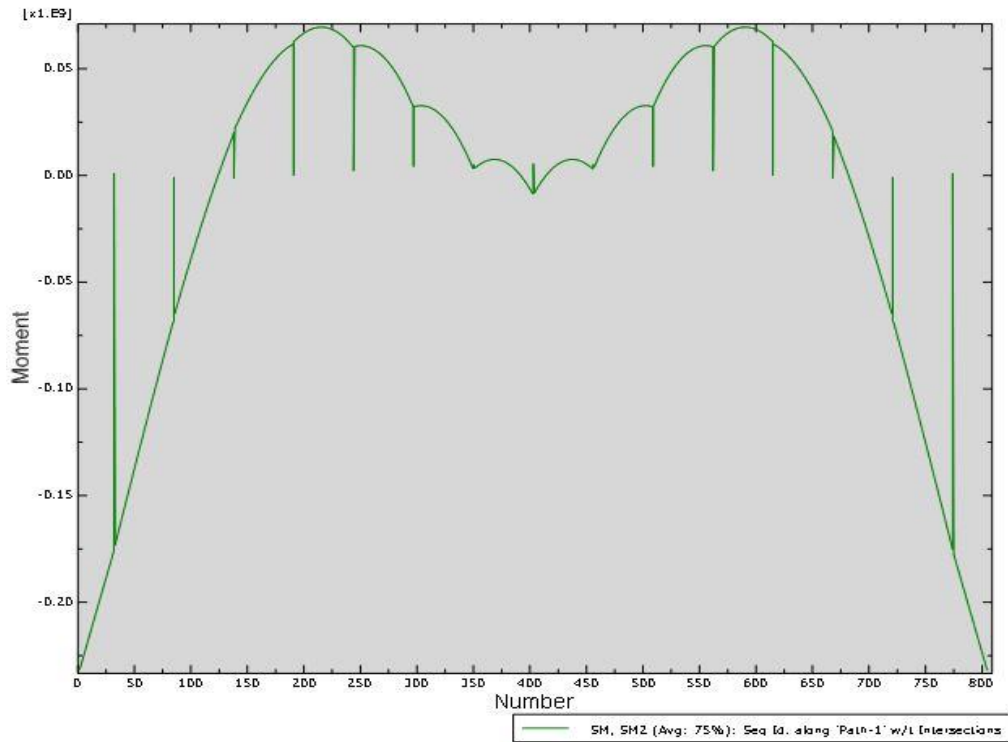


Figure 50: Sway bending moment along the elongated straight bridge model with mooring



For $\theta_{cr} = 82.5$ deg.

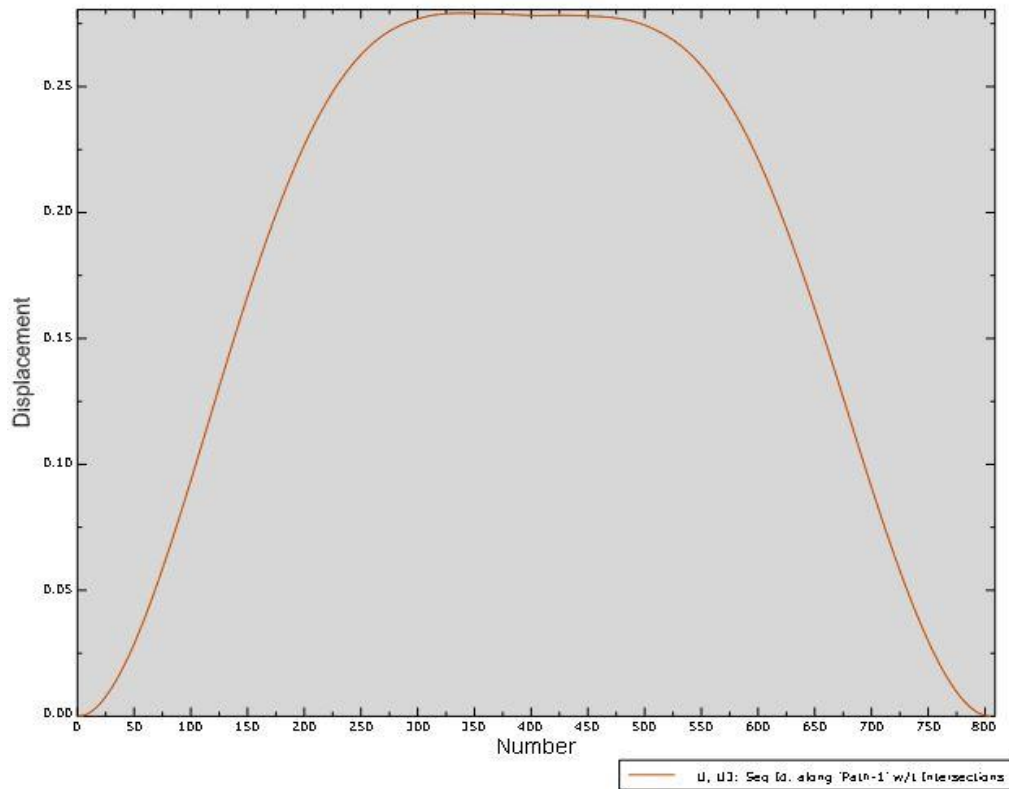


Figure 51: Sway displacement along the elongated straight bridge model with mooring

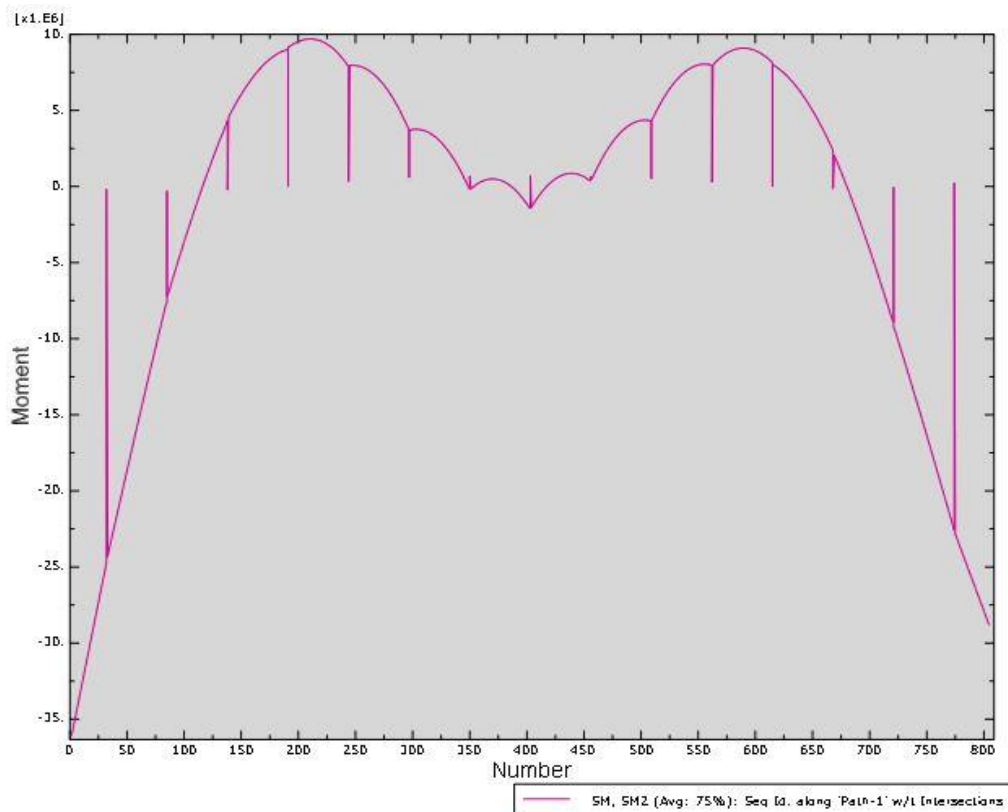


Figure 52: Sway bending moment along the elongated straight bridge model with mooring

7.3.5 Elongated curve bridge model

$$F(t) = (-155992 \cdot \cos\theta) \cdot \sin(0.1891t + \Phi i) \quad \text{Eq. 7.23}$$

For $\theta = 0$ deg.

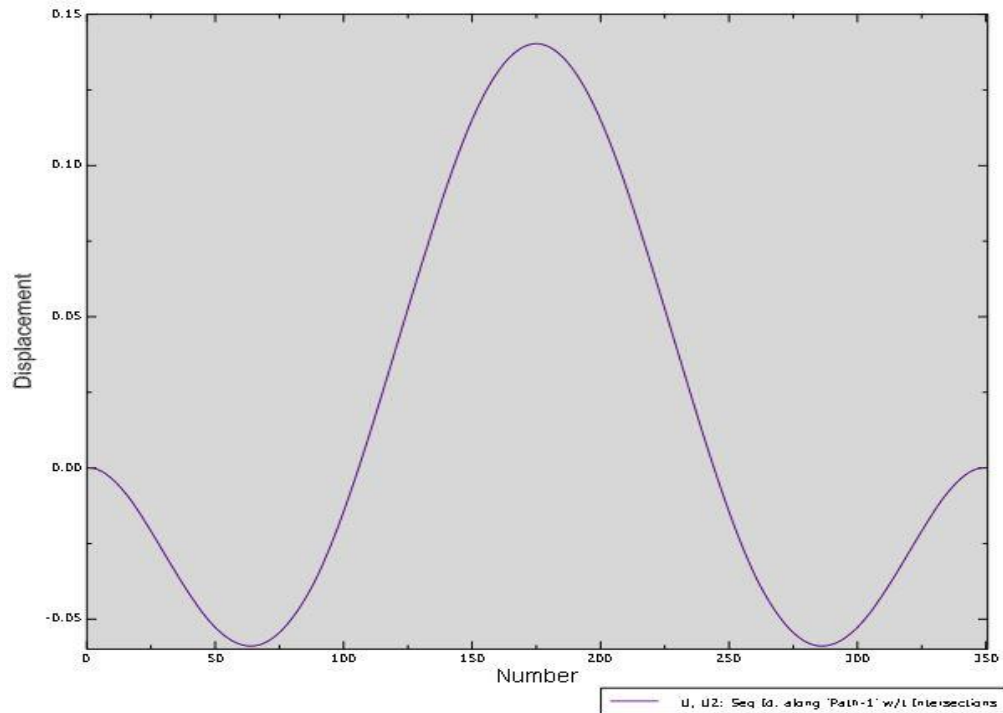


Figure 53: Sway displacement along the elongated curve bridge model

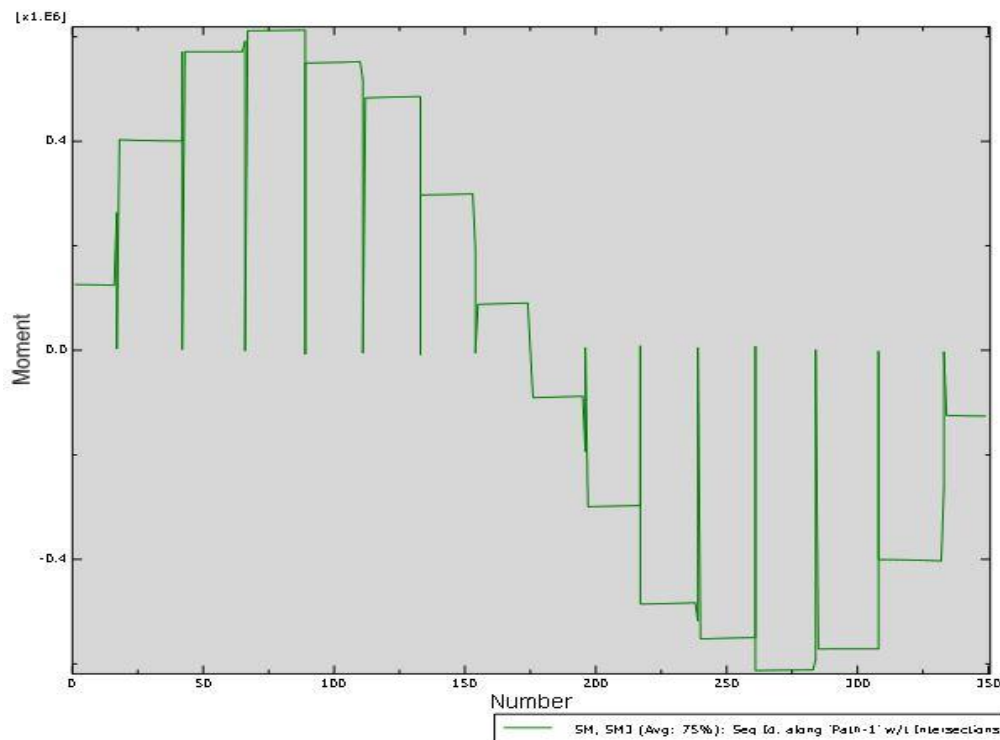


Figure 54: Sway bending moment along the elongated curve bridge model

For $\theta_{cr} = 68.3$ deg.

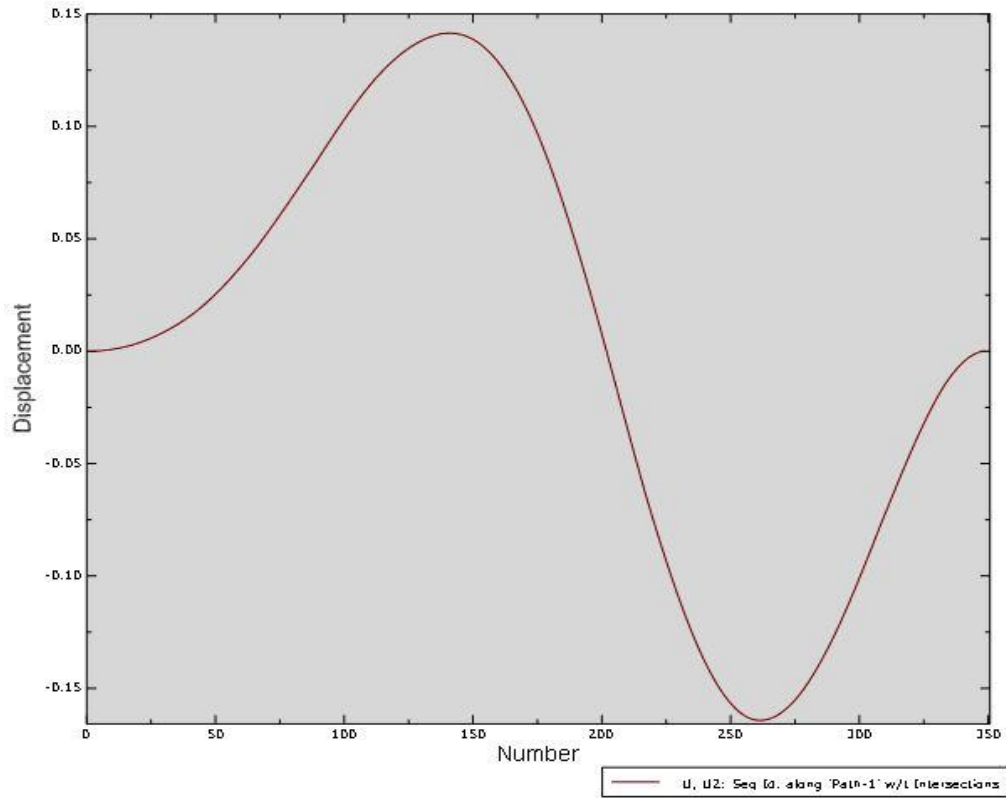


Figure 55: Sway displacement along the elongated curve bridge model

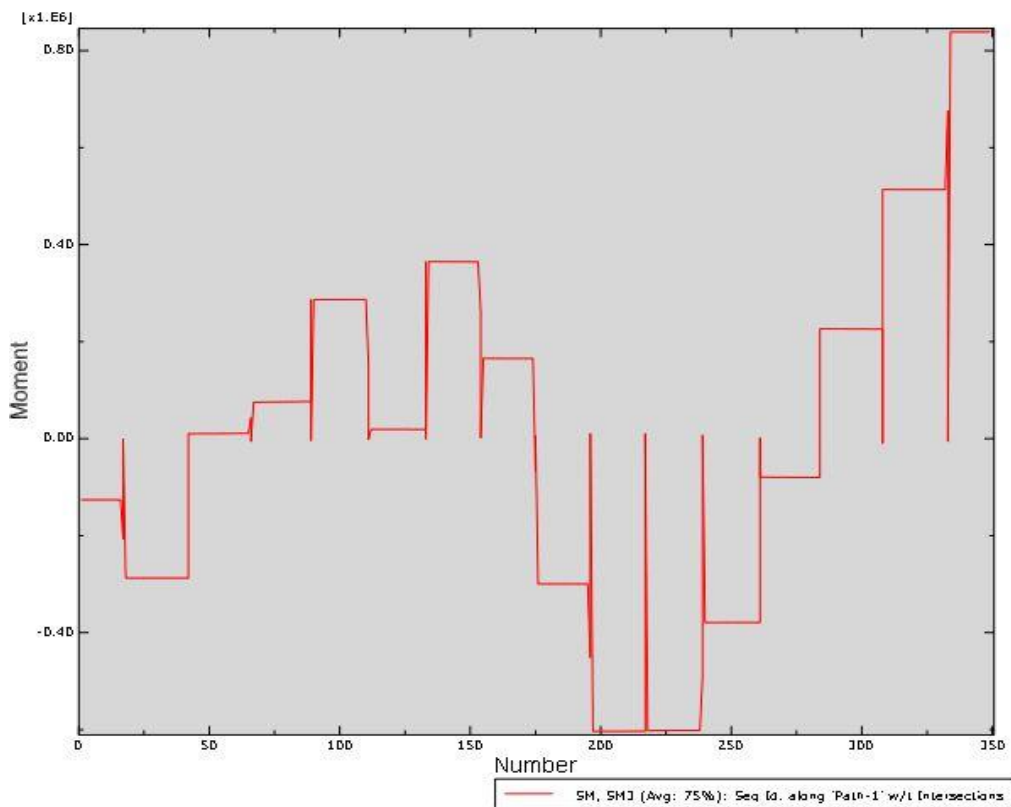


Figure 56: Sway bending moment along the elongated curve bridge model

7.3.6 Elongated curve bridge model with mooring

$$F(t) = (-1338720 \cdot \cos\theta) \cdot \sin(0.6723t + \Phi_i) \quad \text{Eq. 7.24}$$

For $\theta = 0$ deg.

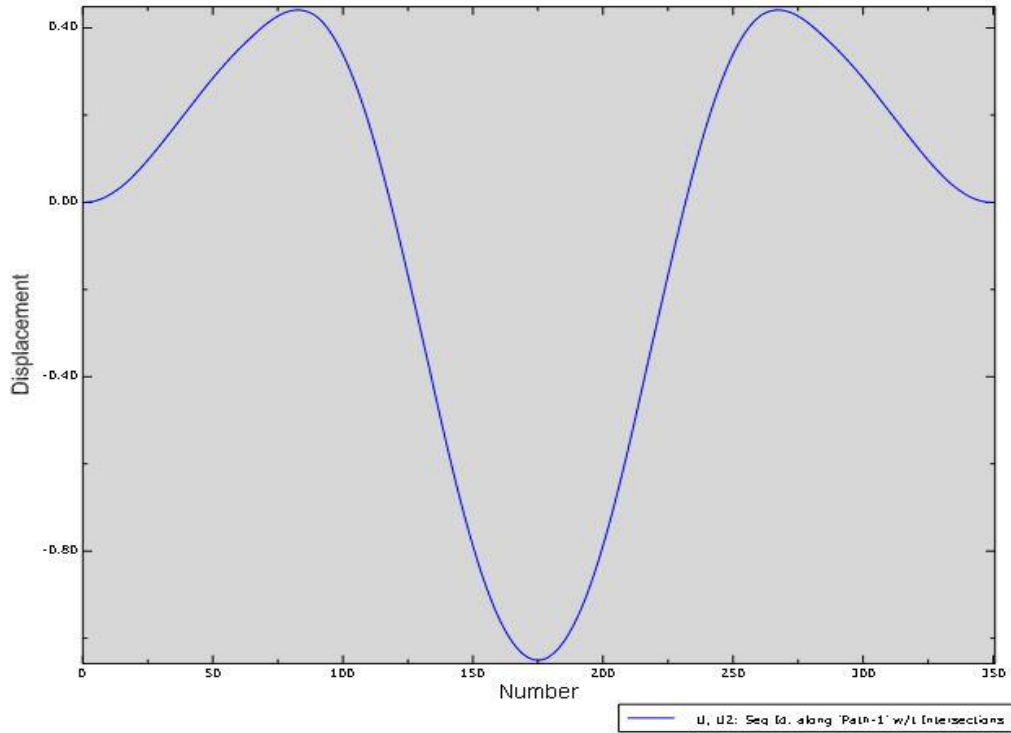


Figure 57: Sway displacement along the elongated curve bridge model with mooring

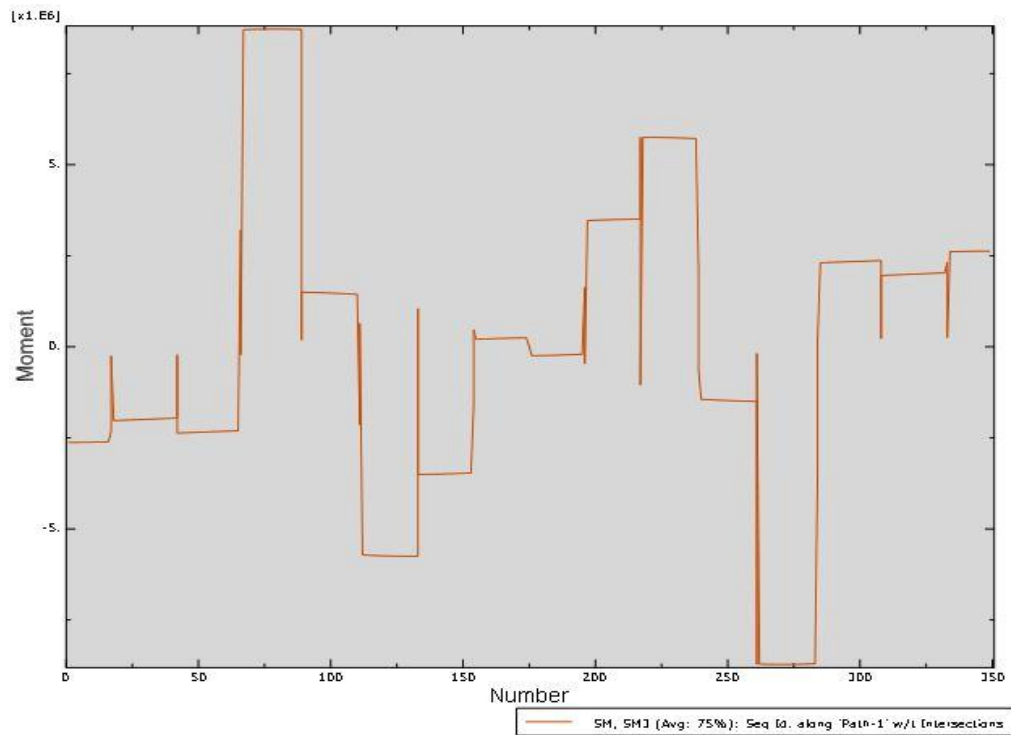


Figure 58: Sway bending moment along the elongated curve bridge model with mooring



For $\theta_{cr} = 64.6$ deg.

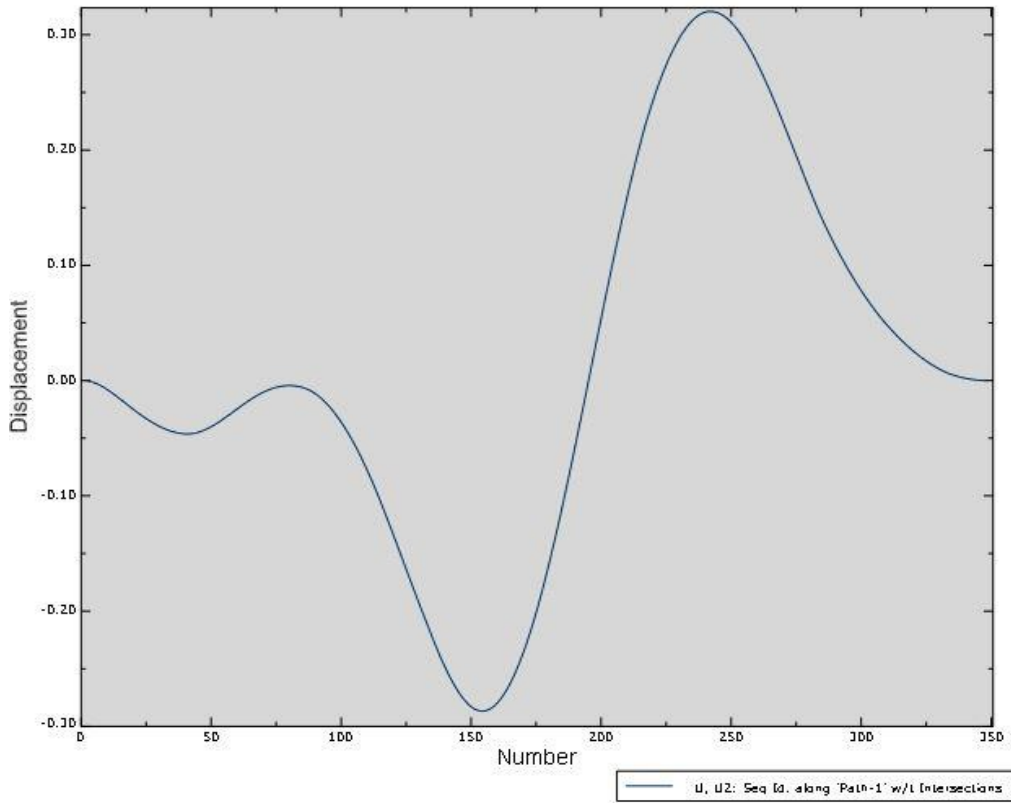


Figure 59: Sway displacement along the elongated curve bridge model with mooring

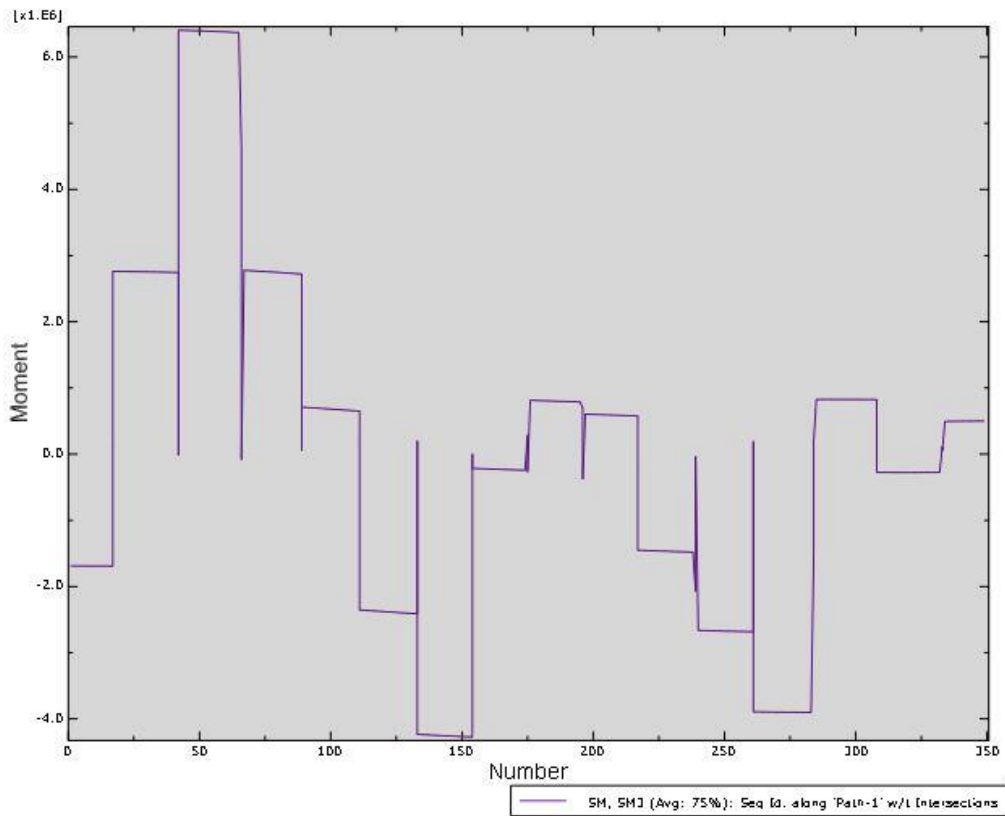


Figure 60: Sway bending moment along the elongated curve bridge model with mooring

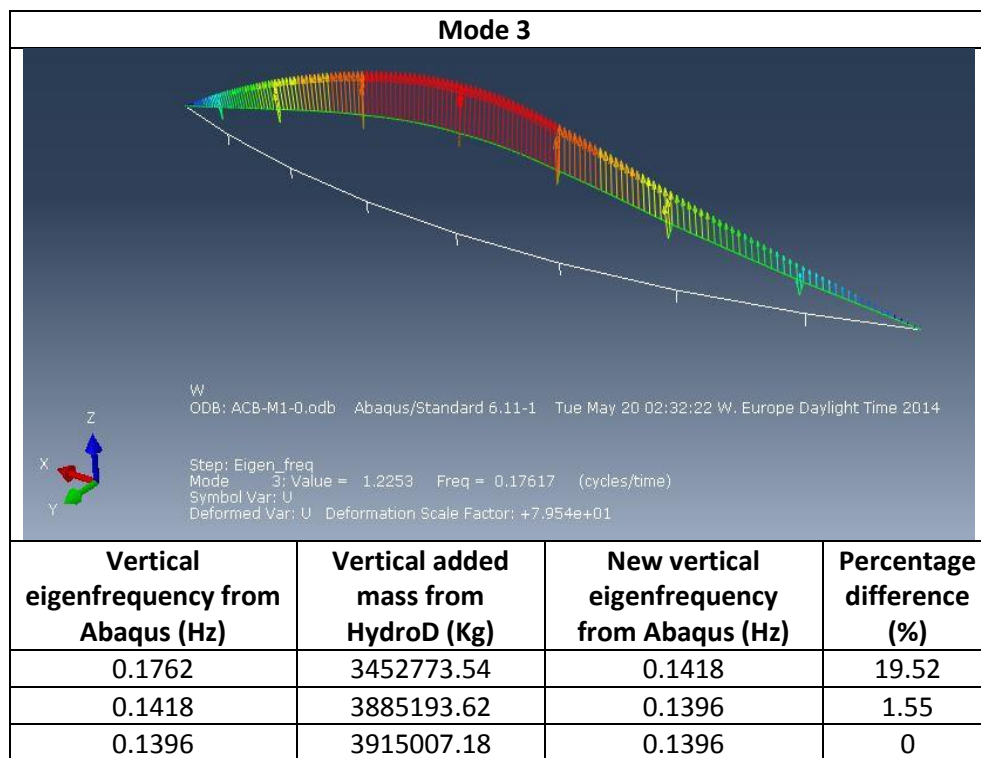
7.4 Heave response

When studying the heave response, the horizontal added mass was replaced with a vertical added mass. For each of the bridge models, the vertical added mass was first updated by iteration of the first heave eigenfrequency before application.

Then similar to the sway response, the pontoons of a model were subjected to a harmonic wave load of the same frequency as the updated heave mode. For a specific wave direction, the corresponding heave force coefficient was obtained from HydroD. The heave displacement and heave bending moment along each model were evaluated at the time instant when maximum response took place.

7.4.1 Curve bridge model

Table 14: Iteration of added mass for first heave eigenmode





For $\theta = 0$ deg.

$$F(t) = 1765570 \cdot \sin(0.8771t + \Phi_i)$$

Eq. 7.25

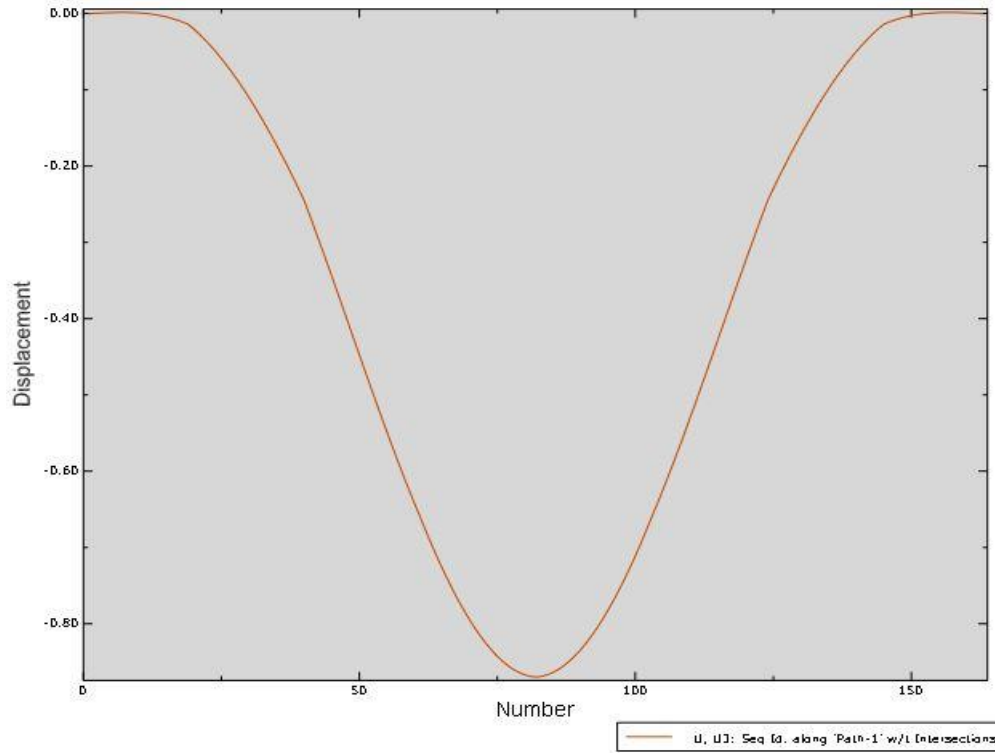


Figure 61: Heave displacement along the curve bridge model

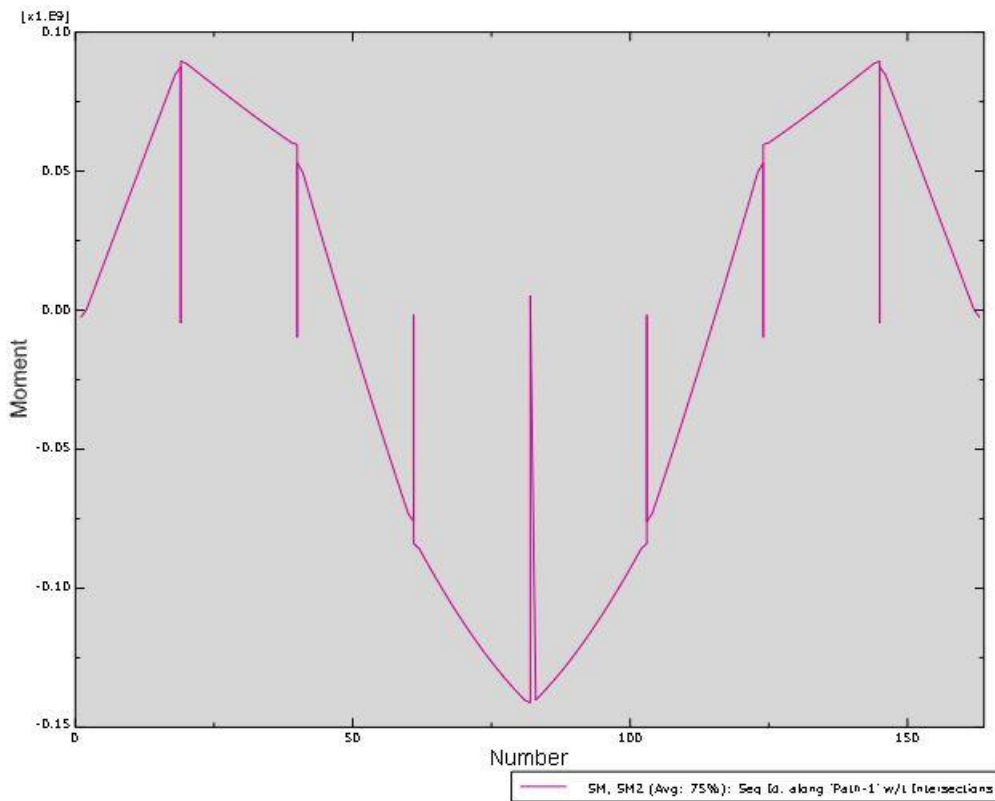


Figure 62: Heave bending moment along the curve bridge model



For $\theta_{cr} = 71.1$ deg.

$$F(t) = 2046400 \cdot \sin(0.8771t + \Phi_i)$$

Eq. 7.26

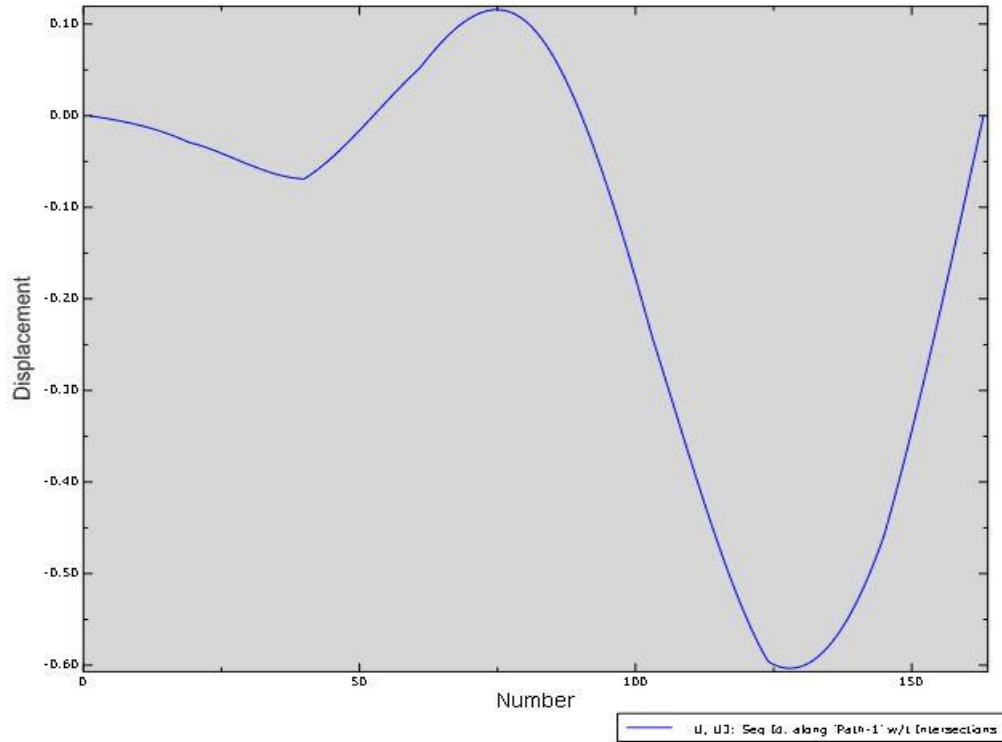


Figure 63: Heave displacement along the curve bridge model

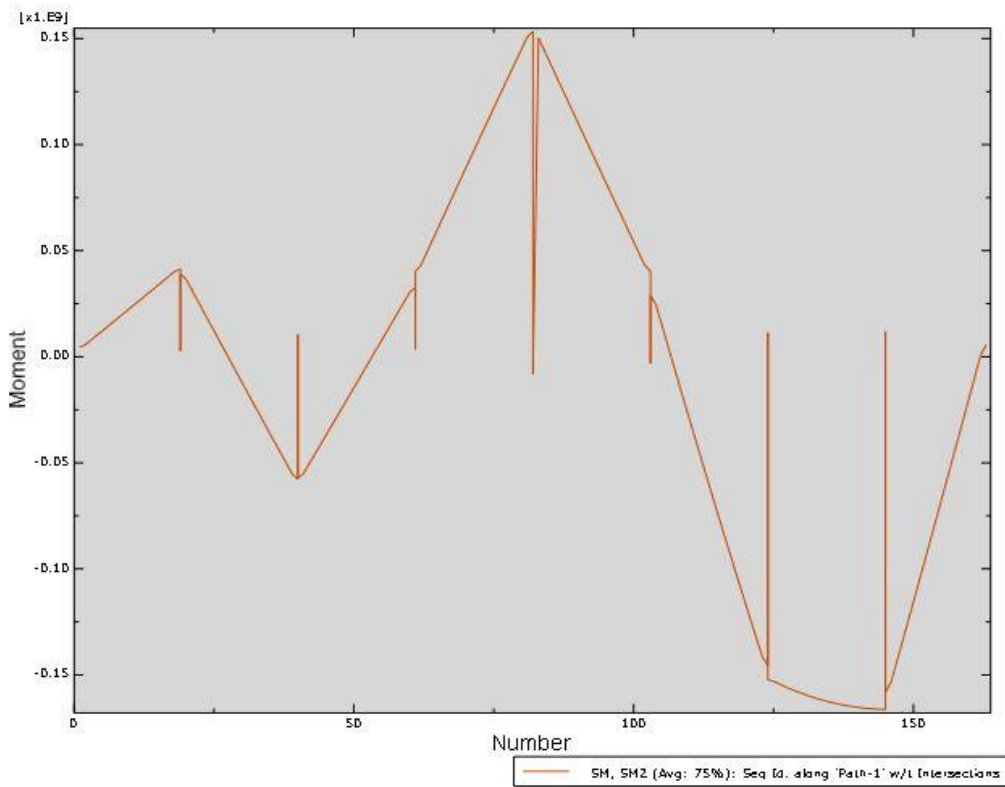
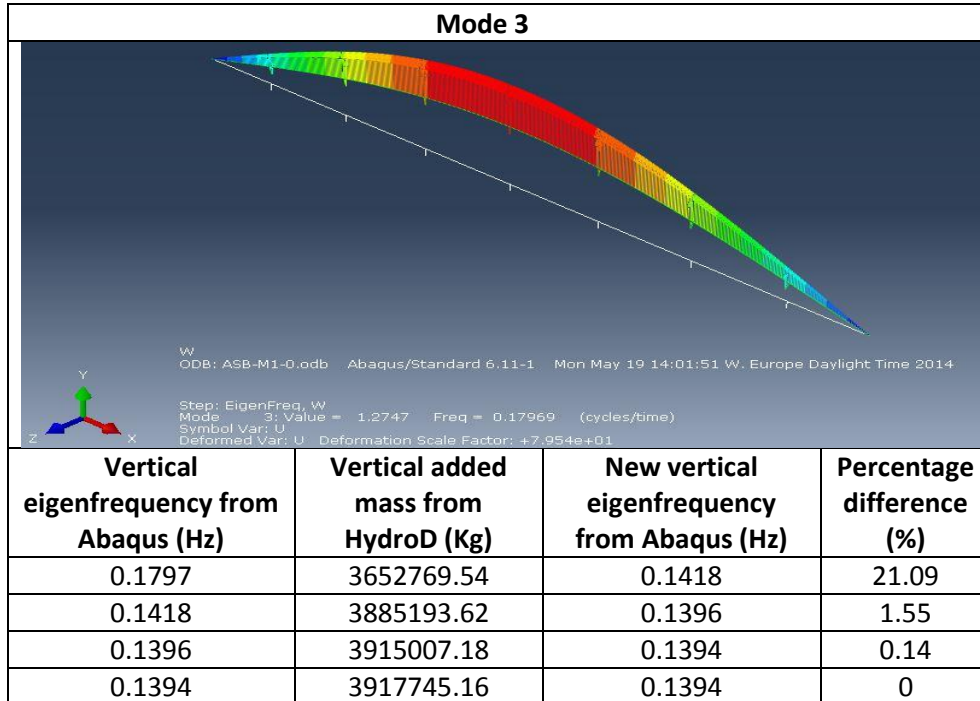


Figure 64: Heave bending moment along the curve bridge model

7.4.2 Straight bridge model

Table 15: Iteration of added mass for first heave eigenmode



For $\theta = 0$ deg.

$$F(t) = 1771410 \cdot \sin(0.8759t + \Phi_i)$$

Eq. 7.27

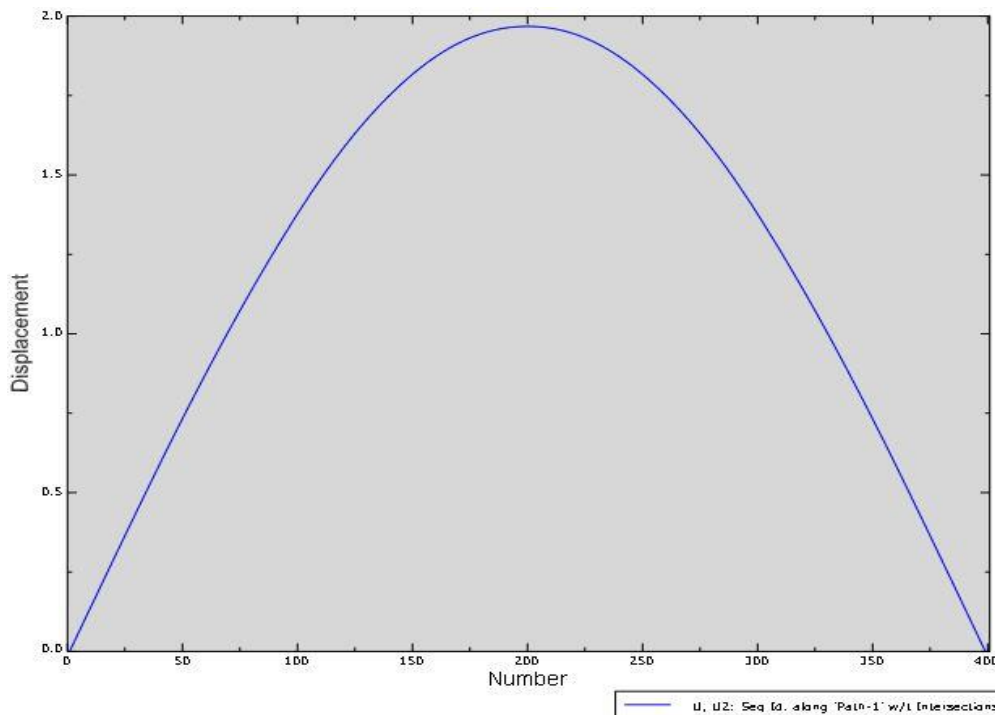


Figure 65: Heave displacement along the straight bridge model

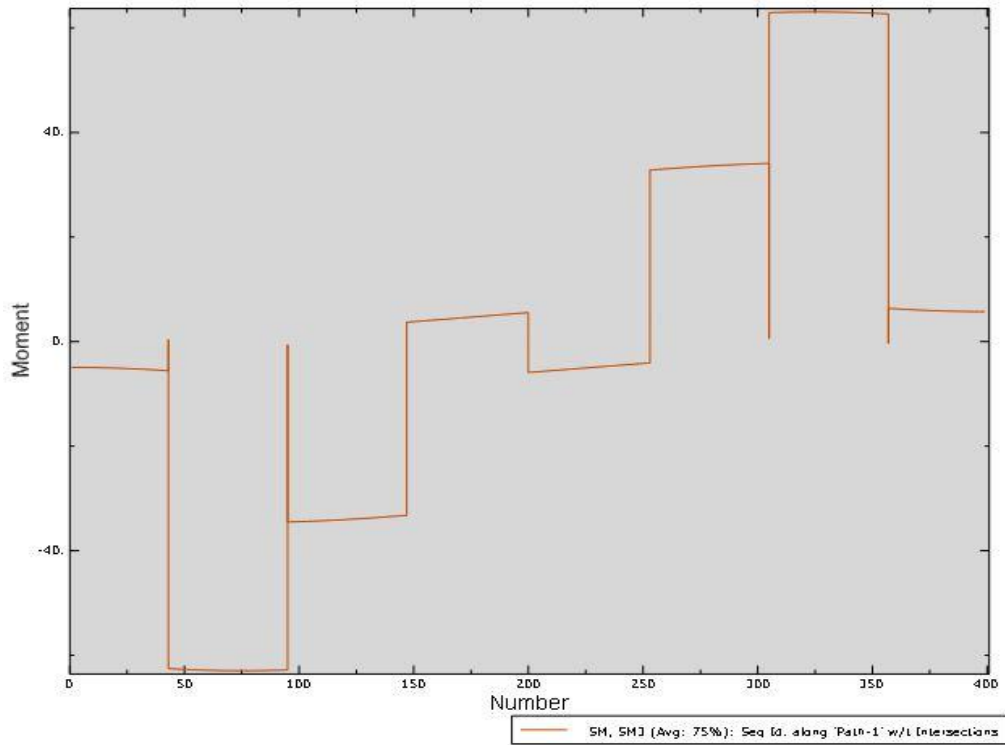


Figure 66: Heave bending moment along the straight bridge model

For $\theta_{cr} = 70.7$ deg.

$$F(t) = 2049390 \cdot \sin(0.8759t + \Phi_i)$$

Eq. 7.28

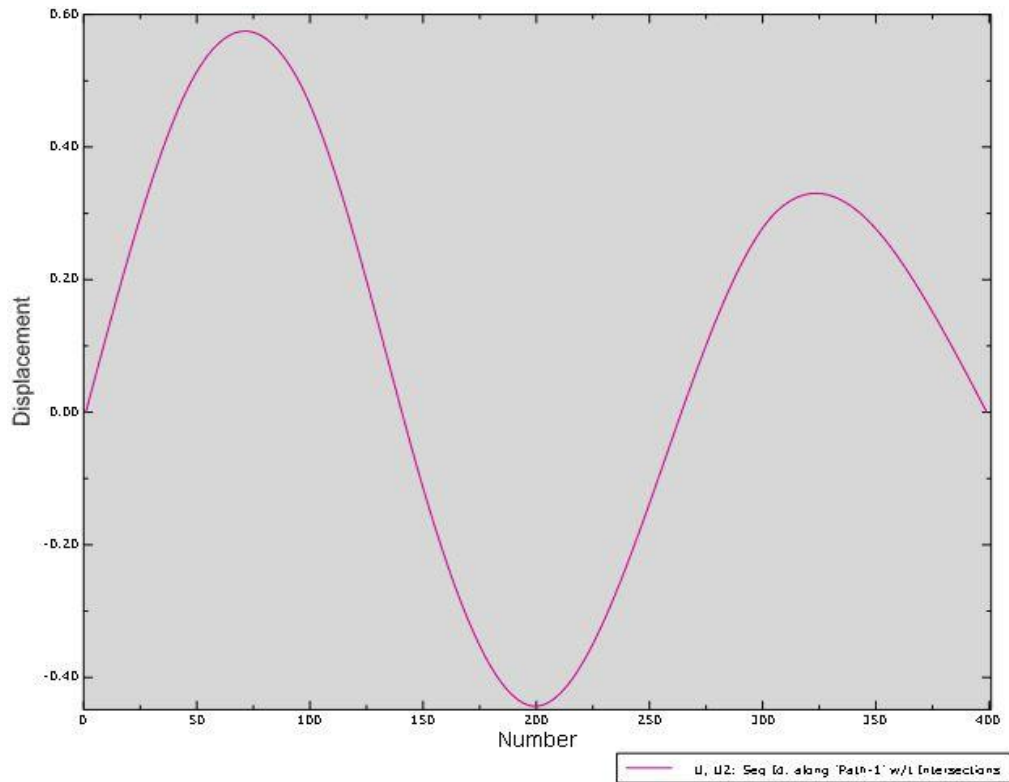


Figure 67: Heave displacement along the straight bridge model

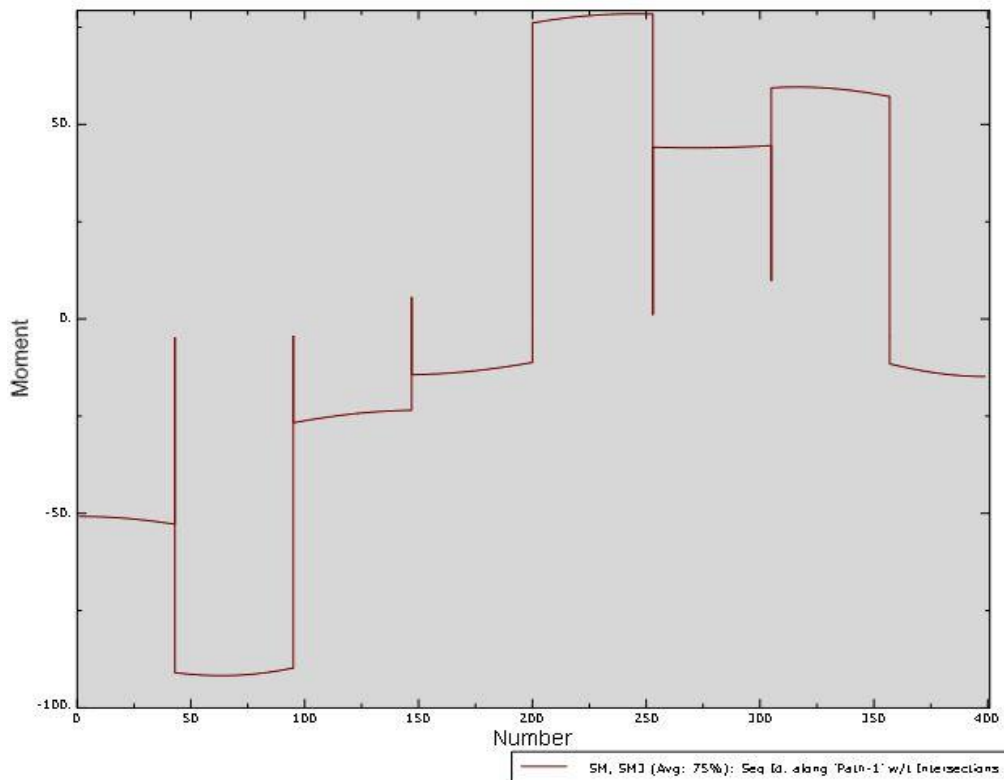


Figure 68: Heave bending moment along the straight bridge model

7.4.3 Elongated straight bridge model

Table 16: Iteration of added mass for first heave eigenmode

Mode 7

Vertical eigenfrequency from Abaqus (Hz)	Vertical added mass from HydroD (Kg)	New vertical eigenfrequency from Abaqus (Hz)	Percentage difference (%)
0.1799	3652769.54	0.1411	21.57
0.1411	3895841.32	0.1389	1.56
0.1389	3925959.10	0.1387	0.14
0.1387	3928697.08	0.1386	0.07
0.1386	3931739.28	0.1386	0



For $\theta = 0$ deg.

$$F(t) = 1800470 \cdot \sin(0.8708t + \Phi_i)$$

Eq. 7.29

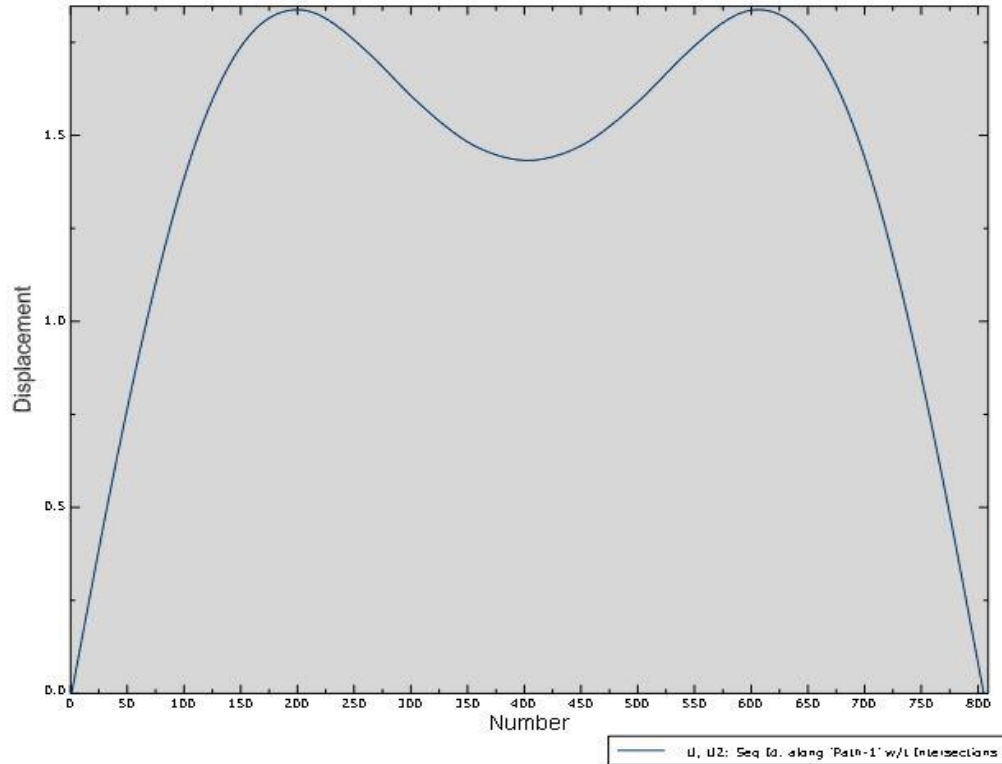


Figure 69: Heave displacement along the elongated straight bridge model

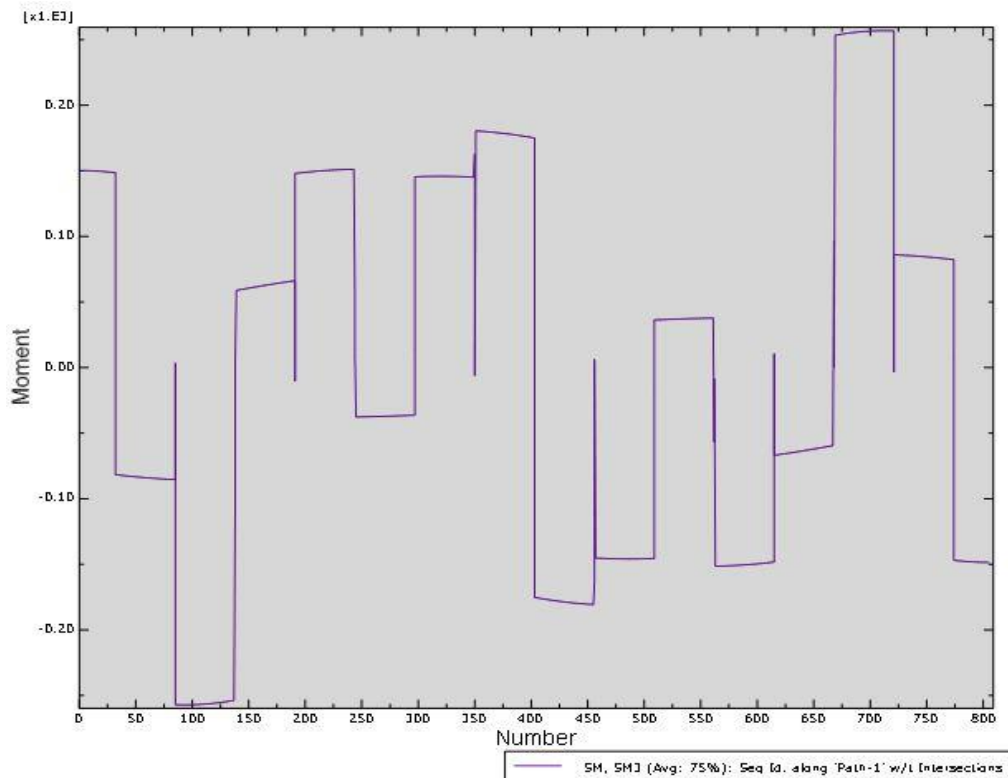


Figure 70: Heave bending moment along the elongated straight bridge model



For $\theta_{cr} = 74$ deg.

$$F(t) = 2081700 \cdot \sin(0.8708t + \Phi_i)$$

Eq. 7.30

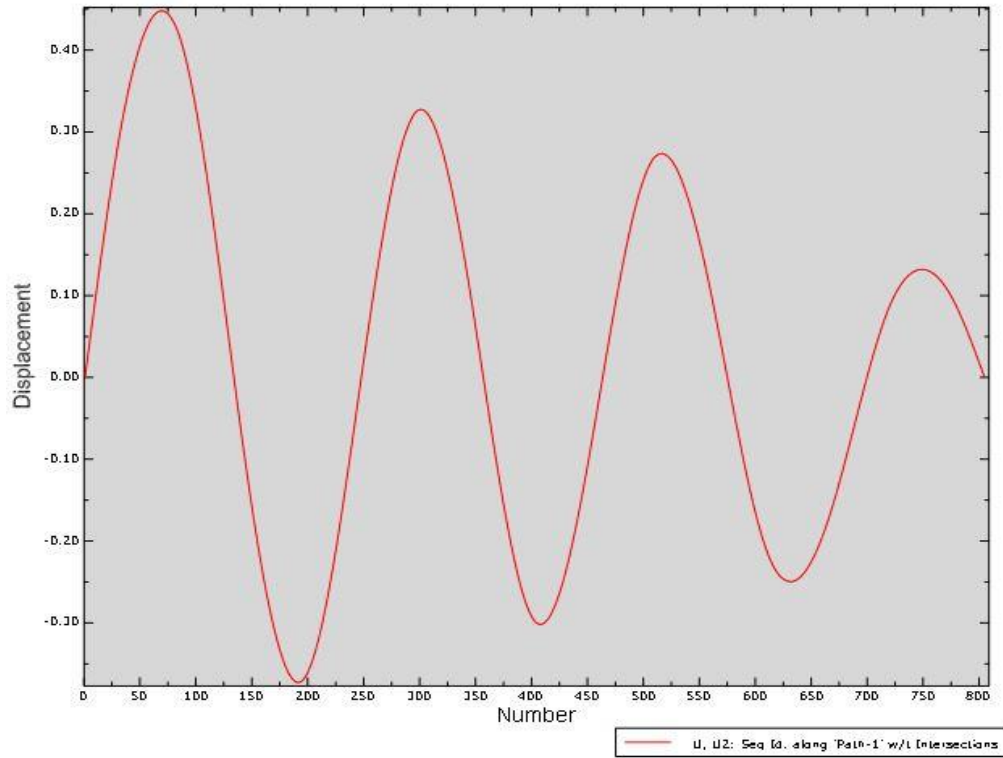


Figure 71: Heave displacement along the elongated straight bridge model

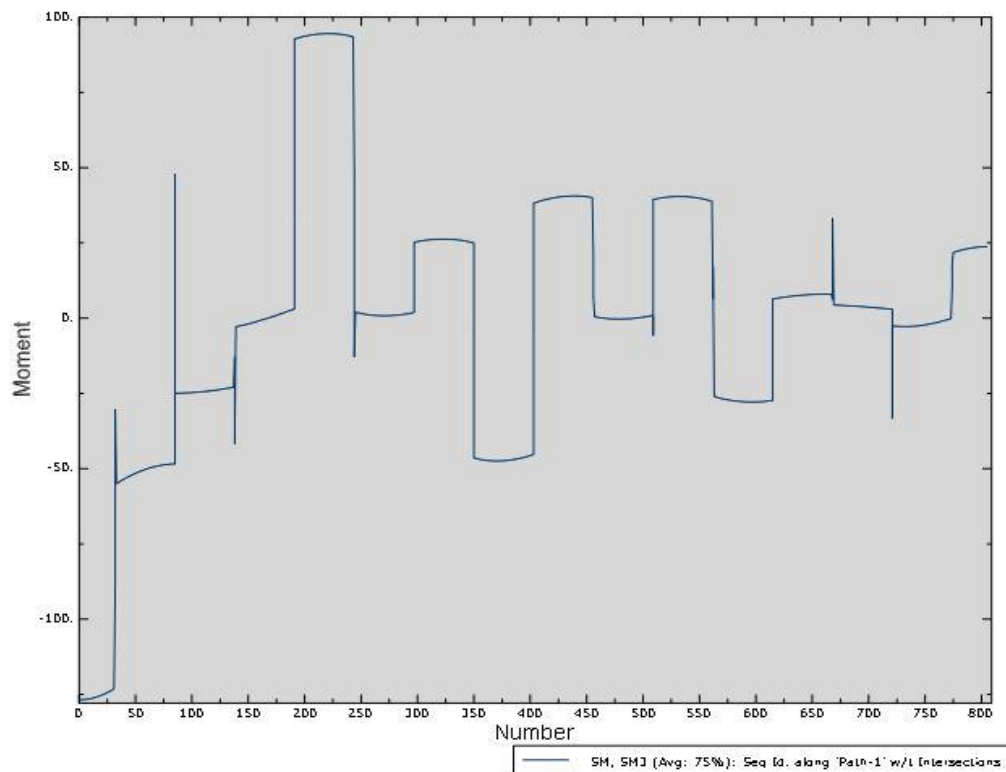
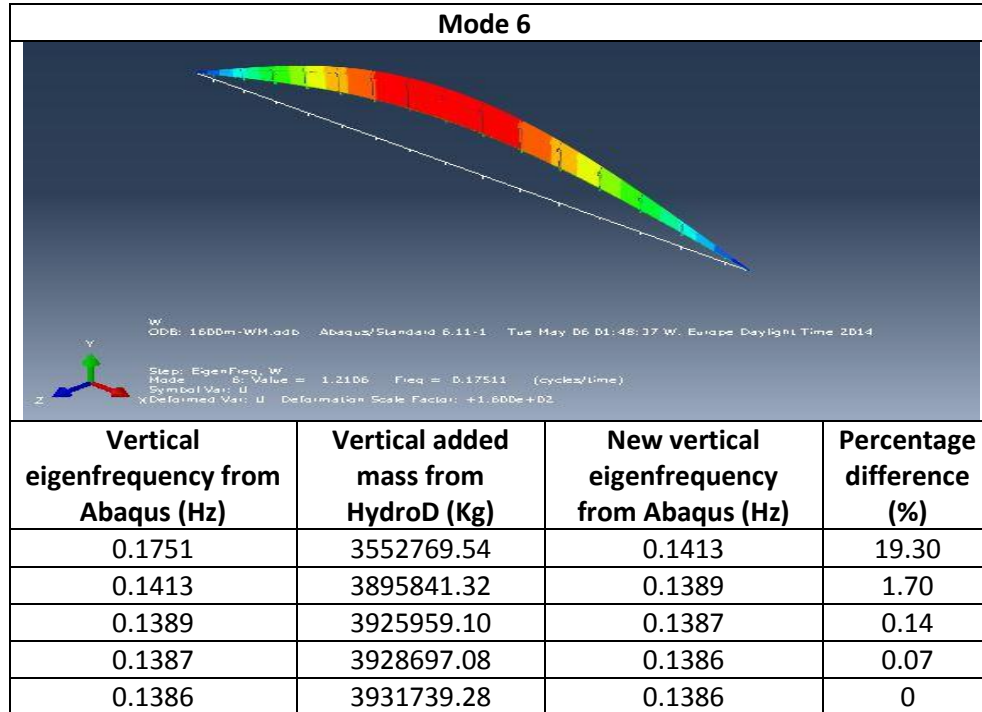


Figure 72: Heave bending moment along the elongated straight bridge model

7.4.4 Elongated straight bridge model with mooring

Table 17: Iteration of added mass for first heave eigenmode



For $\theta = 0$ deg.

$$F(t) = 1800470 \cdot \sin(0.8708t + \Phi_i)$$

Eq. 7.31

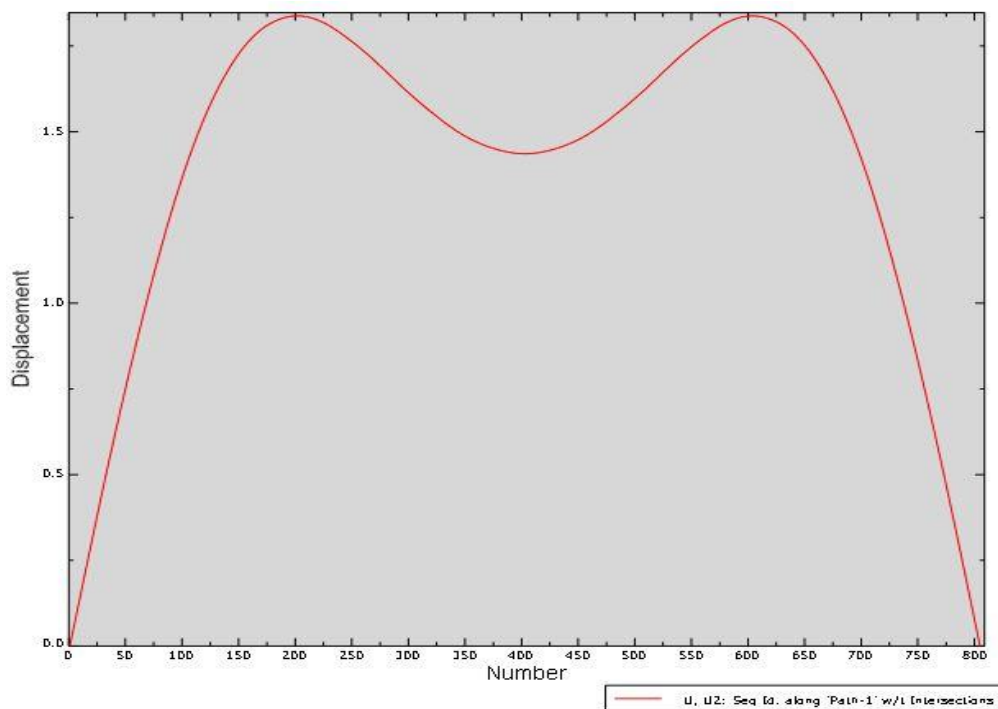


Figure 73: Heave displacement along the elongated straight bridge model with mooring

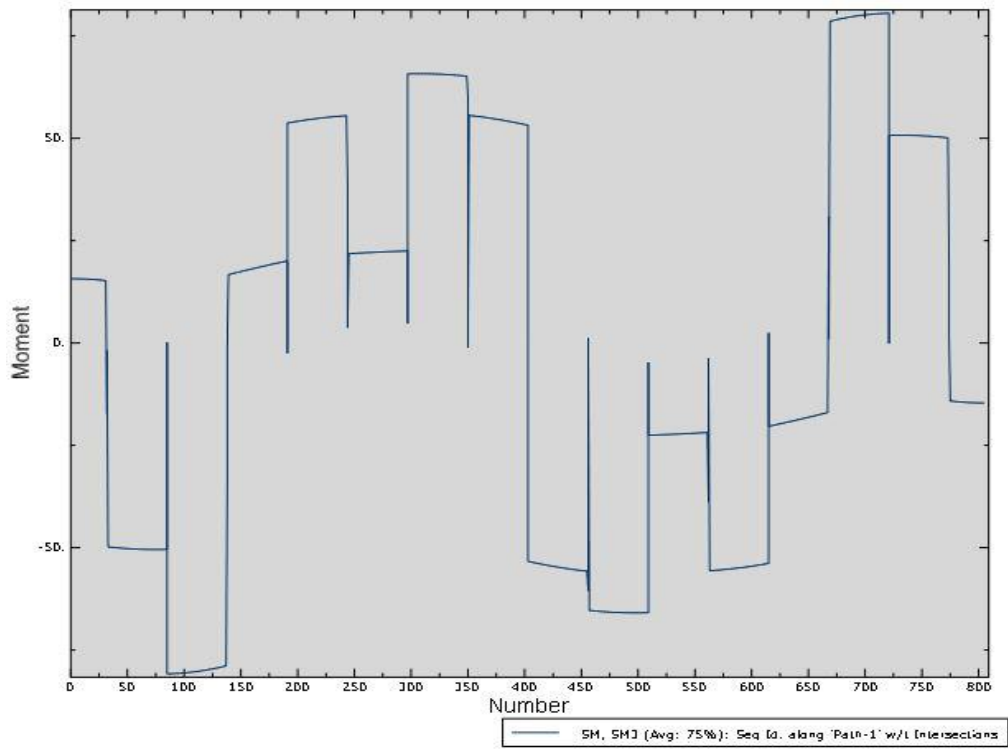


Figure 74: Heave bending moment along the elongated straight bridge model with mooring

For $\theta_{cr} = 74$ deg.

$$F(t) = 2081700 \cdot \sin(0.8708t + \Phi_i)$$

Eq. 7.32

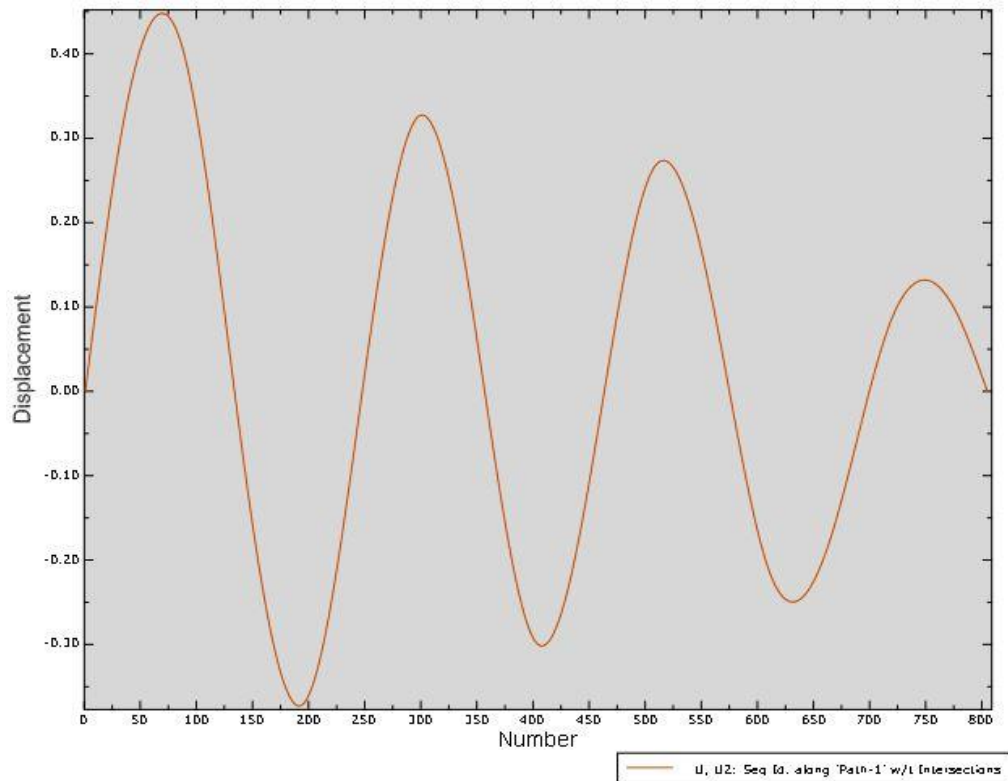


Figure 75: Heave displacement along the elongated straight bridge model with mooring

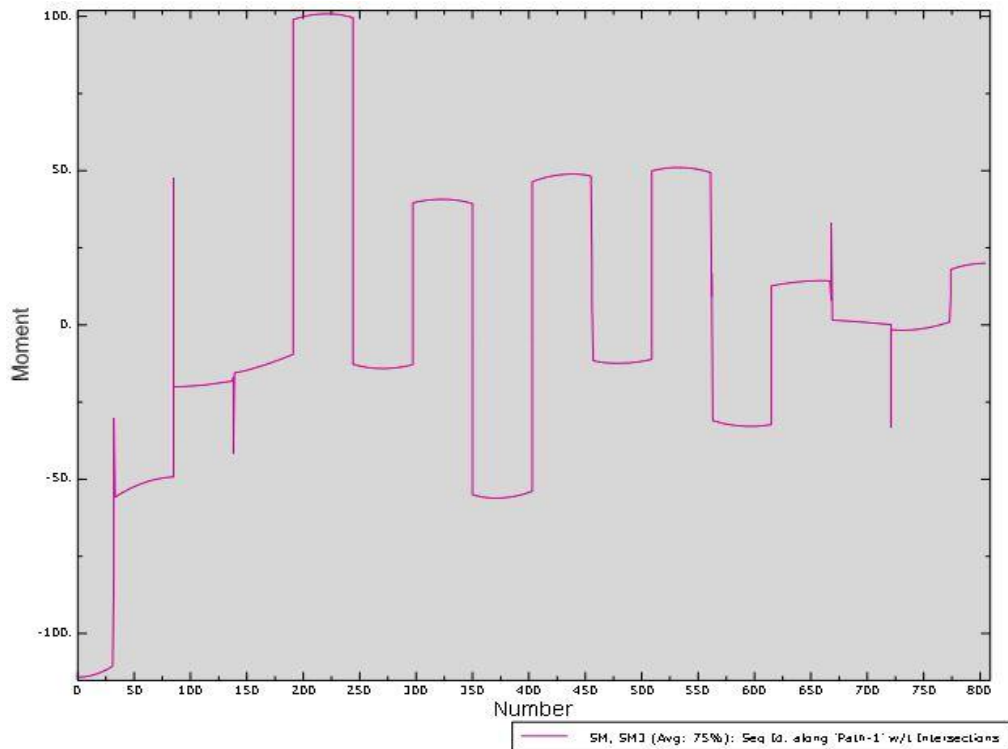


Figure 76: Heave bending moment along the elongated straight bridge model with mooring

7.4.5 Elongated curve bridge model

Table 18: Iteration of added mass for first heave eigenmode

Mode 6			
<small>WJ ODB: EEIadb - Abaqus/Standard 6.11-1 Sun May 04 14:04:48 W. Europe Daylight Time 2014 Step: Eigen_freq Mode: 6; Value = 1.2697 Freq = 0.17934 (cycles/Time) Primary Var: U; Magnitude Deformed Var: U; Deformation Scale Factor: +1.600e+02</small>			
Vertical eigenfrequency from Abaqus (Hz)	Vertical added mass from HydroD (Kg)	New vertical eigenfrequency from Abaqus (Hz)	Percentage difference (%)
0.1793	3653073.76	0.1410	21.36
0.1410	3895841.32	0.1388	1.56
0.1388	3925959.10	0.1385	0.22
0.1385	3931739.28	0.1385	0



For $\theta = 0$ deg.

$$F(t) = 1800470 \cdot \sin(0.8702t + \Phi_i)$$

Eq. 7.33

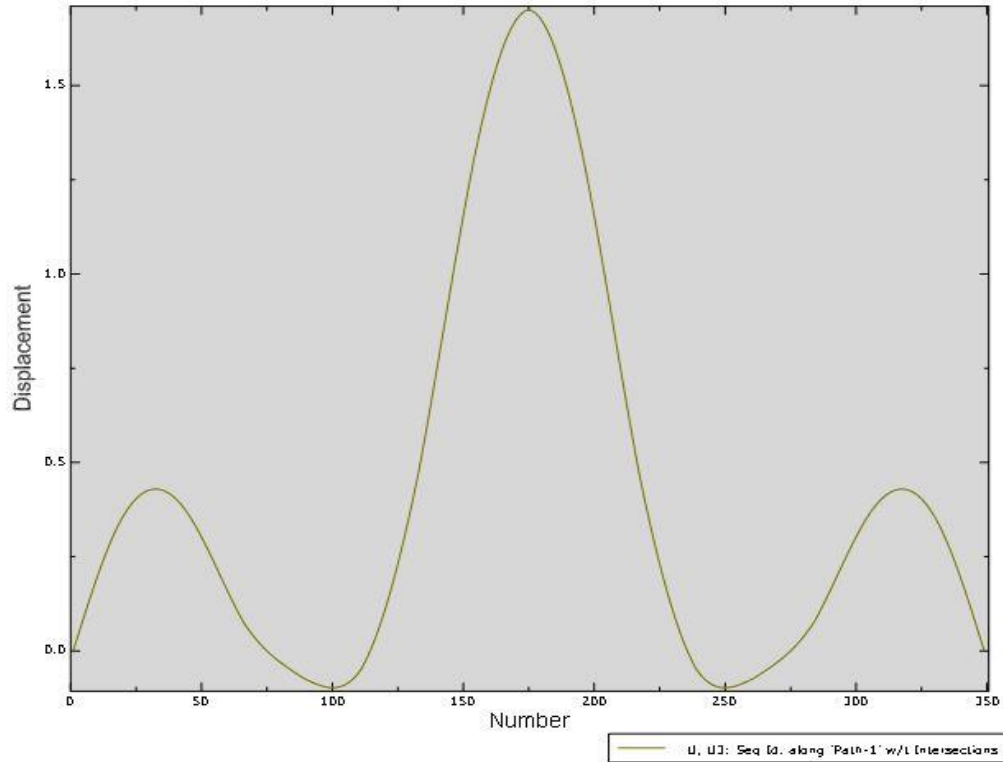


Figure 77: Heave displacement along the elongated curve bridge model

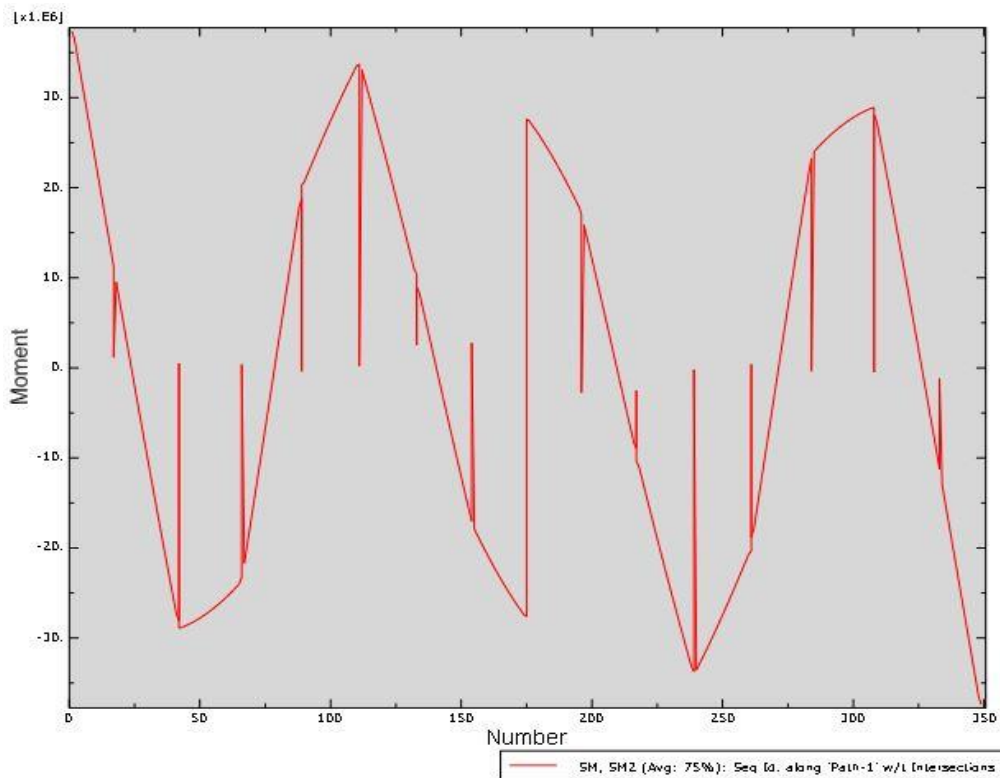


Figure 78: Heave bending moment along the elongated curve bridge model



For $\theta_{cr} = 73.7$ deg.

$$F(t) = 2080800 \cdot \sin(0.8702t + \Phi_i)$$

Eq. 7.34

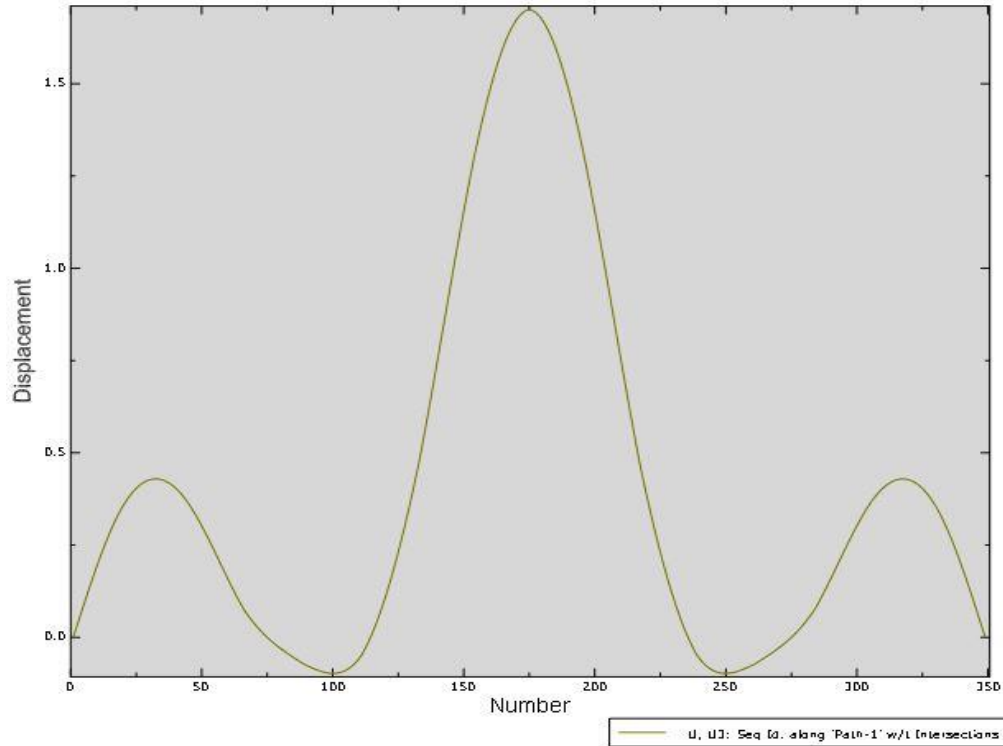


Figure 79: Heave displacement along the elongated curve bridge model

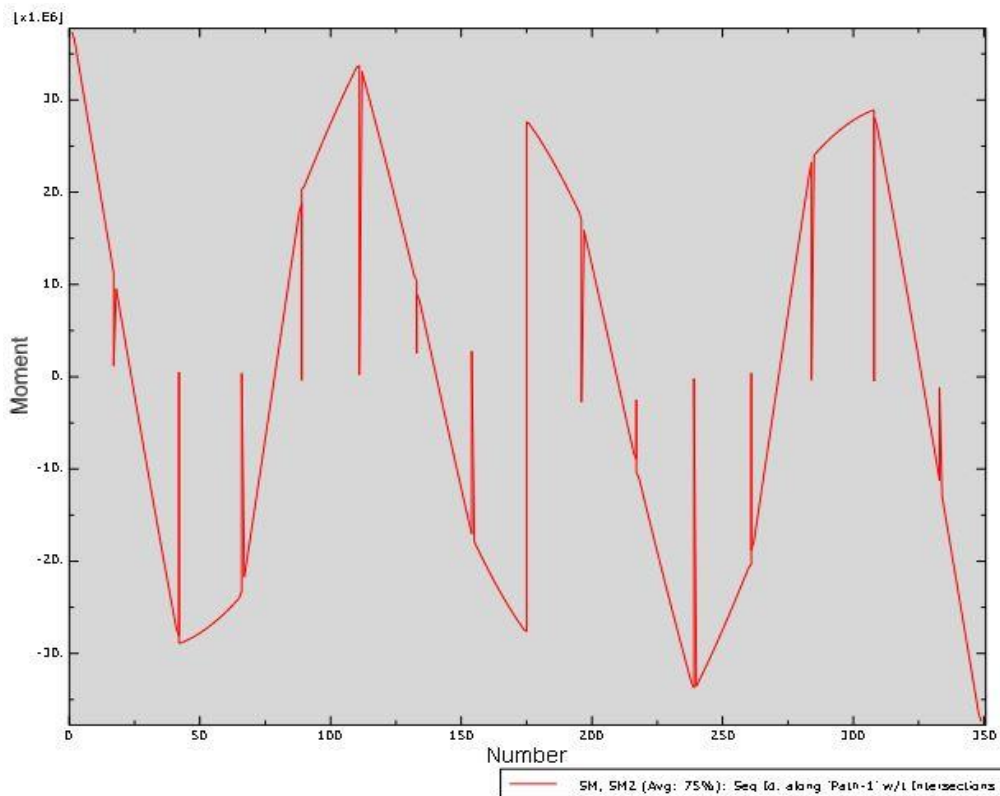
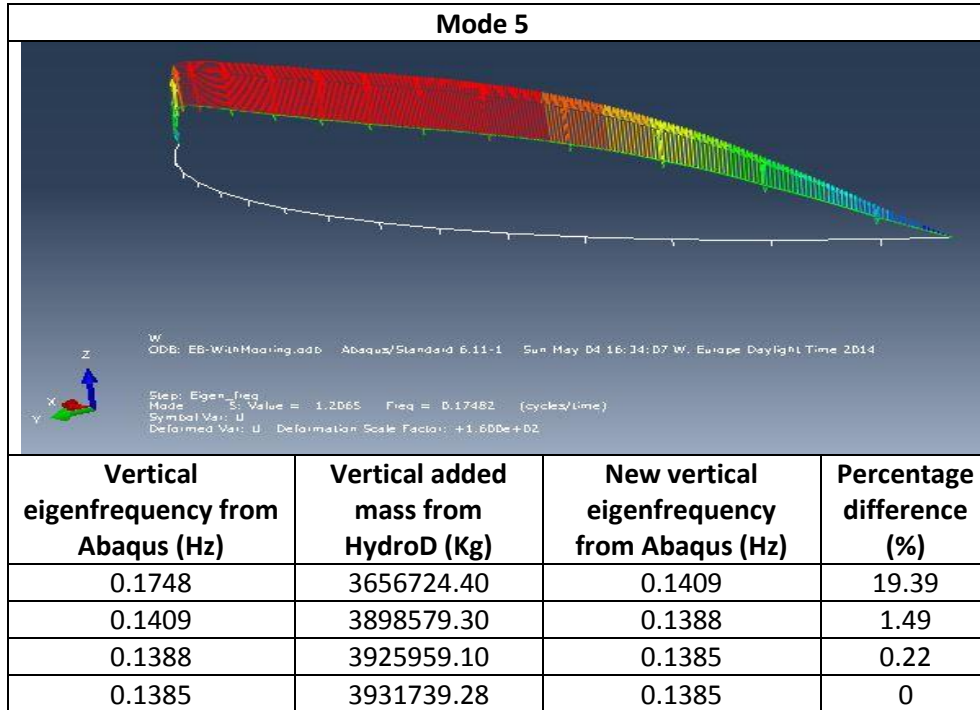


Figure 80: Heave bending moment along the elongated curve bridge model

7.4.6 Elongated curve bridge model with mooring

Table 19: Iteration of added mass for first heave eigenmode



For $\theta = 0$ deg.

$$F(t) = 1800470 \cdot \sin(0.8702t + \Phi_i)$$

Eq. 7.35

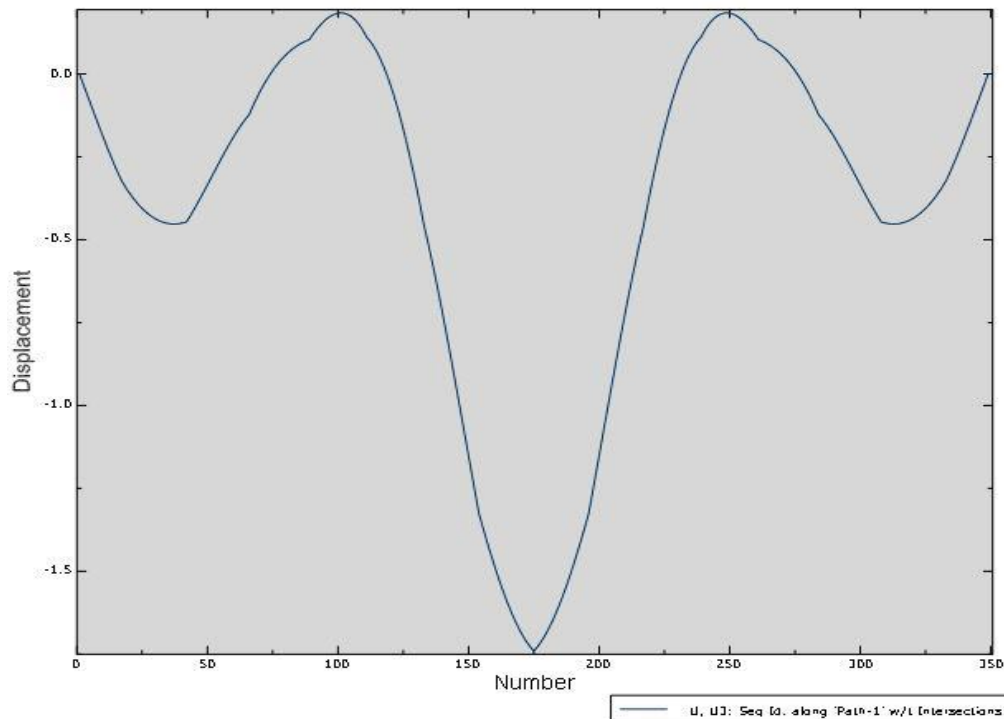


Figure 81: Heave displacement along the elongated curve bridge model with mooring

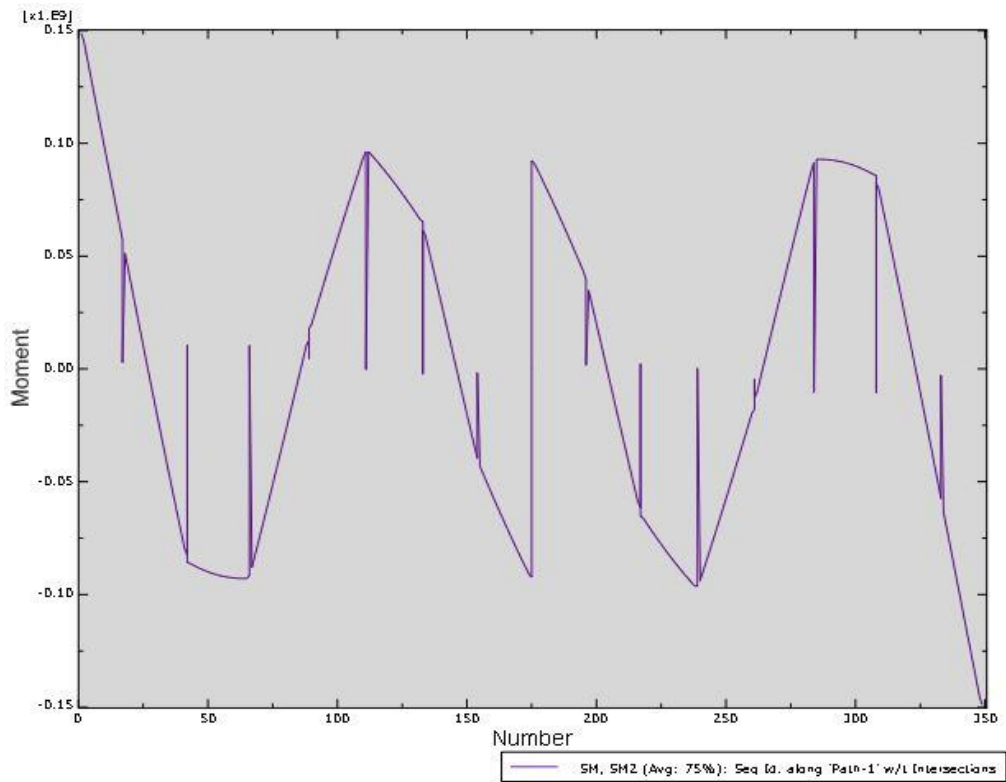


Figure 82: Heave bending moment along the elongated curve bridge model with mooring

For $\theta_{cr} = 73.7$ deg.

$$F(t) = 2080800 \cdot \sin(0.8702t + \Phi_i)$$

Eq. 7.36

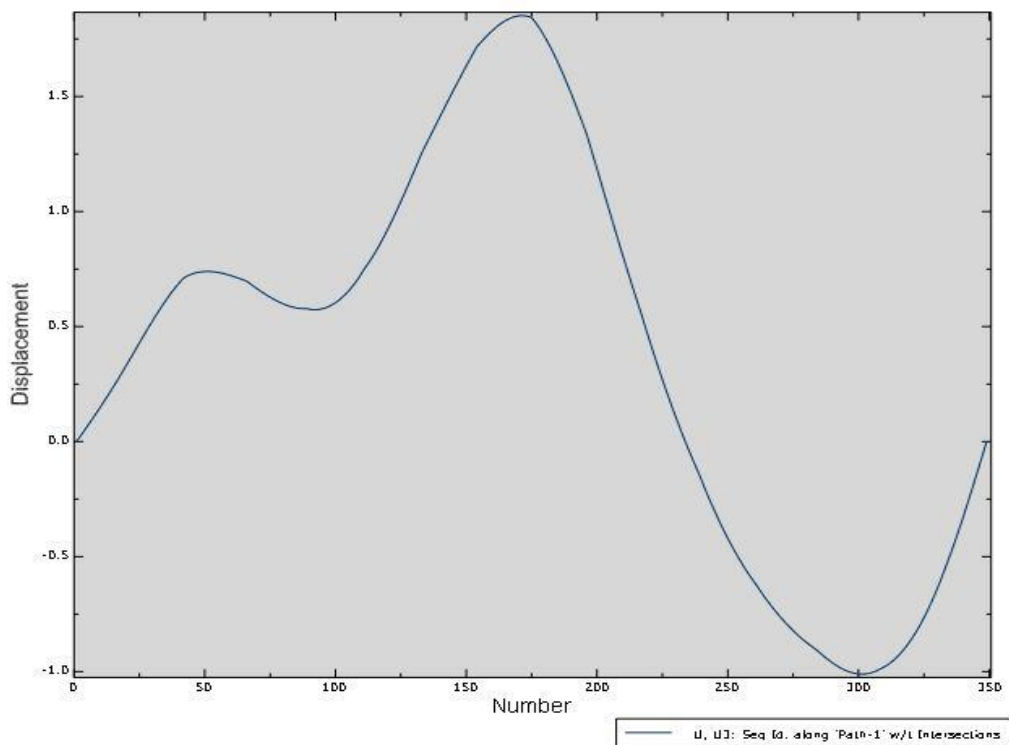


Figure 83: Heave displacement along the elongated curve bridge model with mooring

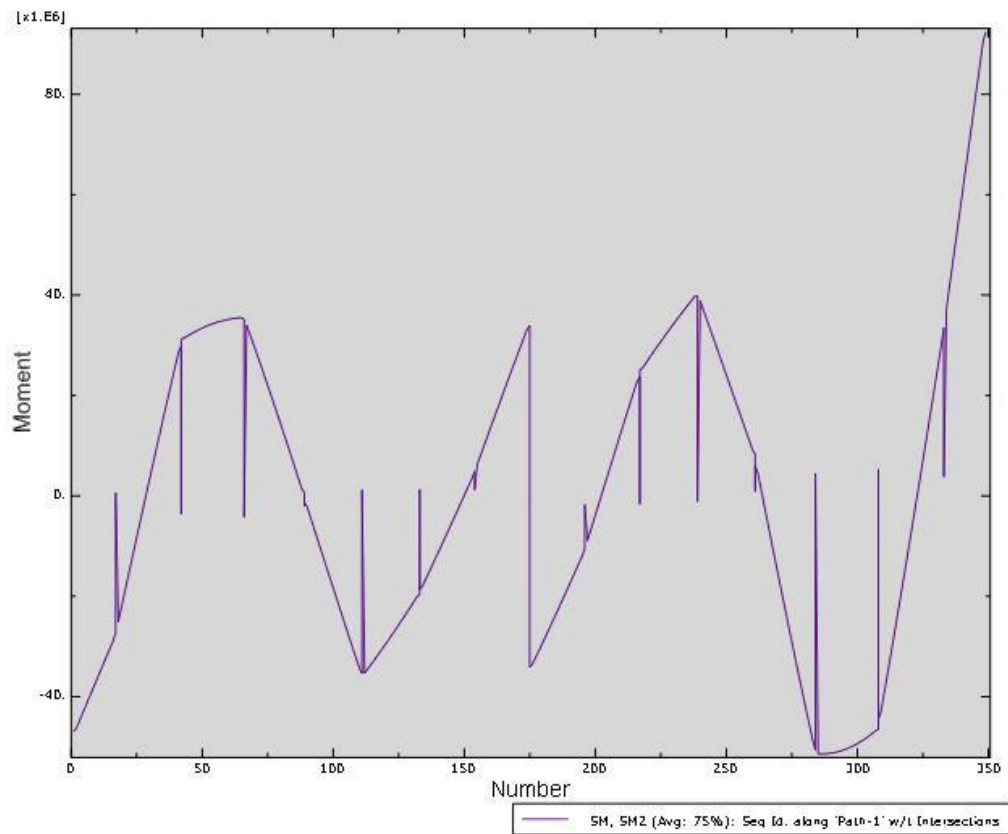


Figure 84: Heave bending moment along the elongated curve bridge model with mooring

8 DISCUSSION

From the results of the static analysis, it is observed that the curve bridge is stiffer compared to the straight bridge in the lateral plane. In the case of a curve bridge, the lateral forces are counteracted by the tensile axial forces. For the same static load, the response of the straight bridge is eleven times that of the curve bridge.

The elongated bridge models are more vulnerable to the static lateral loads, as seen from the results. The sway bending stiffness reduces due to elongation since

$$K = \frac{384Ei}{L^3} \quad \text{Eq. 8.1}$$

where E is Young's modulus of elasticity and I is the moment of inertia. The increased lateral stiffness in the presence of mooring lines minimizes the lateral loads and as a consequence, the response decreases.

The main purpose of the eigenfrequency analysis was to determine the frequency of the first sway and heave modes of a model, and then to determine its response to that frequency wave load. On the basis of what has been explained above, the trends seen in the eigenfrequencies of the models are justified since

$$f = \frac{1}{2\pi} \sqrt{\frac{K}{M}} \quad \text{Eq. 8.2}$$

The first three eigenfrequencies of the simplified model of the Bergsøysundet floating bridge have been compared to that of its more robust model constructed by the Department of Structural Engineering, NTNU.

Table 20: Comparison between the eigenfrequencies of simplified and detailed Bergsøysund bridge models

Mode	Movement	Eigenfrequency of simplified model (Hz)	Eigenfrequency of detailed model (Hz)	Percentage difference (%)
1	Horizontal	0.1061	0.0911	16.5
2	Horizontal	0.1332	0.1653	19.4
3	Vertical	0.1762	0.1950	9.6

One of the constraints of this work has been the non-implementation of the full matrices of the pontoon's mass, hydrostatic stiffness, added mass and hydrodynamic damping. Although the Bergsøysundet floating bridge has two sets of pontoons, a single pontoon type has been used to establish all the pontoons of that bridge model. The differences in the eigenfrequencies could be attributed to these facts.

Negatively damped sway responses have been observed for all the models. The implicit dynamic analysis in Abaqus has some default numerical damping. Sway response analysis with significant numerical damping ($\alpha = -1/3$) failed to stabilize

the response. Hence, external lateral dampers have been applied when studying the sway response of the models. From the dynamic response analysis of the elongated bridges, it is seen that the heave eigenfrequencies are unaffected by the sideways mooring lines. The important results obtained from the dynamic analysis is summarized below

Table 21: Important results of the dynamic analyses

Models	Maximum Sway Bending Moment (Nm)		Maximum Heave Bending Moment (Nm)	
	$\theta = 0 \text{ deg.}$	$\theta = \theta_{cr}$	$\theta = 0 \text{ deg.}$	$\theta = \theta_{cr}$
Curve bridge	2.55E+07	5.75E+06	1.42E+08	1.67E+08
Elongated curve bridge	6.20E+05	8.40E+05	3.70E+07	3.70E+07
Elongated curve bridge with mooring	8.75E+06	6.40E+06	1.50E+08	9.00E+07
Straight bridge	2.75E+08	1.75E+07	64	91.7
Elongated straight bridge	5.20E+07	5.30E+07	265	125
Elongated straight bridge with mooring	2.35E+08	3.63E+07	80	113

Evaluation of these results somewhat undermines the technique used to gauge the critical angle of wave heading. For some of the models, the response is actually lower at the estimated critical angle. As an alternative, iteration was employed to determine the critical angle by directing the wave over a range of angles at small angular increments. Since the bridge models are comparatively less stiff in the vertical plane than in the lateral plane, this has been only done for the elongated straight bridge model in heave mode.

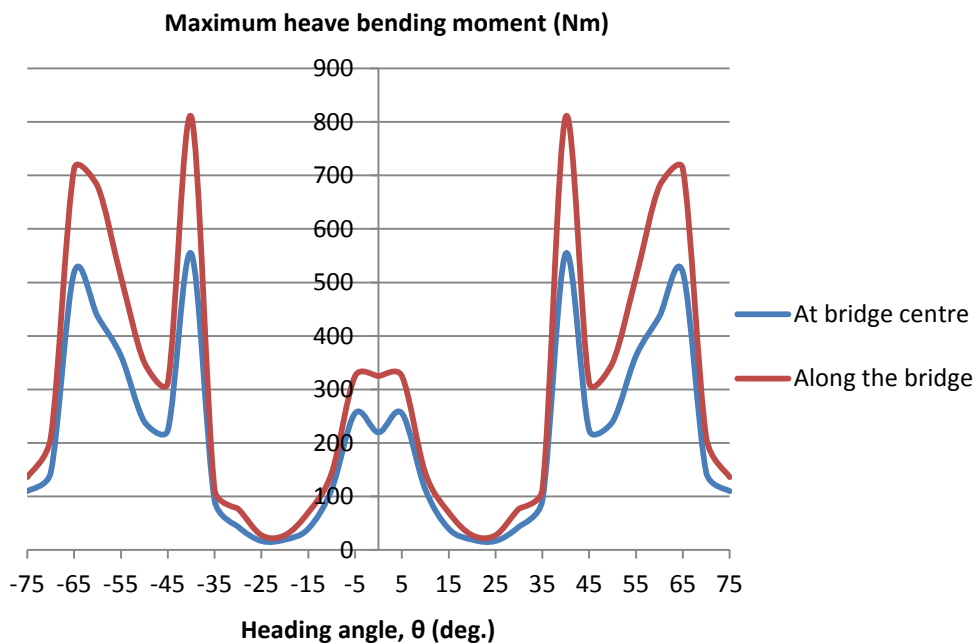


Figure 85: Maximum heave bending moment for the elongated straight bridge model

The response of this model is actually maximum at 40 deg. rather than at 74 deg.

For this particular model and mode, the effect of a $\cos^2\theta$ wave spreading function has also been assessed in a simplified way, within the range $-40 < \theta < 40$. The details can be found in Appendix D.

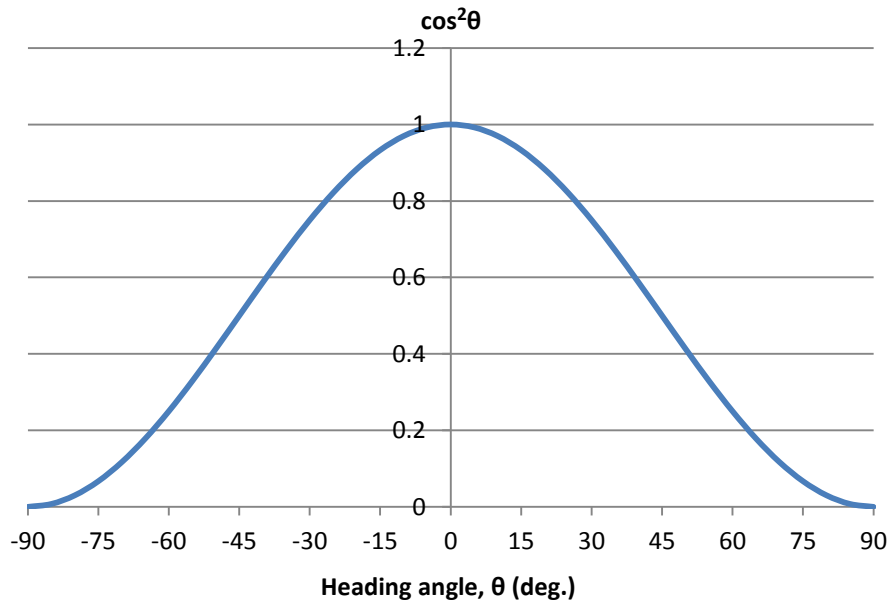


Figure 86: Wave spreading as a $\cos^2\theta$ function

As shown in Figure 86, most of the waves are concentrated in the non-critical region, i.e. in the periphery of the head on direction. Hence, the maximum heave bending moment hovers around the average value of the bending moments in the range $-40 < \theta < 40$, as found in Figure 85. This has been illustrated in Figure 87.

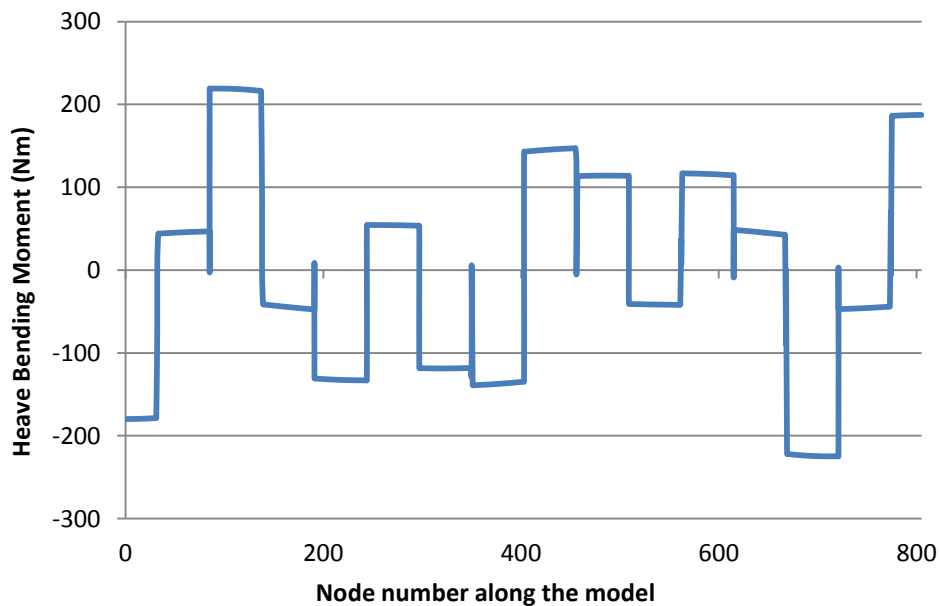


Figure 87: Heave bending moment along the elongated straight bridge model for $\cos^2\theta$ wave spreading function



9 CONCLUSION

The main objective of this thesis has been to analyse the hydrodynamic response of floating bridges with transverse pontoons, when subjected to harmonic regular wave loads. The sway and heave responses have been mainly analysed. For this task, HydroD and Abaqus have been employed for the hydrodynamic and finite element analyses respectively. A number of subjects have been addressed as part of this work.

Reviews have been made of the history, types and existing floating bridges. The relevant theory regarding the loads which are acting on such bridges has also been discussed. Corresponding methods for eigenfrequency, static and dynamic analysis have been elaborated and relevant numerical algorithms have been described.

A simplified beam model of the Bergsøysundet floating bridge has been established in the FEM software Abaqus. The pontoon modelled by Abdillah Suyuthi has been analysed in HydroD and it forms the basis for the bridge model construction. By considering the model of the Bergsøysundet floating bridge as a starting point, additional “synthetic” floating bridge structures have also been constructed and analysed as part of this thesis. Response in the presence of sideways mooring lines has also been contemplated for the elongated bridge models.

For each model, the first sway and heave eigenmodes have been obtained by the eigenfrequency analysis in Abaqus. Each eigenfrequency and the respective added mass are updated by iteration until they are in agreement. Only then, static and dynamic analyses have been carried out for the models. The regular wave load corresponding to the updated eigenfrequency of the mode is acquired from the hydrodynamic analysis in HydroD and applied in Abaqus.

Simplified techniques have been presented to estimate the critical angle of wave heading, as well as the phase difference at each pontoon due to the changing wave direction and shapes of the models. Mixed results have been found at the estimated critical angles. For better estimation, iteration of response at slightly growing heading angle has been conducted for the elongated straight bridge model in heave. For this model, the effect of $\cos^2\theta$ wave spreading function has also been taken into account in a simplified way.

One of the drawbacks of this work has been the non-utilization of the full matrices of the pontoon’s structural model and hydrodynamic parameters. The same pontoon has been used to represent all the pontoons of the Bergsøysundet floating bridge model. The effects of these imperfections have been highlighted by comparing the eigenfrequencies of the simplified and detailed model of the Bergsøysundet floating bridge. Moreover, there is still room for improvement when it comes to modelling the structural damping of the bridge models.



For future work, the use of a more robust model is therefore recommended. The effect of sideways mooring has been only considered for the elongated bridge models. Sideways mooring lines could also be applied on the short length models for a range of stiffness. This task has been restricted to regular waves' responses only. As a part of further study, the actual sea state conditions could be modelled and implemented, and the responses analysed. The scope of work can also be extended to accommodate alternate tangible floating bridge designs.

10 REFERENCES

- [1] Lwin, M., *Floating bridges*. Bridge Engineering Handbook, 2000. **22**: p. 1-23.
- [2] Seif, M. and R.P. Koulaei, *Floating Bridge Modeling and Analysis*. Scientia Iranica, 2005. **12**(2): p. 199-206.
- [3] Watanabe, E. and T. Utsunomiya, *Analysis and design of floating bridges*. Progress in Structural Engineering and Materials, 2003. **5**(3): p. 127-144.
- [4] Wikipedia. Floating Bridge. 2014.
http://en.wikipedia.org/wiki/Floating_bridge. Accessed (05/02/2014)
- [5] Wikipedia. Lacey V. Murrow Memorial Bridge. 2007.
http://en.wikipedia.org/wiki/File:I-90_floating_bridges_looking_east.JPG. Accessed (06/03/2014)
- [6] International Database for Civil and Structural Engineering. Hood Canal Bridge. 2003.
<http://structurae.net/structures/data/index.cfm?id=s0010568>. Accessed (06/03/2014)
- [7] Madison Park Blogger. 2011.
<http://madisonparkblogger.blogspot.no/2011/06/floating-bridge-closed-this-weekend.html>. Accessed (06/03/2014)
- [8] Wikipedia. Admiral Clarey Bridge. 2009.
http://en.wikipedia.org/wiki/File:Admiral_Clarey_Bridge_Open_2009-12-07.jpg. Accessed (06/03/2014)
- [9] Matson, D., et al. *Design and Construction of the William R. Bennett Bridge*. in *IABSE Congress Report*. 2008. International Association for Bridge and Structural Engineering.
- [10] Floating Object Database. Kelowna Floating Bridge. <http://db.flexibilni-architektura.cz/o/96>. Accessed (06/03/2014)
- [11] Wikipedia. Bergsøysund Bridge. 2011.
http://commons.wikimedia.org/wiki/File:Bergs%C3%B8ysundbrua_01.jpg. Accessed (06/03/2014)
- [12] Wikipedia. Nordhordland Bridge. 2011.
http://en.wikipedia.org/wiki/File:Nordhordalandsbrua_towards_north.jpg. Accessed (06/03/2014)
- [13] Wikipedia. Galata Bridge. 2009.
http://en.wikipedia.org/wiki/File:Galata_Bridge_From_Tower.JPG. Accessed (06/03/2014)

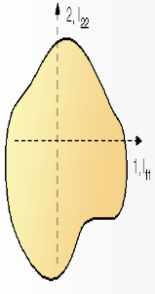
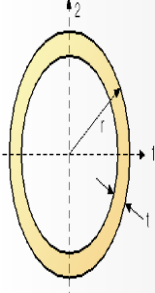


- [14] Movable Bridges in the British Isles. West India Quay Footbridge. 2005.
<http://www.movablebridges.org.uk/BridgePage.asp?BridgeNumber=1122>
Accessed (06/03/2014)
- [15] Seattle Pi. Yumemai Bridge. 2012.
<http://www.seattlepi.com/local/transportation/article/Floating-bridges-of-the-world-2971885.php#photo-2554665>. Accessed (06/03/2014)
- [16] Moe, G., *Design philosophy of floating bridges with emphasis on ways to ensure long life*. Journal of Marine Science and Technology, 1997. **2**(3): p. 182-189.
- [17] Watanabe, E., et al., *Very large floating structures: applications, analysis and design*. CORE Report, 2004. **2**.
- [18] Moan, T., *Finite Element Modelling and Analysis of Marine Structures*. NTNU, Institutt for Marin Teknikk, 2003.
- [19] Simulia, D.S., *Abaqus 6.11 theory manual*. Providence, RI, USA: DS SIMULIA Corp, 2011.
- [20] Faltinsen, O., *Sea loads on ships and offshore structures*. Vol. 1. 1993: Cambridge university press.
- [21] McLean, D.I., *Experimental Response and Analysis of the Evergreen Point Floating Bridge*. 2003, Washington State University.
- [22] The Engineering Toolbox. Drag coefficient.
http://www.engineeringtoolbox.com/drag-coefficient-d_627.html.
Accessed (08/04/2014)
- [23] Georgiadis, C., *Finite element modeling of the response of long floating structures under harmonic excitation*. Journal of energy resources technology, 1985. **107**(1): p. 48-53.



APPENDIX A

Table 22: Bridge sections' properties

Sections*	Profile	Equivalent Cross Sectional Area (m ²)	I ₁₁ (m ⁴)	I ₂₂ (m ⁴)	J (m ⁴)	r (m)	t (m)
1		0.7	10.87	17.26	3.07	—	—
2		0.7	11.64	18.06	3.07	—	—
3		0.7	14.15	20.41	3.07	—	—
4		0.7	16.3	25.83	3.07	—	—
Vertical Section		—	—	—	—	1.9	0.04

*Sections are numbered in ascending order starting from the mid horizontal section of the bridges.

Table 23: Bridge mass data

Property*	Value
Mass of pontoon (Kg)	3040000
Mass of diagonal bracing (kg)	115378
Mass of horizontal bracing (kg)	47948
Mass of legs (kg)	7984
Mass of asphalt (kg)	117600
Rotation mass (kg)	27500

*Except for the mass of pontoon (obtained from Wadam analysis), all other masses were defined at the point of intersection between the truss-work and vertical sections.

Table 24: Material Data

Property	Value
Material	Steel
Desnsity (kg/m ³)	7800
Young's modeulus (GPa)	200
Poisson's ratio	0.3



APPENDIX B

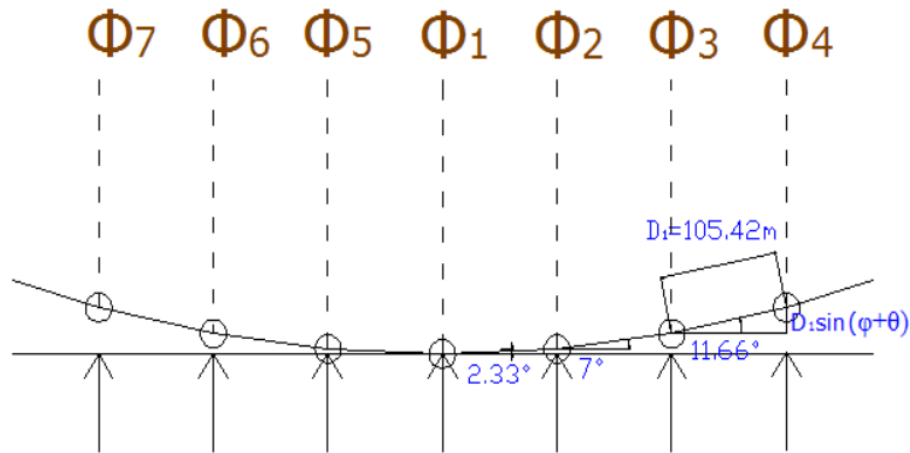


Figure 88: Concept diagram for calculation of phase angles of curve bridge model

Table 25: Phase angles of curve bridge model in sway

Heading Angle, θ (deg.)	Pontoon no. (i)	φ (deg.)	Factor	$\sin(\varphi \pm \theta)$	Factor x $\sin(\varphi \pm \theta)$	Phase Angles, Φ_i (deg.)
0	1					0
	2	2.33	273.86	0.04	11.13	11.13
	3	7.00	273.86	0.12	33.38	44.51
	4	11.66	273.86	0.20	55.35	99.86
	1					0
	5	2.33	273.86	0.04	11.13	11.13
	6	7.00	273.86	0.12	33.38	44.51
7	11.66	273.86	0.20	55.35	99.86	
55.1	1					0
	2	2.33	273.86	0.84	230.79	230.79
	3	7.00	273.86	0.88	242.03	472.82
	4	11.66	273.86	0.92	251.64	724.46
	1					0
	5	2.33	273.86	-0.80	-218.05	-218.05
	6	7.00	273.86	-0.74	-203.84	-421.89
7	11.66	273.86	-0.69	-188.31	-610.20	

Table 26: Phase angles of curve bridge model in heave

Heading Angle, θ (deg.)	Pontoon no. (i)	φ (deg.)	Factor	$\sin(\varphi \pm \theta)$	Factor x $\sin(\varphi \pm \theta)$	Phase Angles, Φ_i (deg.)
0	1					0
	2	2.33	474.10	0.04	19.27	19.27
	3	7.00	474.10	0.12	57.78	77.05
	4	11.66	474.10	0.20	95.82	172.87
	1					0
	5	2.33	474.10	0.04	19.27	19.27
	6	7.00	474.10	0.12	57.78	77.05
7	11.66	474.10	0.20	95.82	172.87	
71.1	1					0
	2	2.33	474.10	0.96	454.41	454.41
	3	7.00	474.10	0.98	463.91	918.33
	4	11.66	474.10	0.99	470.32	1388.65
	1					0
	5	2.33	474.10	-0.93	-441.93	-441.93
	6	7.00	474.10	-0.90	-426.48	-868.41
7	11.66	474.10	-0.86	-408.25	-1276.66	

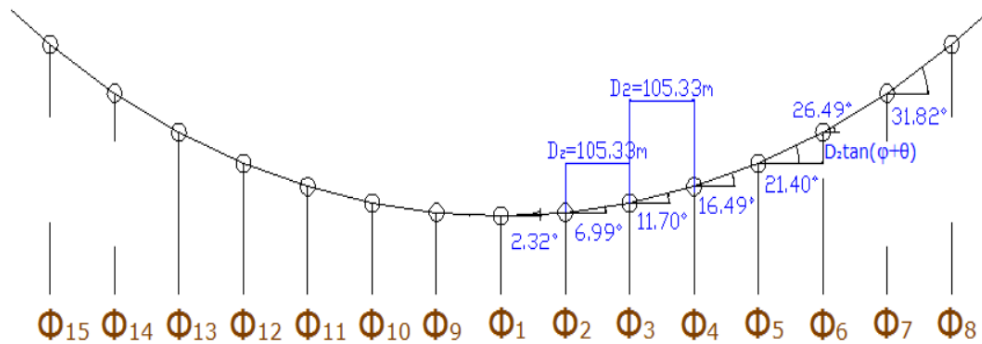


Figure 89: Concept diagram for calculation of phase angles of elongated curve bridge model

Table 27: Phase angles of elongated curve bridge model in sway

Heading Angle, θ (deg.)	Pontoon no. (i)	φ (deg.)	Factor	$\tan(\varphi \pm \theta)$	Factor x $\tan(\varphi \pm \theta)$	Phase Angles, Φ_i (deg.)	
0	1					0	
	2	2.32	22.02	0.04	0.89	0.89	
	3	6.99	22.02	0.12	2.70	3.59	
	4	11.70	22.02	0.21	4.56	8.15	
	5	16.49	22.02	0.30	6.52	14.67	
	6	21.41	22.02	0.39	8.63	23.31	
	7	26.49	22.02	0.50	10.98	34.28	
	8	31.82	22.02	0.62	13.67	47.95	
	1						0
	9	2.32	22.02	0.04	0.89	0.89	
	10	6.99	22.02	0.12	2.70	3.59	
	11	11.70	22.02	0.21	4.56	8.15	
	12	16.49	22.02	0.30	6.52	14.67	
	13	21.41	22.02	0.39	8.63	23.31	
	14	26.49	22.02	0.50	10.98	34.28	
15	31.82	22.02	0.62	13.67	47.95		
68.3	1					0	
	2	2.32	22.02	2.84	62.61	62.61	
	3	6.99	22.02	3.81	83.88	146.49	
	4	11.70	22.02	5.67	124.89	271.38	
	5	16.49	22.02	10.97	241.52	512.90	
	6	21.41	22.02	197.57	4350.95	4863.85	
	7	26.49	22.02	-11.93	-262.81	4601.04	
	8	31.82	22.02	-5.60	-123.38	4477.66	
	1						0
	9	2.32	22.02	-2.24	-49.42	-49.42	
	10	6.99	22.02	-1.83	-40.24	-89.66	
	11	11.70	22.02	-1.52	-33.40	-123.06	
	12	16.49	22.02	-1.27	-28.00	-151.05	
	13	21.41	22.02	-1.07	-23.53	-174.58	
	14	26.49	22.02	-0.89	-19.70	-194.27	
15	31.82	22.02	-0.74	-16.28	-210.56		

Table 28: Phase angles of elongated curve bridge model in heave

Heading Angle, θ (deg.)	Pontoon no. (i)	φ (deg.)	Factor	$\tan(\varphi \pm \theta)$	Factor x $\tan(\varphi \pm \theta)$	Phase Angles, Φ_i (deg.)	
0	1					0	
	2	2.32	466.26	0.04	18.89	18.89	
	3	6.99	466.26	0.12	57.17	76.06	
	4	11.70	466.26	0.21	96.56	172.62	
	5	16.49	466.26	0.30	138.02	310.64	
	6	21.41	466.26	0.39	182.82	493.46	
	7	26.49	466.26	0.50	232.37	725.83	
	8	31.82	466.26	0.62	289.32	1015.15	
	1						0
	9	2.32	466.26	0.04	18.89	18.89	
	10	6.99	466.26	0.12	57.17	76.06	
	11	11.70	466.26	0.21	96.56	172.62	
	12	16.49	466.26	0.30	138.02	310.64	
	13	21.41	466.26	0.39	182.82	493.46	
14	26.49	466.26	0.50	232.37	725.83		
15	31.82	466.26	0.62	289.32	1015.15		
73.7	1					0	
	2	2.32	466.26	4.02	1872.86	1872.86	
	3	6.99	466.26	6.10	2844.18	4717.03	
	4	11.70	466.26	12.43	5795.09	10512.12	
	5	16.49	466.26	-301.56	-140603.77	-130091.65	
	6	21.41	466.26	-11.18	-5214.08	-135305.73	
	7	26.49	466.26	-5.56	-2593.97	-137899.70	
	8	31.82	466.26	-3.60	-1679.01	-139578.71	
	1						0
	9	2.32	466.26	-2.97	-1383.87	-1383.87	
	10	6.99	466.26	-2.32	-1083.17	-2467.04	
	11	11.70	466.26	-1.88	-876.91	-3343.95	
	12	16.49	466.26	-1.55	-723.77	-4067.72	
	13	21.41	466.26	-1.29	-603.05	-4670.78	
14	26.49	466.26	-1.08	-503.69	-5174.47		
15	31.82	466.26	-0.90	-418.06	-5592.53		

Table 29: Phase angles of elongated curve bridge model with mooring in sway

Heading Angle, θ (deg.)	Pontoon no. (i)	φ (deg.)	Factor	$\tan(\varphi \pm \theta)$	Factor x $\tan(\varphi \pm \theta)$	Phase Angles, Φ_i (deg.)	
0	1					0	
	2	2.32	278.29	0.04	11.27	11.27	
	3	6.99	278.29	0.12	34.12	45.39	
	4	11.70	278.29	0.21	57.63	103.03	
	5	16.49	278.29	0.30	82.38	185.41	
	6	21.41	278.29	0.39	109.12	294.52	
	7	26.49	278.29	0.50	138.69	433.21	
	8	31.82	278.29	0.62	172.68	605.89	
	1						0
	9	2.32	278.29	0.04	11.27	11.27	
	10	6.99	278.29	0.12	34.12	45.39	
	11	11.70	278.29	0.21	57.63	103.03	
	12	16.49	278.29	0.30	82.38	185.41	
	13	21.41	278.29	0.39	109.12	294.52	
14	26.49	278.29	0.50	138.69	433.21		
15	31.82	278.29	0.62	172.68	605.89		
64.6	1					0	
	2	2.32	278.29	2.35	653.07	653.07	
	3	6.99	278.29	3.00	836.08	1489.16	
	4	11.70	278.29	4.10	1141.59	2630.75	
	5	16.49	278.29	6.38	1775.10	4405.84	
	6	21.41	278.29	14.34	3989.74	8395.58	
	7	26.49	278.29	-52.56	-14626.53	-6230.95	
	8	31.82	278.29	-8.89	-2473.22	-8704.16	
	1						0
	9	2.32	278.29	-1.90	-529.62	-529.62	
	10	6.99	278.29	-1.58	-438.68	-968.30	
	11	11.70	278.29	-1.32	-367.97	-1336.26	
	12	16.49	278.29	-1.11	-310.27	-1646.53	
	13	21.41	278.29	-0.94	-261.24	-1907.77	
14	26.49	278.29	-0.78	-218.29	-2126.06		
15	31.82	278.29	-0.64	-179.21	-2305.27		

Table 30: Phase angles of elongated curve bridge model with mooring in heave

Heading Angle, θ (deg.)	Pontoon no. (i)	φ (deg.)	Factor	$\tan(\varphi \pm \theta)$	Factor x $\tan(\varphi \pm \theta)$	Phase Angles, Φ_i (deg.)	
0	1					0	
	2	2.32	466.26	0.04	18.89	18.89	
	3	6.99	466.26	0.12	57.17	76.06	
	4	11.70	466.26	0.21	96.56	172.62	
	5	16.49	466.26	0.30	138.02	310.64	
	6	21.41	466.26	0.39	182.82	493.46	
	7	26.49	466.26	0.50	232.37	725.83	
	8	31.82	466.26	0.62	289.32	1015.15	
	1						0
	9	2.32	466.26	0.04	18.89	18.89	
	10	6.99	466.26	0.12	57.17	76.06	
	11	11.70	466.26	0.21	96.56	172.62	
	12	16.49	466.26	0.30	138.02	310.64	
	13	21.41	466.26	0.39	182.82	493.46	
14	26.49	466.26	0.50	232.37	725.83		
15	31.82	466.26	0.62	289.32	1015.15		
73.7	1					0	
	2	2.32	466.26	4.02	1872.86	1872.86	
	3	6.99	466.26	6.10	2844.18	4717.03	
	4	11.70	466.26	12.43	5795.09	10512.12	
	5	16.49	466.26	-301.56	-140603.77	-130091.65	
	6	21.41	466.26	-11.18	-5214.08	-135305.73	
	7	26.49	466.26	-5.56	-2593.97	-137899.70	
	8	31.82	466.26	-3.60	-1679.01	-139578.71	
	1						0
	9	2.32	466.26	-2.97	-1383.87	-1383.87	
	10	6.99	466.26	-2.32	-1083.17	-2467.04	
	11	11.70	466.26	-1.88	-876.91	-3343.95	
	12	16.49	466.26	-1.55	-723.77	-4067.72	
	13	21.41	466.26	-1.29	-603.05	-4670.78	
14	26.49	466.26	-1.08	-503.69	-5174.47		
15	31.82	466.26	-0.90	-418.06	-5592.53		



APPENDIX C

Table 31: Phase angles of straight bridge model in sway

Heading Angle, θ (deg.)	Pontoon no. (i)	Factor	Factor x $\sin\theta$	Phase Angles, Φ_i (deg.)
77.5	1			0
	2	69.83	68.18	68.18
	3	69.83	68.18	136.36
	4	69.83	68.18	204.53
	5	69.83	68.18	272.71
	6	69.83	68.18	340.89
	7	69.83	68.18	409.07

Table 32: Phase angles of straight bridge model in heave

Heading Angle, θ (deg.)	Pontoon no. (i)	Factor	Factor x $\sin\theta$	Phase Angles, Φ_i (deg.)
70.7	1			0
	2	472.34	445.80	445.80
	3	472.34	445.80	891.59
	4	472.34	445.80	1337.39
	5	472.34	445.80	1783.18
	6	472.34	445.80	2228.98
	7	472.34	445.80	2674.77



Table 33: Phase angles of elongated straight bridge model in sway

Heading Angle, θ (deg.)	Pontoon no. (i)	Factor	Factor x $\sin\theta$	Phase Angles, Φ_i (deg.)
22.6	1			0
	2	4.56	1.75	1.75
	3	4.56	1.75	3.51
	4	4.56	1.75	5.26
	5	4.56	1.75	7.01
	6	4.56	1.75	8.77
	7	4.56	1.75	10.52
	8	4.56	1.75	12.27
	9	4.56	1.75	14.03
	10	4.56	1.75	15.78
	11	4.56	1.75	17.53
	12	4.56	1.75	19.29
	13	4.56	1.75	21.04
	14	4.56	1.75	22.79
	15	4.56	1.75	24.55

Table 34: Phase angles of elongated straight bridge model in heave

Heading Angle, θ (deg.)	Pontoon no. (i)	Factor	Factor x $\sin\theta$	Phase Angles, Φ_i (deg.)
74	1			0
	2	466.94	448.85	448.85
	3	466.94	448.85	897.69
	4	466.94	448.85	1346.54
	5	466.94	448.85	1795.39
	6	466.94	448.85	2244.23
	7	466.94	448.85	2693.08
	8	466.94	448.85	3141.93
	9	466.94	448.85	3590.77
	10	466.94	448.85	4039.62
	11	466.94	448.85	4488.47
	12	466.94	448.85	4937.31
	13	466.94	448.85	5386.16
	14	466.94	448.85	5835.01
	15	466.94	448.85	6283.85

Table 35: Phase angles of elongated straight bridge model with mooring in sway

Heading Angle, θ (deg.)	Pontoon no. (i)	Factor	Factor x $\sin\theta$	Phase Angles, Φ_i (deg.)
82.5	1			0
	2	364.16	361.05	361.05
	3	364.16	361.05	722.09
	4	364.16	361.05	1083.14
	5	364.16	361.05	1444.18
	6	364.16	361.05	1805.23
	7	364.16	361.05	2166.27
	8	364.16	361.05	2527.32
	9	364.16	361.05	2888.36
	10	364.16	361.05	3249.41
	11	364.16	361.05	3610.45
	12	364.16	361.05	3971.50
	13	364.16	361.05	4332.54
	14	364.16	361.05	4693.59
	15	364.16	361.05	5054.63

Table 36: Phase angles of elongated straight bridge model with mooring in heave

Heading Angle, θ (deg.)	Pontoon no. (i)	Factor	Factor x $\sin\theta$	Phase Angles, Φ_i (deg.)
74	1			0
	2	466.94	448.85	448.85
	3	466.94	448.85	897.69
	4	466.94	448.85	1346.54
	5	466.94	448.85	1795.39
	6	466.94	448.85	2244.23
	7	466.94	448.85	2693.08
	8	466.94	448.85	3141.93
	9	466.94	448.85	3590.77
	10	466.94	448.85	4039.62
	11	466.94	448.85	4488.47
	12	466.94	448.85	4937.31
	13	466.94	448.85	5386.16
	14	466.94	448.85	5835.01
	15	466.94	448.85	6283.85





APPENDIX D

$$C = \text{Total area under the curve} = \int_{-\pi/2}^{\pi/2} \cos^2 \theta \, d\theta$$

$$A = \text{Area in the range } -40 < \theta < 40 = \int_{-2\pi/9}^{2\pi/9} \cos^2 \theta \, d\theta$$

$$W_{-40 < \theta < 40} = \text{Weight factor} = \frac{A}{C}$$

$$W_{\theta < -40} = W_{\theta > 40} = \frac{1 - A/C}{2}$$

$$F_{\theta < -40} = F_{\theta > 40} = \text{Heave force coefficient for } \theta \rightarrow 40 \text{ deg.}$$

$$F_{-40 < \theta < 40} = \text{Heave force coefficient for } \theta \rightarrow 0 \text{ deg.}$$

$$F_i = \{W_{-40 < \theta < 40} \cdot F_{-40 < \theta < 40} \cdot \sin \omega t\} + \{W_{\theta < -40} \cdot F_{\theta < -40} \cdot \sin(\omega t + \Phi_{i_x})\} + \{W_{\theta > 40} \cdot F_{\theta > 40} \cdot \sin(\omega t + \Phi_{i_y})\}$$

where,

ω = Circular frequency of the heave eigenmode

i = Pontoon no. = {1, 2, 3....15}

F_i = Total heave force on pontoon i

Φ_{i_x} and Φ_{i_y} = Random phase angles at pontoon i

